

Automation of Painted Slate Inspection

BY

Tim Carew (B.Eng.)
carewt@eeng.dcu.ie

Submitted for the requirement of
Degree of Master of Engineering (M.Eng.)
by research to Dublin City University

Supervised by Prof. Paul F. Whelan

School of Electronic Engineering
Dublin City University

October 2002

Declaration

I hereby certify that this material, which I now submit for assessment on the programme of study leading to the award of Master of Engineering is entirely my own work and has not been taken from the work of others save and to the extent that such work has been cited and acknowledged within the text of my work.

Signed: Tim Covert

ID No.: 99145731

Date: October 21, 2002

Acknowledgements

I would like to express my sincere thanks to Paul Whelan and Ovidiu Ghita for their help, guidance and encouragement during the course of this project.

Thanks also to Paul Loughman and Michael Murray for their advice and interest in my project and for their guidance on the needs of the industrial partner.

I would also like to thank my colleagues and members of the Vision Systems Laboratory, particularly Robert Sadleir and John Mallon. A special word of thanks to Ovidiu Ghita for his unfailing enthusiasm and encouragement throughout.

Many thanks to Tegral Building Products Ltd and to Enterprise Ireland for their financial support of this project.

I would also like to thank the external examiner, Prof. Roy Davies, for the time he put into the examination of this work and for the suggestions that he made.

Last, but not least, I wish to thank my wife Martina for her endless encouragement and support and without whom this project would have been impossible for me.

Table of Contents

Acknowledgements.....	3
Table of Contents.....	4
Table of Figures.....	6
List of Tables.....	8
Abstract.....	9
1. Introduction.....	10
1.1 Background to the inspection task.....	10
1.2 Motivation for automating inspection.....	12
1.3 Principal components of a machine vision system.....	13
1.4 Report outline.....	17
2. Relevant Prior Research.....	18
2.1 Prior research on inspection of slates.....	18
2.2 Prior research on inspection of ceramics.....	18
2.2.1 Illumination and image capture.....	20
2.2.2 Image analysis algorithms.....	22
2.2.2.1 Edge faults.....	22
2.2.2.2 Substrate faults.....	23
2.2.2.3 Paint faults.....	24
2.3 Prior research on texture.....	26
2.4 Usefulness of prior work to slate inspection.....	28
3. Image Capture.....	29
3.1 Introduction.....	29
3.2 Description of the slate and paint process line.....	29
3.3 Principle of operation.....	30
3.4 Test bed description.....	33
3.5 Tests using collimated lighting.....	35
3.5.1 Profile of reference slates.....	37
3.5.2 Summary of test results.....	39
3.5.3 Effect of concavity and convexity on signal level.....	40
3.6 Tests using diffuse lighting.....	40
3.6.1 Profile of reference slates.....	41
3.6.2 Signal levels for selected defects.....	42
3.7 Optical solution for successful image capture in the presence of depth profile.....	43
3.7.1 Test results using defocused light line.....	45
3.8 Discussion.....	47
3.9 Prototype inspection system description.....	48
4. Image Processing Algorithm Design.....	50
4.1 Introduction.....	50
4.2 Reference slate characterisation.....	50
4.3 Defect slate characterisation.....	54
4.4 Image processing methods investigated.....	57
4.4.1 Grey level statistical methods.....	57
4.4.2 Grey level difference methods.....	58
4.4.3 Local binary pattern methods.....	60
4.4.4 Morphological methods.....	61
4.4.5 Convolution methods.....	62
4.5 Algorithm design.....	62

4.5.1 Global mean threshold method	63
4.5.2 Adaptive signal threshold method	63
4.5.3 Labelling method	64
4.5.4 Edge detection method.....	65
4.5.5 Detection of shallow template mark by vertical projection.	65
4.6 Algorithm testing	68
4.6.1 Paint faults	68
4.6.2 Substrate faults.....	71
4.6.3 Preliminary robustness testing	76
4.6.4 Discussion.....	77
4.7 Transfer to the production prototype	78
4.7.1 Slate edge detection and region to inspect selection.....	79
4.7.2 Nail hole inspection	80
4.7.3 Tests using prototype inspection system.....	80
5. Robustness Tests.....	83
5.1 Introduction.....	83
5.2 Experimental details.....	83
5.3 Experimental results.....	84
5.3.1 Reference slates	84
5.3.2 Defective slates	87
5.4 Additional experiments and results.....	88
5.4.1 Testing with slate rotated 90°	88
5.4.2 Full slate imaging.....	89
5.4.3 Conveyor speed characterization	90
5.5.4 Effect of slate colour on inspection capability.....	91
5.6 Discussion	92
6. Conclusions.....	93
6.1 Proposed next steps to commercialisation	93
6.2 Equipment recommendations for industrial version of inspector.....	94
6.3 Further applications of an automated inspection system	95
References.....	97
Bibliography	101
Publications arising from this research	102
Appendix A – Detailed Robustness Tests Results.....	A-1
Appendix B – Prototype Inspector Equipment List.....	B-1
Appendix C – Popular Image Processing Techniques.....	C-1
C.1 - Difference statistics.....	C-1
C.2 – Local binary patterns.....	C-3
C.3 – Application of binary morphology.....	C-5
Appendix D – Classification of Defects by Type.....	D-1
Appendix E – Defect Naming Abbreviations.....	E-1

Table of Figures

Figure 1: A selection of defects found on painted slates.	10
Figure 2: Block diagram of an industrial machine vision system, TSI (1998).	14
Figure 3: Factory view of installed machine vision systems, TSI (1997).	15
Figure 4: Flow chart of generalised machine vision system design.	16
Figure 5: Model of reflectance for slate surface.	31
Figure 6: Test bed arrangement.	33
Figure 7: Test bed showing slate, fibre line light and camera	34
Figure 8: Horizontal profiles of reference slates.	37
Figure 9: Mean subtracted from row data shown in Figure 8.	38
Figure 10: Definition of signal amplitude.	39
Figure 11: Signal amplitude of paint and substrate faults by collimated lighting.	40
Figure 12: Vertical profile of slates with significant depth profile variation.	41
Figure 13: Mean grey level of defects imaged using diffuse lighting.	42
Figure 14: Fibre light guide with lens attachment.	43
Figure 15: Modified line light and lens arrangement; side and front views.	44
Figure 16: Light band MD profile according to camera view angle.	45
Figure 17: A selection of substrate defects of type template mark and lump.	46
Figure 18: Amplitude of defect signals imaged with defocused light line.	46
Figure 19: A selection of paint defects of type efflorescence, insufficient paint, paint droplet, shade variation, paint debris and missing paint.	47
Figure 20: Conveyor and slate inspection system.	49
Figure 21: Mean grey level variation for successive samples.	51
Figure 22: Reference sample under test in the Neatvision environment.	51
Figure 23: Slate image bref5 and section a1 shown on right.	53
Figure 24: A 150 x 150 pixel sub-section from bref5 and its grey level histogram. ...	53
Figure 25: A selection of paint defects and their grey level histograms.	56
Figure 26: A selection of substrate defects and their grey level histograms.	57
Figure 27: Difference statistic ($0^\circ + 90^\circ$) applied to reference and defect image.	58
Figure 28: Comparison of DiffXY histograms for reference and defect images.	59
Figure 29: Comparison of LBP and LBP/C binned histograms.	61
Figure 30: Slate defect detection block diagram.	62
Figure 31: Label algorithm.	64
Figure 32: Edge detection algorithm.	65
Figure 33: Vertical projection algorithm explanation.	66
Figure 34: Projection method traces for grey and binary images.	67
Figure 35: Comparison between the four component algorithm and the projection algorithm for detecting a shallow template mark.	67
Figure 36: Image processing image output for selected paint faults.	71
Figure 37: Image processing image output for selected substrate faults.	75
Figure 38: Mean grey levels for reference images.	85
Figure 39: Inspection output for samples with 300 mm edge facing forward.	89
Figure 40: Inspection output of full slate for sample no. 164 and no. 194.	90
Figure 41: Graphs of variation in slate width measurements.	90
Figure 42: Mean grey levels of colour slates.	91
Figure 43: Paint process line with automated sorting of defective slates.	96
Figure A.1: Insufficient paint and no paint sample mean grey levels.	A-1
Figure A.2: Efflorescence samples no. 164 and no. 165 detection results.	A-2

Figure A.3: Shade variation samples no. 183 and no. 185 detection results.....	A-3
Figure A.4: Mean grey levels of nozzle drip samples.....	A-4
Figure A.5: Nozzle Drip samples no 181. and no. 173 detection output.....	A-4
Figure A.6: Small paint fault detection result output.....	A-5
Figure A.7: Template marks no. 39 and no. 195 detection output.....	A-6
Figure A.8: Detection output for no. 56 and no. 66 lump defects.....	A-6
Figure A.9: Depression no. 205 and no. 38 detection output.....	A-7
Figure A.10: Bad edge no. 79 and no. 82 detection output.....	A-8
Figure B.1: Conveyor and slate inspection system.....	B-1
Figure C.1: Difference statistic calculation, source and difference images.....	C-2
Figure C.2: Local binary pattern calculation.....	C-3
Figure C.3: Typical LBP images and histograms.....	C-4
Figure C.4: Horizontal line SE applied to detection of horizontal template mark.	C-6
Figure C.5: Vertical line SE applied to detection of a horizontal template mark...	C-6
Figure C.6: Horizontal SE applied to detection of a vertical template mark.....	C-7
Figure C.7: Vertical SE applied to detection of a vertical template mark.....	C-7
Figure C.8: Horizontal line SE applied to a reference image.....	C-8
Figure C.9: Comparison of vertical and horizontal (top row) SE results when applied to a vertical template mark.....	C-9
Figure D.1: Reference slate and large depression imaged by triangulation.....	D-3

List of Tables

Table 1: Defect type and size definitions.....	11
Table 2: Ceramic tile and slate defect category comparison.	19
Table 3: Slate properties.	30
Table 4: Signal amplitude calculations for selected defects.	39
Table 5: Defect signal levels when using diffuse light source.....	42
Table 6: Measurements on 150 x 150 pixel sub-sections of reference bref1.....	52
Table 7: Processing loop results for selected paint defects.....	68
Table 8: Processing loop results for selected substrate defects.	72
Table 9: Summary data for Thrutone reference slates.	76
Table 10: Processing loop results for various substrate defects.....	77
Table 11: Image and data output for selected defect types.	81
Table 12: Summary of inspectorv2 inspection results.	84
Table 13: Summary of inspection of reference slates.	86
Table 14: Summary of defect detection rates.....	88
Table 15: Inspection results for samples tested when full size slate was imaged.....	89
Table 16: Equipment recommendations for factory inspector.....	95
Table A.1: Paint fault detection results.....	A-2
Table A.2: Nozzle drip sample inspection results.....	A-3
Table A.3: Template mark defect detection results.....	A-5
Table A.4: Depression inspection results.....	A-6
Table A.5: Bad edge defect detection details.....	A-8
Table A.6: Miscellaneous defect type detection results.....	A-8
Table B.1: Equipment list.....	B-2
Table D.1: Relation of algorithm component to defect type.....	D-1
Table D.2: Algorithm component triggered by defect type.....	D-2
Table E-1: Defect naming abbreviations used in the report.....	E-1

Abstract

This thesis is concerned with the problem of how to detect visual defects on painted slates using an automated visual inspection system. The vision system that has been developed consists of two major components. The first component addresses issues such as the mechanical implementation and interfacing the inspection system with the optical and sensing equipment whereas the second component involves the development of an image processing algorithm able to identify the visual defects present on the slate surface.

The visual defects can be roughly classified into two distinct categories. In this way, substrate faults occur when the slate is not fully formed or has excess material whilst paint faults describe a slate of uneven colour or gloss level. A key element in successfully imaging the slate surface defects is the illumination set-up. After extensive testing, an effective collimated lighting topology was selected and is described in detail. Imaging the slate surface was challenging because it is dark coloured, glossy and has depth profile non-uniformities.

A four component image processing algorithm was designed to detect the range of defect types. The constituent components are global mean threshold, adaptive signal threshold, labelling, edge detection and labelling. Having proven a solution on the laboratory test bed, a prototype conveyor-based inspection system was assembled in order to replicate a factory-style environment. Robustness tests were performed on 400 slates and a 97% success rate was achieved. This thesis is concluded with a discussion on the feasibility of progressing this project to installation on an automated production line.

1. Introduction

The aim of this work is to develop an on-line sensor capable of measuring and classifying the quality of surface finish on painted slates produced in a conveyor style production line. The sensor needs to adapt to a wide variety of surface textures and colours. Each inspected slate will be classified as having a surface finish of acceptable or not acceptable quality. The classification results are intended for informing a reject mechanism when defective slates are found.

This section of the thesis begins with an overview of the industrial task and some motivating factors related to this research. A formal definition of the defects is provided. A generalised machine vision system is presented.

1.1 Background to the inspection task

Slates are used to cover roofs of buildings. While their primary function is to prevent water ingress to the building they also have a decorative function. The slates are manufactured using primary raw materials of cement, mineral and synthetic fibres. While generally flat in appearance, the fibre cement slate can have one of a number of surface textures. This surface profile remains visible after the painting process.

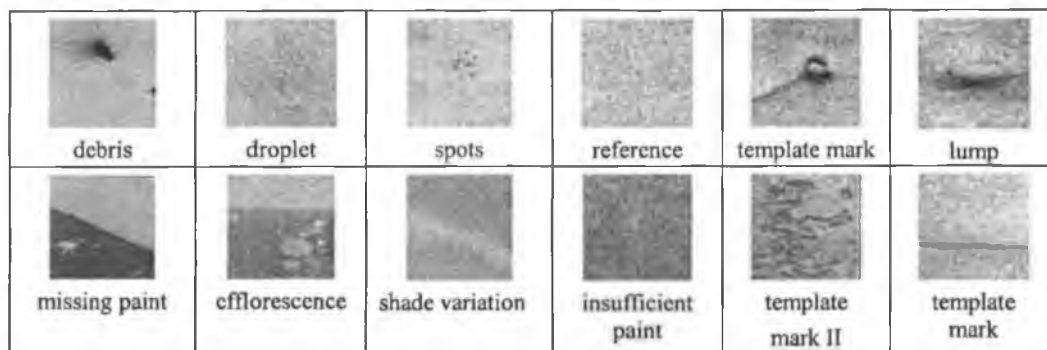


Figure 1: A selection of defects found on painted slates.

The formed slates are painted at high speed (approximately 40,000 slates per 8 hour shift). The painted slate is dried, inspected and stacked in a continuous mode production line. The slates arrive at the inspection station via a conveyor system. Visual inspection is carried out by operators and is at production line speed. Slates not meeting inspection criteria are put aside for rework or rejection.

There are two principal defect type categories: substrate and paint. Substrate faults include incomplete slate, lumps, depressions and template marks. Paint faults include no paint, insufficient paint, paint droplets, efflorescence, paint debris and orange peel. A listing is given in Table 1.

Table 1: Defect type and size definitions.

No.	Defect type	Defect size	Description
1	Lumps	$2.0 \text{ mm} < \{L, W, \phi\} < 50 \text{ mm}$ and $\pm 0.1 < D < \pm 3.5 \text{ mm}$	Excess material on surface. Often conical shape
2	Depressions	$2.0 \text{ mm} < \{L, W, \phi\} < 50 \text{ mm}$ and $\pm 0.1 < D < \pm 3.5 \text{ mm}$	Insufficient material on surface. Inverse conical shape
3	Holes	$\phi = 4.5 \text{ mm}$	Hole in slate to assist insertion of nails. Absence indicates fault (but not rejection of slate)
4	Incomplete slate	Any $W \neq W_{\text{expected}} \pm 3.0 \text{ mm}$ Any $L \neq L_{\text{expected}} \pm 3.0 \text{ mm}$	W, L dimensions not conforming to specification
5	Poor quality edge	$W = 0.2 \text{ mm} * L > 10 \text{ mm}$	Edge not straight or having a feathery feel
6	Template mark	$0.5 < \{L, W\} < 600 \text{ mm}$ $0.1 < \{D, H\} < 3.0 \text{ mm}$.	Excess material on surface (depressions also) caused by damage to forming template – any shape
7	Template mark II	$1.0 \text{ mm} < d < \text{all slate}$	Texture variation on surface, usually roughness
8	Insufficient paint	$20 \text{ mm} < \{W, L, \phi\} < \text{all slate}$	Shade variation due to insufficient paint usage
9	Missing paint	$2 \text{ mm} < \{W, L, \phi\} < \text{all slate}$	No paint or paint missing from portion of slate
10	Droplet	$2.0 \text{ mm} < \{W, L, \phi\} < 15 \text{ mm}$ and $0.05 \text{ mm} < D < 0.5 \text{ mm}$.	Excess paint on surface, dried and cracked
11	Efflorescence	$\phi > 5.0 \text{ mm}$	Contaminant on surface preventing correct adherence of paint
12	Paint debris	$2 \text{ mm} < \{W, L, \phi\} < 50 \text{ mm}$	Dried paint debris encrusted on slate surface giving rough texture
13	Orange peel	$20 \text{ mm} < \{W, L, \phi\} < \text{all slate}$	Shade variation caused by overheating slate
14	Barring	$W = 10 \pm 5 \text{ mm} \ \& \ 20 < L < 600 \text{ mm}$	Shade variation caused by uneven heating of slate
15	Spots	$1 \text{ mm} < \{W, L, \phi\} < 5 \text{ mm}$	Localised shade variation
16	Nozzle drip	$W = 10 \pm 5 \text{ mm} \ \& \ 20 < L < 600 \text{ mm}$	Shade variation caused by uneven paint delivery from nozzle

17	Wax mark	$5.0 < \{W, L, \emptyset\} < 50 \text{ mm}$	Splash of wax on top surface
----	----------	---	------------------------------

Inspection in the context of the slate paint line is the process of determining whether the product can be considered visually acceptable. The default condition is that the product is acceptable and is only classified as reject if the inspector can determine that at least one of the defects listed in Table 1 exists on the slate. This type of inspection is called visual inspection as it is based on pictorial information perceived from human sensation. Automated visual inspection is considered here to be visual inspection effected by means of a machine vision system.

An interesting aspect of the inspection process is that the acceptance or rejection of a slate surface quality is a function of the surface quality of other slates in the same batch. Slates containing gross faults will be rejected in all situations but a slate, *A*, with minor faults will be accepted if the tendency in that batch is for the majority of slates to contain minor faults. This is because uniformity is one of the factors which makes the slates appear aesthetically pleasing when viewed en-masse on a roof. The same slate, *A*, would be rejected if it appeared in a perfectly formed batch. An automated inspection system can mimic this inspection function using a sliding acceptance threshold or it can facilitate sorting of acceptable quality slates into batches of similar uniformity.

The inspection system in use at the industrial partner's factory is an in-line, manual system. The industrial partner states that the existing system is very discerning and does not generate false triggers. An automatic system must emulate this achievement.

1.2 Motivation for automating inspection

The principal uses of visual inspection are:

- To classify product for quality so that defective units may be rejected.
- To measure properties of the product with a view to controlling the production process.
- To gather statistics on production process efficiency for management purposes.

Tobias et al (1995) list some of the key factors that influence the adoption of machine vision systems in industry. These are increased productivity, improved product quality, absence of human inspectors performing dull and monotonous tasks, high-speed inspection (matched by high-speed production) and reduced human labour costs. Furthermore, advances in fields of sensors, processors, memory and hardware components facilitates the design of cost-effective machine vision systems that meet industries high-speed requirements for 100% inspection.

These issues were specifically addressed by Porter et al (1985) when they controversially postulated that the use of human labour for low level repetitive tasks has no economical or social justification while the development of these technologies require technicians, programmers, maintenance workers and operators, jobs that offer better work conditions and require higher skills. Thus, the incorporation of automation in manufacturing industry is not necessarily about the displacement of labour, but more as an answer to the expectation of an increasingly educated labour force and the compliance to the recent realities of the world economy (Ghita 2000).

The industrial partner stated that the benefits to them of installing an automated inspection system include:

- Estimated savings of Euro 35,000 per annum.
- Monitoring of rejects contributing to the aforementioned cost savings.
- A faster response to problems/potential problems.
- Statistical analysis of the detailed information provided by the inspection system should facilitate corrective/preventative action.
- Defense of existing sales by complimenting the complaint reduction program in place at the factory.
- Improvement to competitive position, in particular, by using the advanced technology as a marketing tool when publishing marketing/technical literature.

1.3 Principal components of a machine vision system

A commercial machine vision system is shown in Figure 2. This system is for inspecting continuous web products such as paper and plastic film.

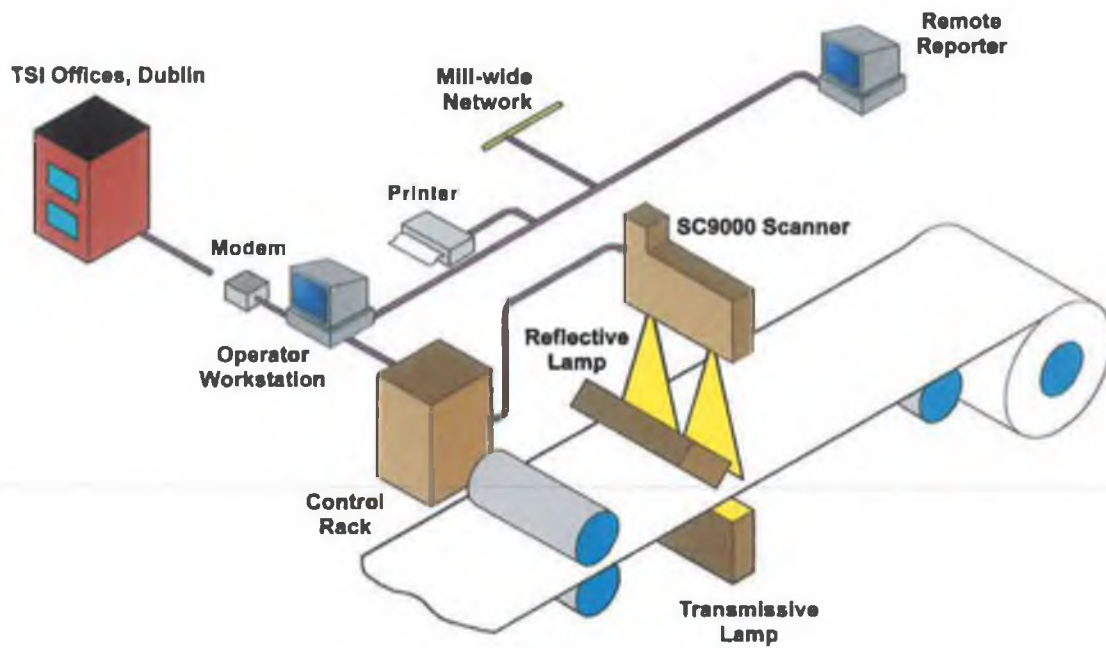
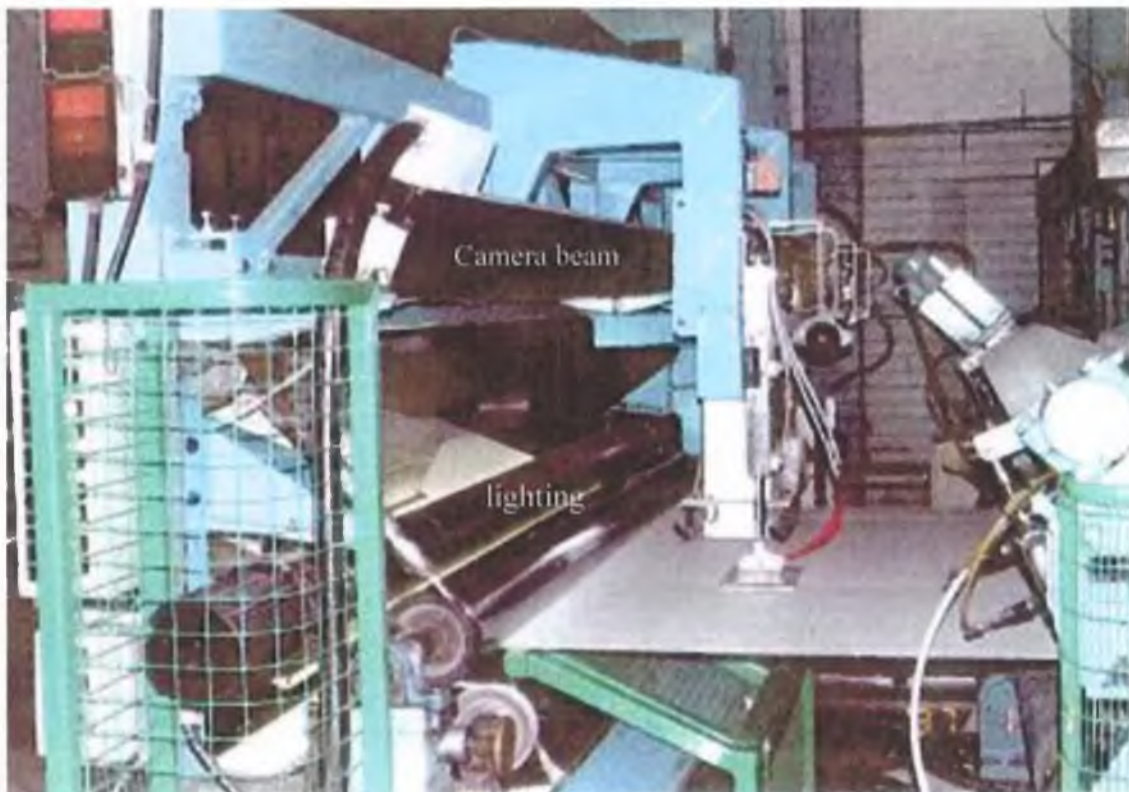


Figure 2: Block diagram of an industrial machine vision system, TSI (1998).



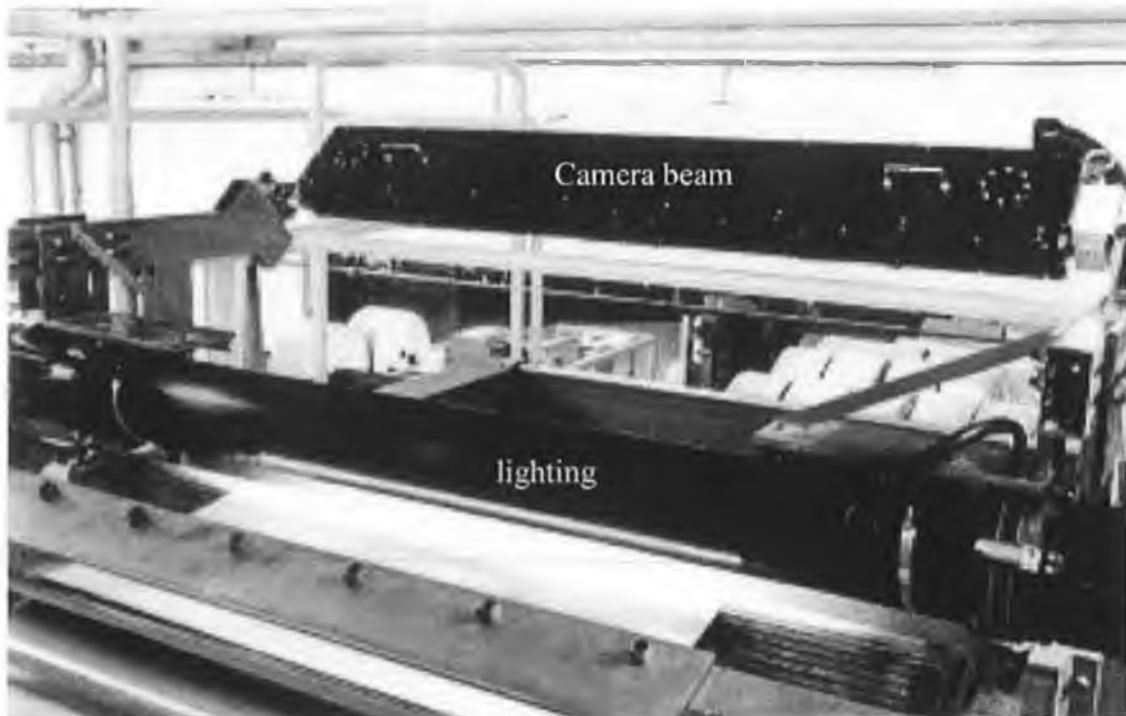


Figure 3: Factory view of installed machine vision systems, TSI (1997).

The principal physical components of a typical machine vision system are as follows:

Lighting	One or more lamps (with optical elements such as mirrors, lens, diffuser) to create appropriate lighting to highlight the defects.
Scanner	Single or multiple CCD camera arrays to capture images of the material and defects at appropriate resolution.
Control rack	For local control of cameras and lighting and for interfacing with the production line. Image processing and image analysis also take place in the control rack.
Operator workstation	For communication of inspection results to the line operator, compilation of statistics and for data entry by line operator, factory engineer and field service engineer.
Enclosures	Sensitive components must be protected from the factory environment in enclosures of appropriate standard. E.g., IP65 where moisture and dust are a danger and cabling needs correct shielding to prevent noise coupling from motors.

Non-essential components of the machine vision system shown in Figure 2 are:

Modem link to supplier	For remote system monitoring and remote field service. The modem link also facilitates download of upgrade software.
Remote reporter	Inspection reports are sent (usually via site network) to a remote workstation and can be viewed using the same user interface as that of the operator station. Production managers and site engineers often use this type of facility.

A detailed discussion of machine vision system design is beyond the scope of this review. Whelan (1997) gives a review of the system engineering issues in industrial inspection.

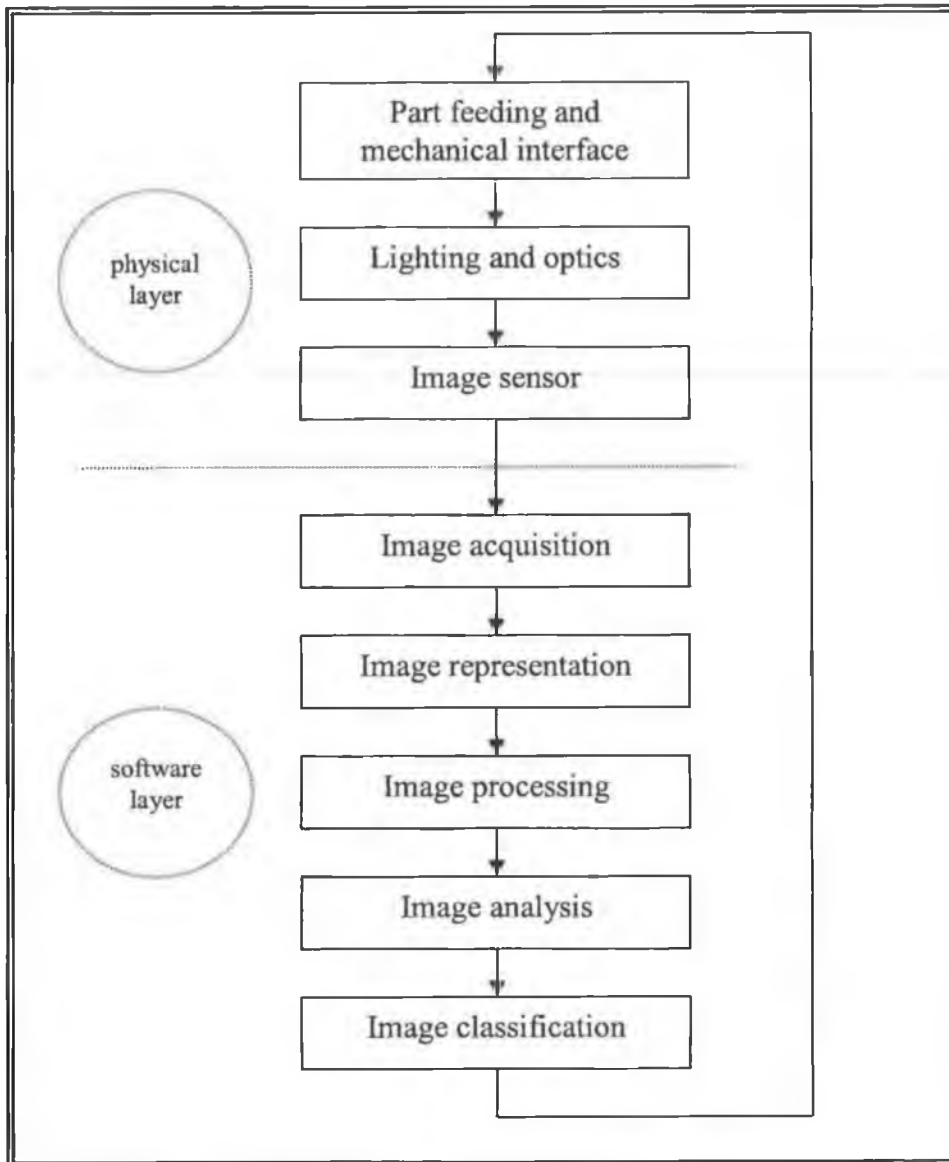


Figure 4: Flow chart of generalised machine vision system design.

1.4 Report outline

The prior research work into ceramic tile inspection and texture analysis is described in Chapter 2.

Chapter 3 begins with a description of the image capture test bed built for experimentation with lighting techniques and progresses to a description of the principal imaging methods tested, the problems encountered and the devised opto-mechanical solution. The prototype system built to replicate factory conditions is also described in this chapter. Its description is included here even though the image processing algorithm was developed prior to the design and procurement of the prototype system. This layout was chosen to keep opto-mechanical descriptions in the same chapter.

The image processing algorithm is described in Chapter 4.

The robustness testing of the image processing algorithm and the prototype inspection system is described in Chapter 5.

Chapter 6 concludes the report with discussion and suggestions on further work to progress the project to its possible installation on a production line.

2. Relevant Prior Research

A review of relevant work follows with particular focus on ceramics inspection and texture analysis. Image capture, image processing and image analysis techniques were sought that could be drawn upon while seeking a solution to the current inspection task.

2.1 Prior research on inspection of slates

No relevant prior work on inspection of slates was found during this review.

2.2 Prior research on inspection of ceramics

Many references to inspection of ceramics (tiles) were found in the literature. Though the production processes for slates and ceramic tiles are very different, the visual inspection process for ceramic tiles can be considered applicable to slates. Both products are rectangular in shape, have varying thickness, have textured surfaces and arrive at the inspection point via a conveying system. Both products exhibit the two principal defect type categories of substrate and paint (colour).

Boukouvalas et al (1995) list typical ceramic tile defects. Table 2 compares the ceramic tile defect list with defect types found at the slate manufacturers production site. The level of similarity is not immediately obvious from the defect type naming categories until one considers that the last seven defect types listed are shade or tone variations, so that they can be considered to be a subset of colour variations. Template mark and template mark II are substrate faults; template marks can be viewed as a type of lump and template mark II as a texture variation. All researchers reviewed for this report treat substrate and colour defect types separately. Distinct imaging processing, image analysis and lighting techniques are employed.

Tiles have a much broader range of surface finishes than slates. Whereas slates are of single colour and have a relatively uniform surface¹ finish, tiles can be plain, two colour, multi-coloured and heavily textured. This may lead one to assume that the

¹ Relief slates are the exception having a heavily textured surface.

task of inspecting slates may be simpler than that of tiles. As a cautionary note, the defects associated with slates may not be as obvious to a machine vision system as those exhibited by tiles. The true situation will become clearer during sample testing.

Table 2: Ceramic tile and slate defect category comparison.

Defect type	Defect size for tiles	Defect size for slates
Bumps (lumps)	0.3 mm < d < 5 mm	1.0 mm < d < 50 mm
Depressions	$\phi < 5.0$ mm	$\phi > 2.0$ mm
Cracks	0.3 mm < d < 5 mm	n/a
Holes	$\phi > 0.25$ mm	$\phi = 4.5$ mm
Incomplete slate	n/a	Any $W^2 \neq W_{\text{expected}} \pm 3.0$ mm Any $L \neq L_{\text{expected}} \pm 3.0$ mm
Poor quality edge	n/a	$W = 0.2$ mm * $L > 10$ mm
Template mark	n/a	1.0 mm < d < all slate
Template mark II	n/a	1.0 mm < d < all slate
Dirt	0.3 mm < d < 5 mm	n/a
Drops	0.3 mm < d < 3 mm	n/a
Water drops	5 mm < d < 50 mm	n/a
Undulations	5 mm < d < 50 mm	n/a
Texture	0.3 mm < d < 50 mm	n/a
Colour	0.3 mm < d < 50 mm	n/a
Insufficient paint	n/a	$\phi > 10.0$ mm
Missing paint	n/a	$\phi > 2.0$ mm
Droplet	n/a	$\phi > 2.0$ mm
Efflorescence	n/a	$\phi > 5.0$ mm
Paint debris	n/a	$\phi > 1.0$ mm
Orange peel	n/a	$\phi > 10.0$ mm
Barring	n/a	$W > 2$ mm * $L > 10$ mm

Two commercial companies, Surface Inspection Ltd (UK) and Massen GmbH (Germany), offer in-line ceramic tile inspection systems. These systems inspect for both substrate and colour faults. Inspection throughput³ is one sixth of the rate required for slates. Integral precision conveyor and centraliser are features of these products.

² W = width, L = length.

³ For product area inspected. A direct comparison is difficult due to differing fault categories.

2.2.1 Illumination and image capture

The minimisation of spatial and temporal illumination variations is reported as being crucial to successful defect detection. Good results are reported by Boukouvalas et al (1994) when variations are less than 2%. Boukouvalas et al (1997) report that replicating human eye capability involves resolving grey scale data to less than one grey scale pixel level⁴. In experiments on the response of human eye, Hubel (1988) found that our eyes begin to respond to regions having intensity variations greater than 2% relative to the background intensity levels. The absolute intensity levels⁵ are of little relevance to a human observer since eyes do not respond to absolute values of light intensity⁶.

Spatial corrections of illumination variations are effected by curve fitting or by pixel level multiplications with factors determined using a calibration pattern, Boukouvalas et al (1997, 1999). Line scan cameras are invariably used (though area scan cameras were used in early tests by Boukouvalas et al (1997)) in an effort to reduce spatial illumination non-uniformities. It is easier to control the intensity uniformity of a long, narrow strip of light than that of an area large in two dimensions. Temporal variations were corrected by placing a reference surface in the field of view of the imaging system and correcting for variations using multiplication. Ideally, one would want to replicate the human eye invariance to grey scale illumination variations; no techniques to achieve this are reported in work concerning ceramics inspection.

All researchers of ceramics inspection reviewed here used different imaging sub-systems and processing techniques to detect substrate and paint fault types. Boukouvalas et al (1999) image substrate defects such as lumps and depressions using collimated lighting with fluorescent lamps as light source. Their imaging system

⁴ For colour comparisons.

⁵ Absolute intensity level is the radiant intensity. Radiant intensity is defined as the radiant flux per unit solid angle radiated in a given direction from a point source and is measured in units of watts per steradian (Pinson, 1985).

⁶ For example, a newspaper looks roughly the same, black letters on white paper, whether it is viewed in a dimly lit room or outdoors on a sunny day. The radiant intensity from the white paper is twenty times higher in the outdoor situation relative to the indoor situation (Hubel, 1988). Most image sensors respond directly to absolute intensity levels and the sensor calibrated to work efficiently indoors would need to be recalibrated to work outdoors.

relies on specular reflections whereby the lighting and camera angles relative to the surface being imaged are equal. Light incident on the tile at angle, θ , will be reflected from the tile and into the camera at the same angle, θ , when the surface quality is acceptable and will be reflected at a different angle, $\theta \pm \delta$ ⁷, when a substrate defect is encountered. An absence of light arriving at the camera signifies the possible presence of a defect. The same researchers also experimented with dark field detection⁸, whereby the camera is located where light from an acceptable surface will not reach it and light from defects will arrive at the camera and signal a defect. This lighting method may have been used to image glossy, light coloured tiles as the intensity of reflected light might have bloomed⁹ the camera. Marik et al (1995) reject grazing incidence in favour of illumination at 23° claiming this angle of illumination leads to better quantification of the faults.

Boukouvalas et al (1997) create a further imaging and processing sub-system to image substrate defects of type crack and hole using diffuse lighting with halogen lamps as source. The tile is indirectly illuminated and a reflecting baffle is used to create diffuse illumination.

Colour shade comparison is the subject of several papers. Diffuse lighting methods are usually employed and often with colour cameras. Peñaranda et al (1997) use a fibre optic light guide placed directly above the tile to create a linear strip of light from halogen light sources. The light guide appears to be located 90° to the tile and the camera view angle is not specified. Boukouvalas et al (1997) locate the camera directly above the tile and use the same diffuse lighting technique as they used for detecting cracks and holes.

Boukouvalas et al (1997, 1999) are circumspect about resolution used and it is inferred from the assumption that they are inspecting 200 x 200 mm square tiles and they use a 1,024 pixel CCD sensor for substrate faults, a 3,100 pixel CCD sensor for crack and hole faults and an 8,640 pixel CCD sensor for colour faults. This gives

⁷ δ is determined by the geometry of the structural fault.

⁸ Identifying exact location of product edge may be a difficulty with this method.

⁹ Blooming is the term used to describe an effect whereby an image sensor is 'dazzled' by incoming light intensity and cannot respond with a reliable signal.

CD¹⁰ resolutions of 0.2, 0.07 and 0.025 mm respectively. Even if the system had been designed to cater for 600 mm wide tiles (largest tile size available) the CD resolutions would be 0.6, 0.2 and 0.07 mm respectively. Peñaranda et al (1997) use a CD and MD resolution of 0.5 mm.

Most researchers into ceramic tile inspection used 8-bit digitisation with the exception of Peñaranda et al (1997) who opted for 12-bit digitisation. Kauppinen (2000) uses an optical arrangement similar to that used by Peñaranda et al (1997) to image parquet slabs, placing the camera at 0° to the product and the fibre optic light guide ~20° to the product. 12-bit digitisation of the colour line scan camera output is used by Kauppinen where data is used for colour grading and defect detection.

Kälviäinen et al (1998) compare colour classification using RGB camera and spectral camera and produce comparable results with each method for the grading of brown tiles. Neural net comparison methods are applied by these researchers to classify the tiles. They made no correction for spatial variation in illumination thereby contributing to a high number of miss-classifications.

2.2.2 Image analysis algorithms

2.2.2.1 Edge faults

Poor quality edge and incomplete slates are not listed as fault types found on tiles. Some work on edge location and on region of interest extension to accommodate local operator techniques is reported. Boukouvalas et al (1999) extend the image at the edges by mirroring so that the same fault detection techniques used in the inner zone can be extended to the edges.¹¹ Peñaranda et al (1997) segment the tile image from the background without using computationally expensive rotation. They assume the tiles have good edges and use a morphological operator to locate the corners. The angle of rotation of the tile with respect to the camera view line can be estimated from knowledge of corner locations. The image data is in digital format and a straight line between the tile corners is approximated using short line lengths and shifting from

¹⁰ CD = Cross Direction. MD = Moving Direction (of tile).

row to row in the image in *staircase* fashion. The number of steps and the length of each line in the *staircase* are determined from the rotation angle calculated from the corner locations and the tile dimensions. In this way, the region of interest (tile) is extracted from the background.

2.2.2.2 Substrate faults

For uniformly coloured tiles, Boukouvalas et al (1999) use 2 x 1-D convolvers (one horizontal and one vertical) to detect the possibility of defects and a version of template matching (expected signal in case whereby a defect exists) to verify defect existence. Spot defects on light-coloured plain tiles are detected using a single 1-D convolver, optimised for spot detection. This function is followed by a threshold operation.

Petrou (1993) reports that optimal filter coefficients used in the convolvers can detect features with widths within a factor of 1.5 of the feature for which the filter is optimised. Features of defects on slates do not follow any pattern for size and shape and will most likely be a limiting factor in the usefulness of this technique to slate inspection.

Morphological operations are used by Boukouvalas et al (1997) to identify thin structures such as crack defects. Performance was reported as being similar to that achieved by human operators in the case of uniformly coloured tiles. The method is reported to be ineffective for some kinds of textured tiles. More complicated techniques based on Wigner distributions¹² are employed when multi-coloured and heavily textured surfaces are being inspected - excellent results have been reported using these techniques. A co-joint spatial and spatial frequency representation of the Wigner distribution is used to maximise the detection of signatures of regular patterns. This method is more applicable to multi-coloured and heavily textured

¹¹ Necessary for local neighbourhood operators such as convolvers but not for statistical techniques.

¹² The Wigner distribution is represented by the attributes computed for each pixel that encapsulates both the local spectral and phase properties of the local Fourier transform. The Wigner distribution is computed within a 7 x 7 square window in the referenced implementation (Kittler et al, 1994).

surfaces and may be useful if relief slates are considered. A significant disadvantage of the Wigner approach is the onerous¹³ computational demand.

Morphological methods have been successfully applied to detection of defects on ceramics. Müller and Nickolay (1994) explain how to apply morphological techniques to detect cracks and sink holes in heavily textured tiles. Selection of appropriate structuring elements may prove difficult for slates due to the range of defect sizes. A distinct advantage of morphological techniques is that they are suitable for real time operation.

2.2.2.3 Paint faults

A simple average of grey level intensity values is used by Boukouvalas et al (1995) to grade plain tiles and they use the average of grey level intensity values of each colour band in the case of two colour tiles. This method seems to work well when temporal and spatial illumination variations are carefully measured and factored into calculations. The same researchers proposed a variation to this method for randomly textured tiles by comparing the histogram distributions of a reference and sample tile using statistical comparison methods such as Chi-square, Correlation Coefficient and L_1 norm. In order to be able to compensate for the illumination changes with respect to time, the reference tile has to be permanently imaged. This approach has some drawbacks including the requirement to use some of the CCD imaging area to image the reference tile and there is no assurance that the surface characteristics of the reference tile will not be affected by the industrial environment (dust, accidental positional shift, surface scratch, etc).

Fioravanti et al (1995) propose sub-dividing the image into square blocks and classifying each block separately on the basis of its rank functions. A morphological filter defined as a close less open¹⁴ operator is applied to the image. An anomaly presence degree measurement (APD) is computed for square blocks of dimension 40 x 40 pixels of the filter image and this measurement is compared to that of a standard. The APD is null when the measurements are equal and increases in proportion to the

¹³ Processing time is 200~250 seconds on a 256 x 256 image using a SUN-SPARC 2.

disparity between the standard and the tile under test. A square block is classified as defective when an APD threshold is exceeded. Boukouvalas et al (1997) chose to use rank functions over histogram distribution comparison as they felt it gave more detailed information about the type and spatial location of the fault.

An approach, based on K-means clustering, is used by Boukouvalas et al (1997) for multi-colour tiles to segregate the tile into its chromatic classes. The number of clusters is initially chosen to be high to minimise under-segregation. These small clusters are transformed into CIE-Luv colour space and the small clusters are merged into super-clusters using perceptual merging into chromatic classes that are perceptually uniform. The image is then split into a stack of binary images, one for each chromatic category. The structural features area, perimeter fractality and elongatedness are calculated for each blob in each binary image. Standard measurements are computed in a training phase. Any unclassified pixels found during inspection are labelled as colour defects. The structural integrity of each colour blob is checked using the calculated structural features. This method is unlikely to be used in this application, as slates are uniform and of single colour.

Peñaranda et al (1997) and Finney et al (1994) compute the grey level intensity histograms, extract the peaks and calculate the mean and standard deviation for each peak. A variety of measures of similarity are proposed including neural net methodologies by Finney et al (1994). Among the measures proposed by Boukouvalas et al (1995), the correlation coefficient appears to be optimum as it has a bounded range allowing for *a priori* selection of thresholds. Finney et al (1994) advise histogram smoothing to facilitate peak extraction. The first order statistical methods are grey level dependent and close control of illumination level is crucial to successful implementation using these methods.

Most researchers into ceramic tile inspection use an industrial CCD camera connected to a frame grabber card installed in a standard PC whereas Boukouvalas et al (1997) built a system based on the VME Bus.

¹⁴ $CIO(I) = Close(I) - Open(I) = Erosion(Dilation(I)) - Dilation(Erosion(I))$ where I is the image.

2.3 Prior research on texture

One approach to describing a slate is to quantify it by its texture content. The texture of an acceptable quality slate will be known *a priori* (from a training and calibration stage) and any significant deviation from this standard texture can be considered as a defect. A considerable research effort has been expended on texture analysis and some of the techniques developed should be relevant for this application.

Although no formal description of texture exists, one intuitively views this descriptor as providing a measure of properties such as smoothness, roughness, coarseness, contrast, orientation of local features, etc. A slate having a substrate fault no longer has a smooth surface (relative to that of an acceptable slate) and slates having paint faults will have regions of differing contrast.

The three principal approaches used in image processing to describe the texture of a region are statistical, structural, and spectral (Haralick et al 1979). Statistical approaches yield characterisations of textures as smooth, coarse, grainy and so on. These descriptors are exactly the sort used to quantify slates and grade them as acceptable or reject. Structural techniques deal with the arrangement of image primitives, such as a description of texture based on regularly spaced parallel lines and are not applicable to this application. Spectral techniques are based on properties of the Fourier spectrum and are used primarily to detect global periodicity in an image by identifying high-energy, narrow peaks in the spectrum and are not applicable to this application.

One of the simplest approaches for comparing reference and test images is to use moments of the grey level histogram¹⁵ of an image or region. A feature vector is subsequently computed from the histogram. This feature vector is finally compared with that of a known good reference and is classified as a defect if the difference between the reference and the test is greater than a pre-determined threshold. Peñaranda et al (1997) use the first and second moments of the grey level intensity histogram in their work and combine these moments to create the feature vector.

¹⁵ The histogram is not encapsulating the grey level spatial distribution of the pixels within the image section (Julesz, 1965).

Measures of texture computed using only grey level intensity histograms suffer from the limitation that they carry no information regarding the relative positions of pixels with respect to each other¹⁶ (Boukouvalas et al 1997). This limitation can be overcome to a certain extent by performing a vertical and horizontal projection of the image and searching for peaks and valleys in the projections, Whelan et al (1999). A further useful technique is to consider the slate as an agglomeration of sub-regions and compute intensity histograms for each sub-region. The spatial location of the fault would then be localised to the sub-region.

Haralick et al (1973) were the first to use grey-tone spatial-dependent matrices to characterise image texture. Also called the co-occurrence approach, the efficacy of this method in distinguishing different textures is well reported, Weszka et al (1976). It does not provide information concerning the spatial location of defects and is computationally inefficient.

Unser (1986) noted that difference statistics, a subset of the co-occurrence matrix can yield similar information with considerably less computational effort. Tobias et al (1995) experimentally evaluated Unser's findings regarding difference statistics to detect defects on ceramics. They reported good results for gross defects in a laboratory environment. In this approach, the co-occurrence matrix is not computed; the grey level differences are computed for fixed separation of 1 or 2 pixels.

Ojala et al (1996) compare feature histogram distributions of standard and defective images and create the histograms from the grey level differences between neighbouring pixels or from local binary patterns (LBP). They have tested their methods on a variety of surfaces including painted surface and sheet metal. Reported results are good, especially when combinations of features are selected for input to the similarity measurement block. These methods have the attractive feature of being computationally efficient and LBP has a further advantage of being grey scale invariant, thereby reducing the influence of illumination variations.

¹⁶ This restriction is not necessarily a limiting factor for slate inspection as the industrial partner is primarily interested in an ACCEPT/REJECT response from the inspector without regard to the type and location of the defect.

Tamura et al (1987) investigated which features of texture best correspond to visual perception. The best measures were found to be coarseness, contrast, line-likeness and directionality. Their definition of contrast gave good results and is likely to be useful for detection of paint faults.

$$\text{Contrast, } F_{con} = \frac{\sigma}{(\alpha_4)^n} \quad (1)$$

where, σ is the standard deviation of the grey level intensity histogram

$$\alpha_4 = \frac{\mu_4}{\sigma^4}$$

μ_4 is kurtosis of the grey level intensity histogram.

n is a positive number and was set at $\frac{1}{4}$ following experimentation.

2.4 Usefulness of prior work to slate inspection

It would appear that automated inspection of painted slates is a realistic and achievable target, when one considers the reported successes with tiles. Some of the image capture and image processing and analysis techniques have been identified as having been successfully applied to the similar applications in ceramic inspection.

The principal findings concerning image capture are that substrate and paint fault types are best inspected using different imaging sub-systems. The imaging system should control the conveyor to ensure good image capture and every effort should be made to obtain spatially and temporally uniform illumination.

The principal findings concerning image processing and analysis are that convolution and morphological methods would appear most appropriate for detection of substrate defect types. Statistical texture analysis methods based on intensity, grey level differences or local binary pattern histograms are likely to be appropriate for detection of paint defect types. These approaches will be tested in the subsequent project stages.

3. Image Capture

3.1 Introduction

This section of the report is focussed on laboratory investigations into the identification of image capture techniques that can be used to detect the visual defects on slates. There were three key challenges to be overcome to develop a solution.

Getting a sufficiently strong signal level from the slate was the first challenge. It further transpired that the slate surface profile is often deformed by concavity or convexity. The tests became a balancing act between making the system sensitive enough to discern the defects while being simultaneously insensitive to the acceptable thickness and profile variations. The third principal challenge was to generate a strong signal to noise ratio for each defect type so that a computationally inexpensive processing method becomes viable. The continuous stream of video data will need to be processed in real time and weak signals requiring computationally expensive algorithms would make the task more difficult.

Prior work investigations indicate that every effort should be made to eliminate non-uniformities in the image capture arrangement and that this can best be achieved using a combination of line scan cameras and a uniform band of light across the product. Researchers into ceramic tile inspection have used specular reflection light field method, specular reflection dark field method and diffuse lighting techniques. These three methods were investigated.

The industrial partner supplied 100 slates for use in these initial tests. Most slates contained one or more defect types. A good range of defect types were contained within the samples. 10 slates contained no defects and were used as references.

3.2 Description of the slate and paint process line

The slate is a fibrous cement product of rectangular shape. The primary usage is as a roofing material. While a number of slate sizes, surface profiles and colours are produced, the subject of this research is focussed on a single size slate whose

dimensions are given in Table 3. Some slates have three circular nail holes of diameter 4.5 mm located 15 mm from front, end and left edges. The slate can be coloured jet black or dark grey and has a high gloss surface finish. One of a range of black pantone colours is used in any single production run. The painted surface is nominally flat.

A description of the paint line process is as follows: slates manufactured 14 days previously in large slabs are loaded onto the conveyor system and separated into individual slates. They are pre-heated, spray-painted, post-heated and dried prior to arrival at the inspection point. After inspection the slates are stacked and wrapped. The inspection is the only manual operation on this highly automated process.

Table 3: Slate properties.

Dimension	Nominal	Tolerance
Length	600 mm	±3 mm
Width	300 mm	±3 mm
Thickness ¹⁷	4.0 mm	±0.1 mm
Local flatness profile	±0.1 mm	±0.1 mm
Concavity	±0.05 mm	±5 mm
Convexity	±0.05 mm	±5 mm

3.3 Principle of operation

The basic material properties of importance in considering the interaction of light with the slate surface are emissivity, reflectance, absorptance and transmittance. Radiant energy (from a light source) incident upon the slate may be absorbed or reflected¹⁸. Materials generally absorb and emit radiation at the same rate. The emitted radiation from the slate surface is too low to be of practical interest. Therefore, reflectance is the radiometric property of importance.

Irradiance is defined as the radiant flux density incident upon a surface and has units of watts per square meter. Radiance is radiant flux in a given direction from a surface that is normalised with respect to both surface area and unit solid angle. For viewing

¹⁷ Thickness for an entire production run will not vary but the thickness for a particular production run can be within the range $3.7 < t < 4.4$ mm. Most slates are produced to meet the 4.0 mm specification.

¹⁸ The slate is opaque and radiant energy will not be transmitted through the material.

angles normal to the surface, units are watts per square meter per steradian. Consideration must be made for the fact that the apparent surface area decreases in direct relation with $\cos \theta$, where θ is the reflectance angle. Reflected light can take the form of diffuse reflection, specular reflection or a combination of both types of reflection.

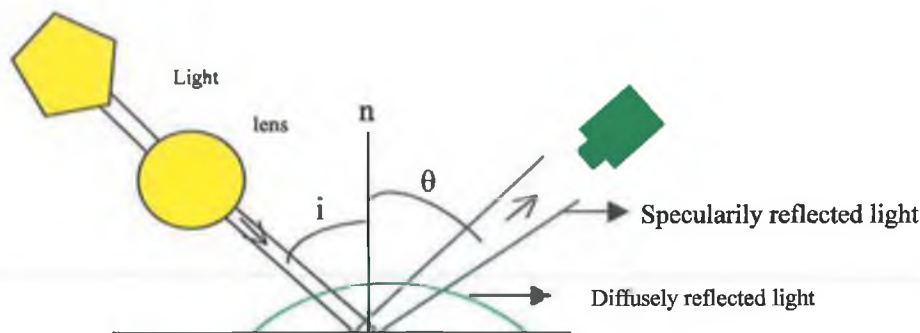


Figure 5: Model of reflectance for slate surface.

Planar surfaces for which the radiant intensity varies with the cosine of the angle between the viewing direction and the surface normal are called Lambertian (or diffuse) surfaces. If I_n is the radiant intensity normal to the surface, then the radiant intensity at angle θ , I_θ , is given by

$$I_\theta = I_n \cos \theta \quad - \text{ Lambert's cosine law} \quad (3-1)$$

The effect of Lambert's cosine law on radiance from a surface is to make the radiance (from a Lambertian surface) independent of the viewing angle. Radiance in the viewing angle θ is defined in Equation 3-2

$$L_\theta = \frac{\delta I}{\delta A} = \frac{I_\theta}{dS} = \frac{I_n \cos \theta}{dA \cos \theta} = L \quad (3-2)$$

Object reflectances are not all Lambertian and can have a component of specular reflection whereby a larger percentage of incident light is reflected at an angle of reflection equal to the angle of incidence. The percentage of light reflected specularly depends on the degree of specularity of the surface. A good approximation of the slate surface is obtained by modelling it as being Lambertian with a strong additional reflectance near the specular reflectance angle (Davies,

1997). This model can be represented by the following equation where the first term represents the diffuse reflection and the second term represents the specular reflection.

$$R = R_0 \cos i + R_1 \cos^m \theta \quad (3-3)$$

where

R = surface reflectance,

R_0 = Lambertian reflectance at the normal position,

R_1 = specular reflectance at the specular reflectance position with
typical values in range 10% ~ 80%,

m is in the range 1 ~ 10,

θ = angle between actual emergence direction and the ideal specular
reflection direction.

Experimental data suggests up to 80% of light is reflected specularly and approximately 20% is reflected diffusely from slate surfaces¹⁹. Knowledge of these physical properties was utilized to devise the following imaging strategy.

The strategy used to get sufficiently strong light intensity at the sensor relies on using the strong reflecting properties of the glossy surface. Light incident on the slate will be reflected with angle of incidence equal to angle of reflection. A collimated light source will help maximise efficiency. The slate surface profile is specified as being uniform to ± 0.1 mm. A smooth transport mechanism that maintains slate aspect with respect to light source and sensor should be sufficient to make this method work.

Defect detection method for paint and substrate fault types will be similar. Paint faults have reduced gloss levels and there will be a reduction in light levels arriving at the sensor. Substrate faults will direct light away from the sensor on their rising and falling edges and should be detectable due to the reduced signal level. A smooth transport mechanism should enable detection of both paint and substrate faults with a single lighting arrangement. An alternative approach for detecting paint faults is to use the cloudy day illumination technique and flood the slate with diffuse light.

¹⁹ There are many unknown parameters that hinder an accurate evaluation between the level of specular and diffuse light arriving at the camera. These parameters include variation in gloss levels, depth profile variations and uneven illumination.

3.4 Test bed description.

A Basler Model L102 line scan CCD camera was used as the sensing device and the video data was captured and transferred to computer hard drive using a Euresys model Multi frame grabber card. The slate was illuminated using a fibre optic light guide illuminated by a 150W halogen bulb driven by a DC regulated lamp controller. No light intensity feedback sensor was used. An aperture lens was placed in front of the fibre light guide. This arrangement creates a highly collimated source.

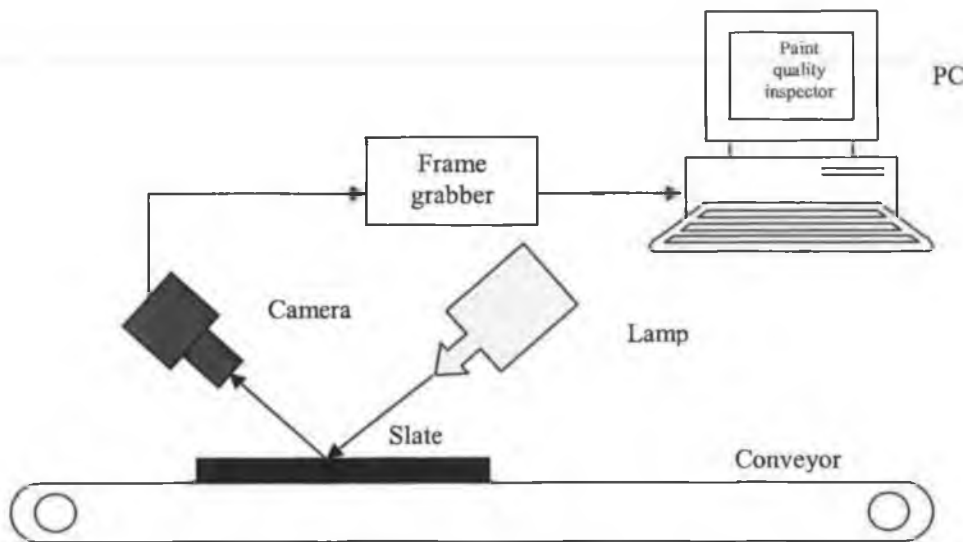


Figure 6: Test bed arrangement.

The camera was fixed in position 700 mm distance from the slate and the lighting was separated from the slate by a distance of 84 mm. An f28 mm lens was used with aperture set to 2.8. A micro-positioner was attached to the camera to facilitate fine adjustment of the camera view line.

A guide for slate conveyance was made from Bosch extrusions. The slate was inserted between slots in the extrusion and this ensures the slate travels smoothly in the x and y -axes. There is scope for 5 mm movement in the z -axis. Slate weight will keep it on the lower edge of the slot and there should not be any z -axis movement. Slates were pulled by hand along the extrusions.

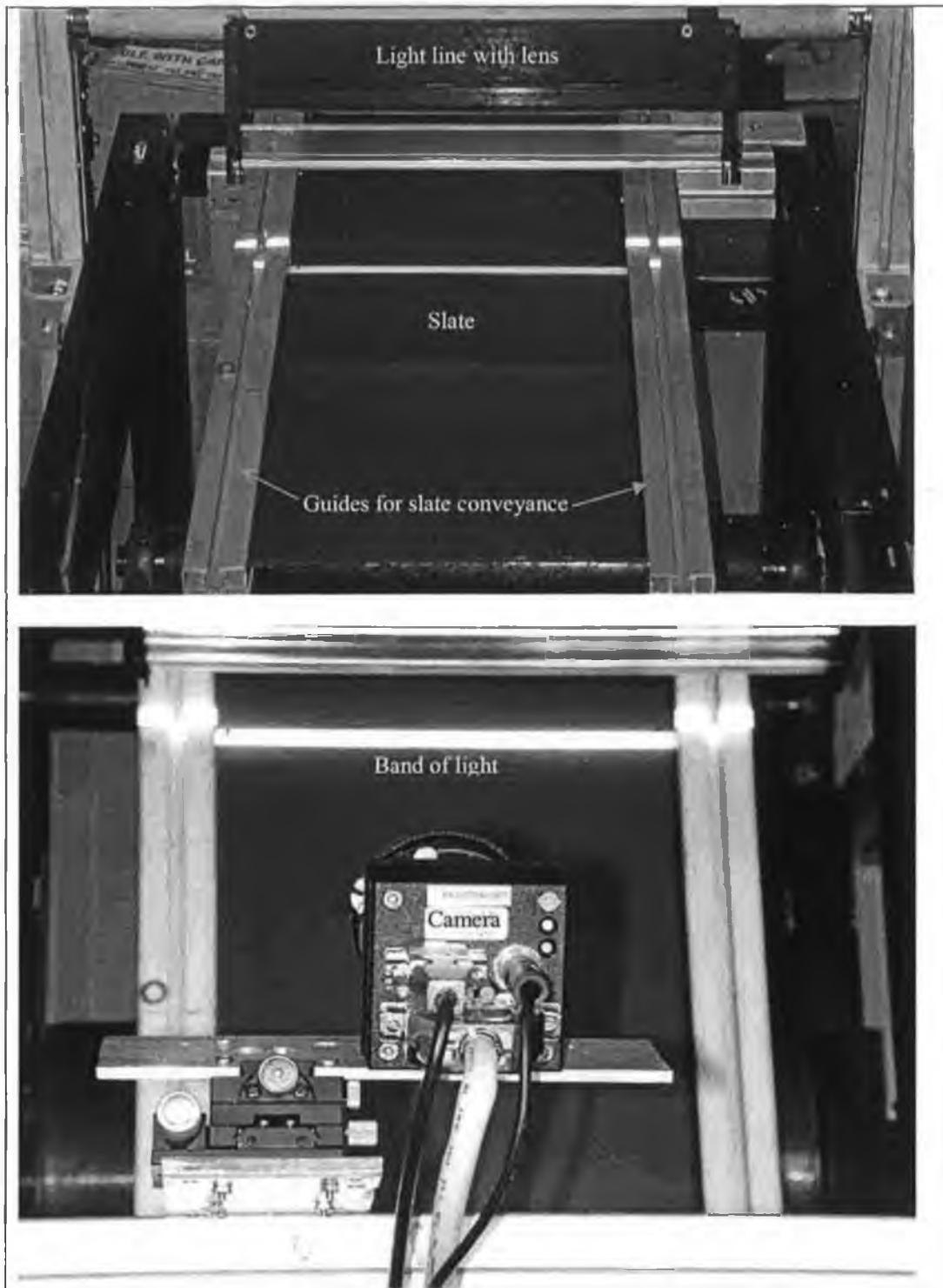


Figure 7: Test bed showing slate, fibre line light and camera

Camera control and frame capture was implemented using the Euresys software environment. The slates were moved past the inspection point at relatively constant speed and frames of width 2,000 pixels and length 600 lines were captured and transferred to computer memory. Regions of interest were extracted from these

frames and filed for analysis. The Neatvision (2000) image analysis software and MS Excel spreadsheet packages were used to implement off-line analysis.

3.5 Tests using collimated lighting

A halogen source was input to a fibre light guide to create a highly collimated and intense band of light across the slate. The focussed band of light is only 5 mm wide. Aligning the sensor with this band of light turned out to be a very difficult task. The mechanical rigidity of the supporting frames and slate transport mechanisms established themselves as major sources of signal capture errors. The solution was to source rigid brackets and to strengthen the mounting frame and transport mechanism.

Focussing the sensor on a 5 mm wide band of light from a distance of 700 mm involves an adjustment arc of less than one half of one degree. Micro-adjustors were used to facilitate fine adjustment. By the time all of these items had been procured many of the sample slates exhibited a curved depth profile variation. The depth profile followed no pattern and took the form of concavity in some samples and convexity in others and ranged from negligible to 5 mm over the slate length and up to 2 mm along the slate width. This impacted severely on image capture capability.

Initial feedback from the industrial partner was to the effect that the depth profile variations were caused by either uneven drying in the warm laboratory conditions or inappropriate stacking conditions. Fresh samples were made available and it was noted that some of these also had curved depth profiles. It transpired that the usability of slates is not affected by curved depth profiles of up to 5 mm so that the industrial partner was correct from his perspective in saying that the slate was flat. From a machine vision perspective a whole new level of complexity had been introduced.

The curved depth profile raises and lowers the absolute position of the band of light and the view position of the camera. When the slate position is elevated the band of light shifts to the left while the sensor view position shifts to the right. With incidence and reflectance angles of 45° , if the slate position rises 1 mm the band of light and camera view point move 1.25 mm in opposite directions. The higher the angle of incidence, the smaller the shift in location of the band of light. However, the

lower the angle of incidence the wider the band of light so that the overall effect of altering the angle of incidence is cancelled.

The curved depth profile also changes the angles of incidence and reflectance. A change in the slate aspect alters the angle of incidence by α , and the angle of reflectance by 2α . A concavity of 0.3 mm will cause an aspect change of 0.43° and will shift a collimated reflected beam by 4 mm when viewing the slate from 700 mm at an angle of 50° .

The most obvious solution is to devise a method to force the slate into a uniform flat shape during inspection. The slate does have some elasticity and it is probably feasible from a mechanical perspective. The slate top surface is easily damaged so a method that operates in contact with the underside of the slate would be preferred. Design of this sort of mechanical handling equipment is beyond the scope of this project. Discussion with the industrial partner clarified that any mechanical means of dealing with the depth profile was unlikely to be successful and equally unlikely to be implemented on the production line.

An alternative approach is to defocus the lens on the fibre light guide. This produces a wider band of light and reduces the collimation. The intensity is reduced in proportion with the amount of defocus. A more intense source was used to compensate for the intensity reduction. Tests were repeated with the lens defocused to its maximum to produce a light band of width 13 mm. Though the effects of the depth profiles are still evident, useful results were obtained. Light intensity was sufficient and even the smallest defects could be imaged.

The lamp angle of incidence was set up at 46° and the camera view angle was located as close as possible to 46° relative to the slate. The exposure setting was 1 millisecond and the grey scale mean values were 160 grey levels for Supercem samples at lamp intensity setting of 77%. The cross direction pixel resolution was 0.21 mm and the moving direction pixel resolution was 0.44 mm. Light levels are 6 times lower than required for production line speeds. There is sufficient spare capacity in the lamp controller to provide a more intense light band but doing so will reduce bulb lifetime to approximately 300 hours.

3.5.1 Profile of reference slates

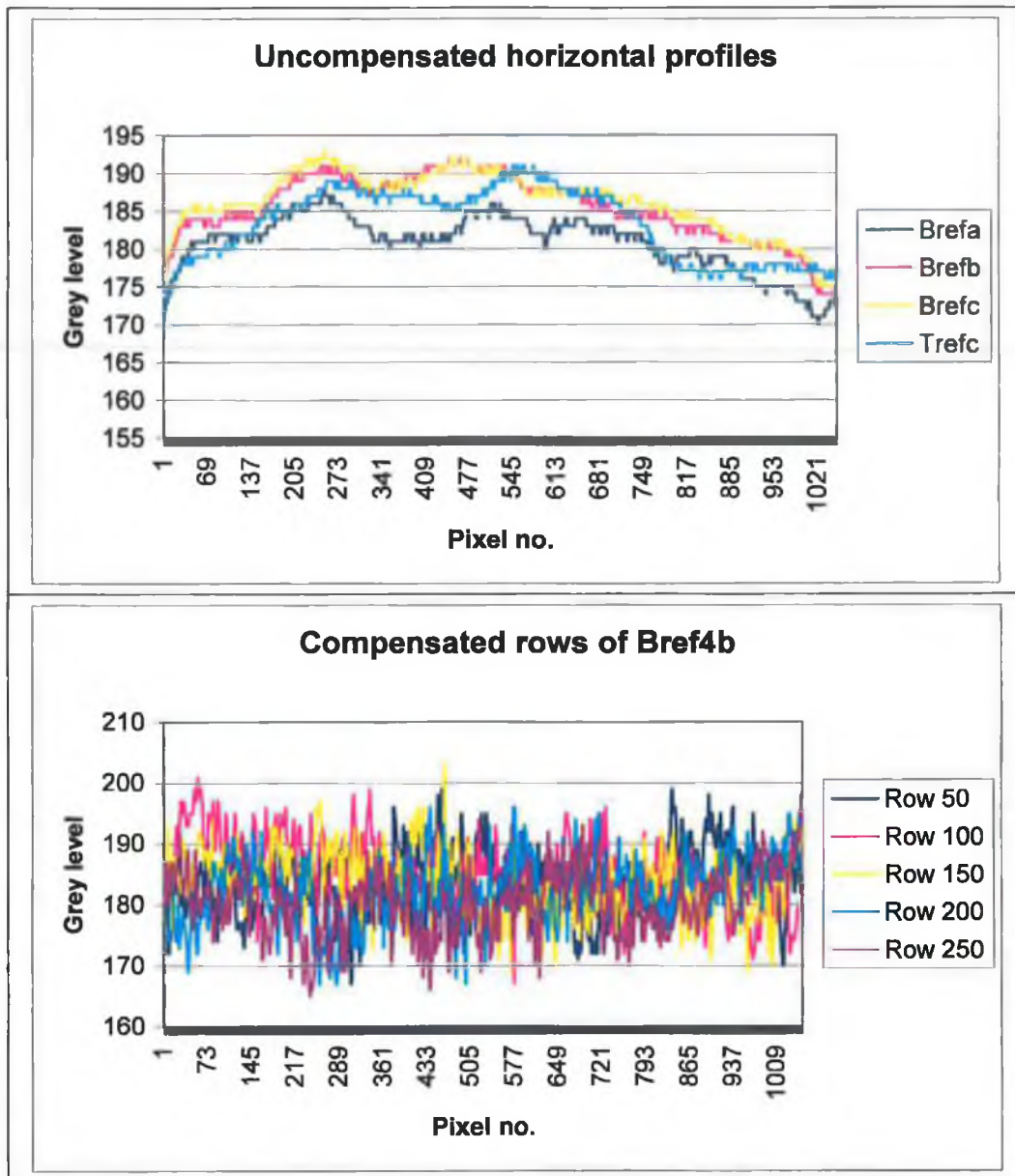


Figure 8: Horizontal profiles of reference slates.

The horizontal profile of Supercem reference slate, bref2, was used as the training image. The image contains 600 successive lines of data representing a 264 mm length of the central 252 mm of the slate. A horizontal profile was calculated by averaging data in columns. The profile is shown in Figure 8 and has 20% non-linearity. The mean grey level was 181. If one subtracts the mean level from the profile the local

noise (or texture information) data is easier to visualise. This is shown in Figure 8 and the noise level due to slate texture is ± 15 grey levels.

A compensation profile was generated to linearise the horizontal profile. The compensation profile reduces variation to 2.5%. Variation for Thrutone sample (Tref3) is reduced from 22% to 12% using compensation data from the Supercem slate. The compensation was expected to have been better and indicates that other sources of image capture noise are present.

The measured variation of the vertical profile is 11% with noticeable drop in mean signal level close to slate start and end. Linearisation of the vertical profile is not possible to be performed in real time as the sensor used is a line scan camera. Vertical profile linearisation can be applied after the slate image has been captured and would generate a high computational demand.

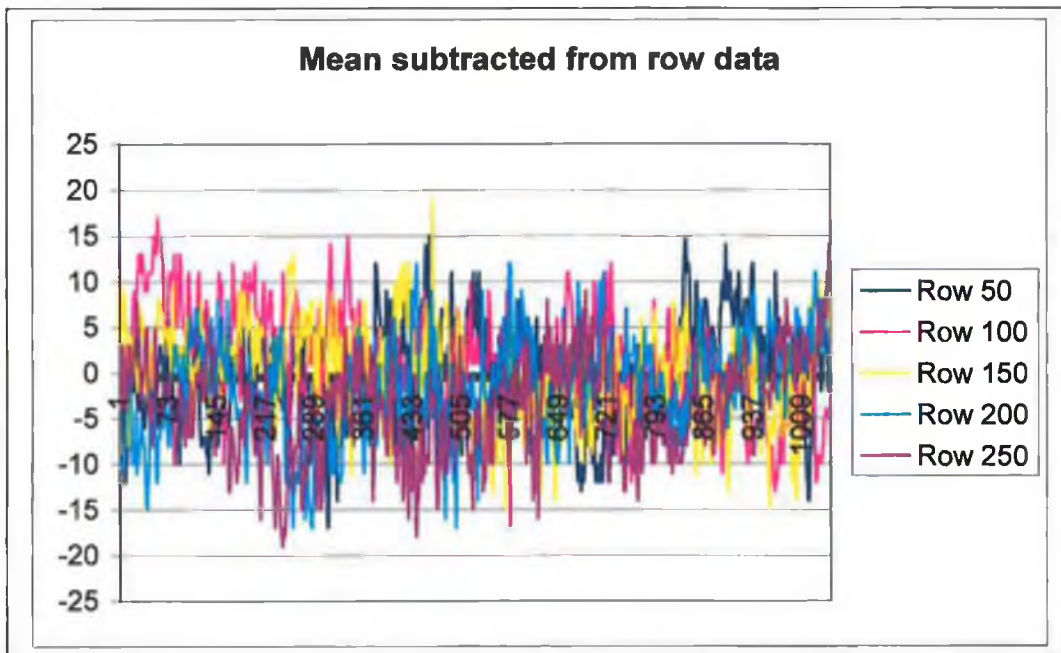


Figure 9: Mean subtracted from row data shown in Figure 8.

3.5.2 Summary of test results

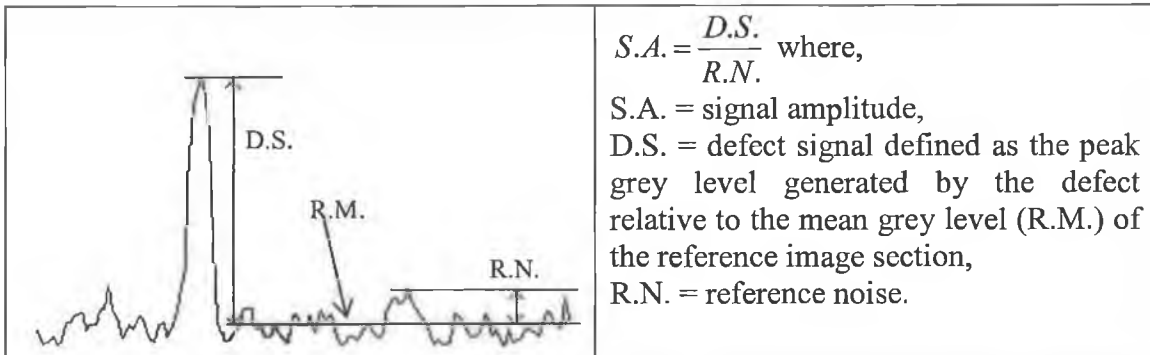


Figure 10: Definition of signal amplitude.

Table 4: Signal amplitude calculations for selected defects.

No.	Defect	Mean	Signal	Amplitude	Detectable
1	Lump – lu20	186	150	2.4	Yes
2	Lump – lu23	180	140	2.7	Yes
3	Lump – lu24	184	125	3.9	Yes
4	Lump – lu25	182	135	3.1	Yes
5	Lump – lu26	191	160	2.1	Yes
6	Insufficient paint – ip73	181	136	3.0	Yes
7	Paint debris - pdu01	172	80	6.1	Yes
8	Paint droplet – pd83	179	150	1.9	Yes
9	Spots – lu24	184	150	2.3	Yes
10	Supercem – bref4	181	166	1.0	Yes
11	Orange peel – op50	181	127	3.6	Yes
12	Efflorescence – ef11	175	150	1.7	Marginal
13	Efflorescence – ef12	181	135	3.1	Yes
14	Efflorescence – ef13	184	145	2.6	Yes
15	No paint - mp03	180	100	5.3	Yes
16	Shade variation - mp03	180	150	2.0	Yes
17	Template mark - tm40	177	145	2.1	Yes
18	Template mark - tm41	189	140	3.3	Yes
19	Template mark - tm42	179	120	3.9	Yes
20	Template mark - tm43	180	150	2.0	Yes
21	Lump - tm41	170	120	3.3	Yes
22	Template mark - tm44	181	150	2.1	Yes
23	Template mark - tm45	188	120	4.5	Yes
24	Template mark - tm46	167	100	4.5	Yes
25	Template mark – dt30	182	135	3.1	Yes
26	Template mark – dt31	179	150	1.9	Yes
27	Template mark – dt32	165	150	2.0	Yes
28	Template mark – dt34	175	140	1.7	Marginal
29	Template mark – dt35	160	100	4.0	Yes
30	Bad edge				Marginal
31	Vertical template mark	181	166	1.0	No

The definition of signal amplitude is illustrated in Figure 10. Defects that generate signal amplitude greater than 2.0 are considered to be detectable.

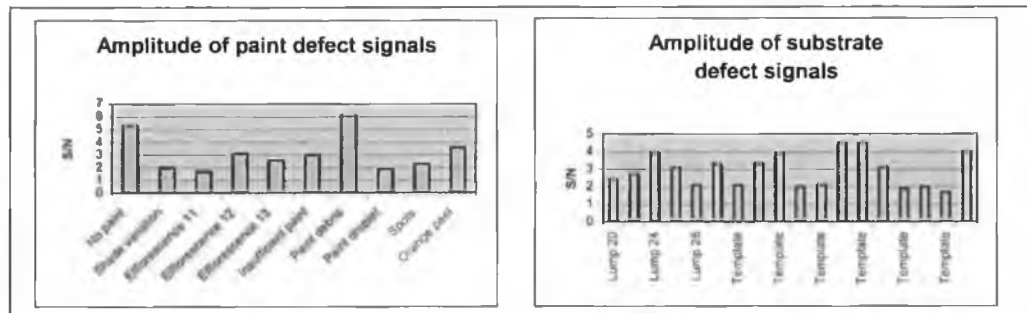


Figure 11: Signal amplitude of paint and substrate faults by collimated lighting.

3.5.3 Effect of concavity and convexity on signal level

The collimated lighting method of image capture is very sensitive to changes in the surface profile of the slate. The effects of severe concavity and convexity are to shift the camera view line outside the illuminated band. Such areas will be erroneously classified as defective. The partially collimated, partially defocused light band is not entirely successful.

3.6 Tests using diffuse lighting

The test bed is the same as that described in Section 3.4 with the exception that an aperture fluorescent light system with integral cylindrical focussing lens (TSI Model AFL9000) was used as the illumination source. The bulb aperture is 60° and light is dispersed equally in a 60° arc. This lighting method creates a wide band of partially diffuse and partially collimated light and it is quite easy to align the camera. The lamp angle of incidence was set up at 50° and the camera was located at 50° relative to the slate. Other lamp angles of incidence were investigated but this arrangement generates the strongest signal level. The exposure setting was 2 milliseconds and the grey scale mean values were 80 grey levels for Supercem samples.

The cross direction pixel resolution was 0.28 mm and the moving direction pixel resolution was 0.62 mm. Light levels are 16 times lower than required so that effective moving direction resolution will be 2.0 mm at production line speeds. Cross

direction resolution is not influenced by production speed and will be set as considered appropriate.

An advantage of this lighting method is that it is relatively immune to slate profile non-uniformities. An obvious disadvantage is that the smaller defects cannot be detected. A review of fault types and sizes shows that many of the paint faults are quite large and can be inspected at a relatively low resolution of 2 mm. A less intense light source would suffice. The effects of depth profile variations do not impact negatively on large size defect detection.

3.6.1 Profile of reference slates

The horizontal profile of the reference slate, bref2, was used as the training image.

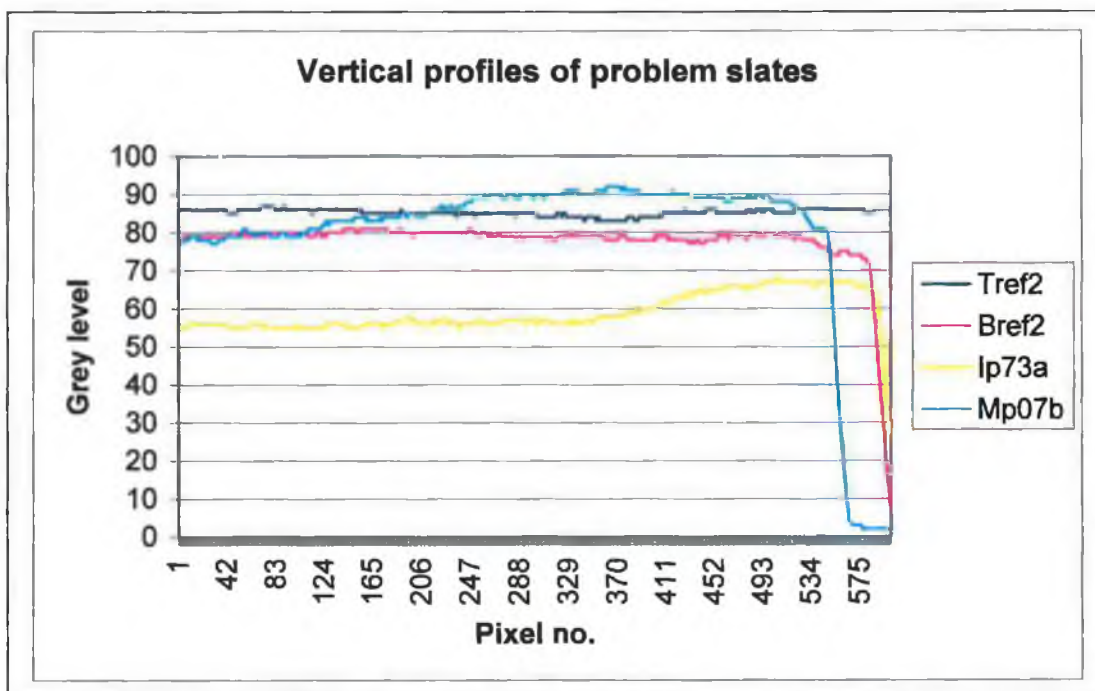


Figure 12: Vertical profile of slates with significant depth profile variation.

The image from which the compensation profile was generated contained 600 successive lines of data representing a 370 mm length of the central 252 mm of the slate. The horizontal profile was calculated by averaging data in columns. The profile has 21% non-linearity. A compensation profile was generated to linearise the horizontal profile. The compensation profile reduces variation to 4%. The measured variation in the vertical profile is 11% with noticeable drop in mean signal level close

3.7 Optical solution for successful image capture in the presence of depth profile

The cylindrical lens of the fibre light guide collimates and focuses the light emerging from the fibres. When optimum collimation and focus is achieved, the spread of the band of light produced on the slate is 5 mm.

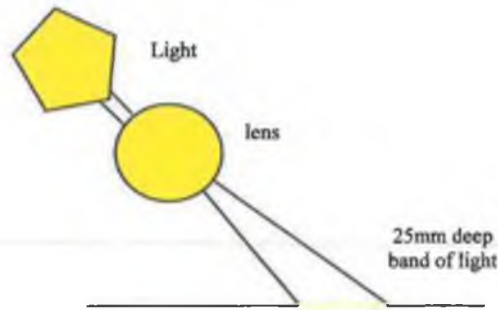


Figure 14: Fibre light guide with lens attachment.

As mentioned earlier, it is very difficult to align the camera onto such a narrow band of light and all previous tests were conducted with the lens defocused sufficiently to produce a 13 mm spread in the band. This was the maximum defocus achievable using the mechanical brackets supplied by the manufacturer. The brackets were modified so that the cylindrical lens on the light guide was brought very close to the fibre ends and the light guide to lens separation was reduced to 5 mm. Light spreads out much more than when the lens was located in its optimal focusing location. A 25 mm wide band of light was created on the slate for the full width of the fibre guide. The 25 mm diameter lens was 70 mm from the slate surface.

Images taken at 1 ms exposure using the 85% setting of the lamp controller generate mean grey levels of 150, sufficient intensity for this application. It was unexpected that intensity levels would remain sufficient because defocus from 5 mm to 13 mm had resulted in a directly proportional drop in intensity levels. Referring to the illumination model outlined in Section 3.3, it can be assumed that the diffusely reflected component of radiance is larger than had been previously estimated. The contribution of the diffusely reflected component to the camera signal will also have increased in direct proportion to the increased width of the light band and the increase in range of angles of incident light from the lens.

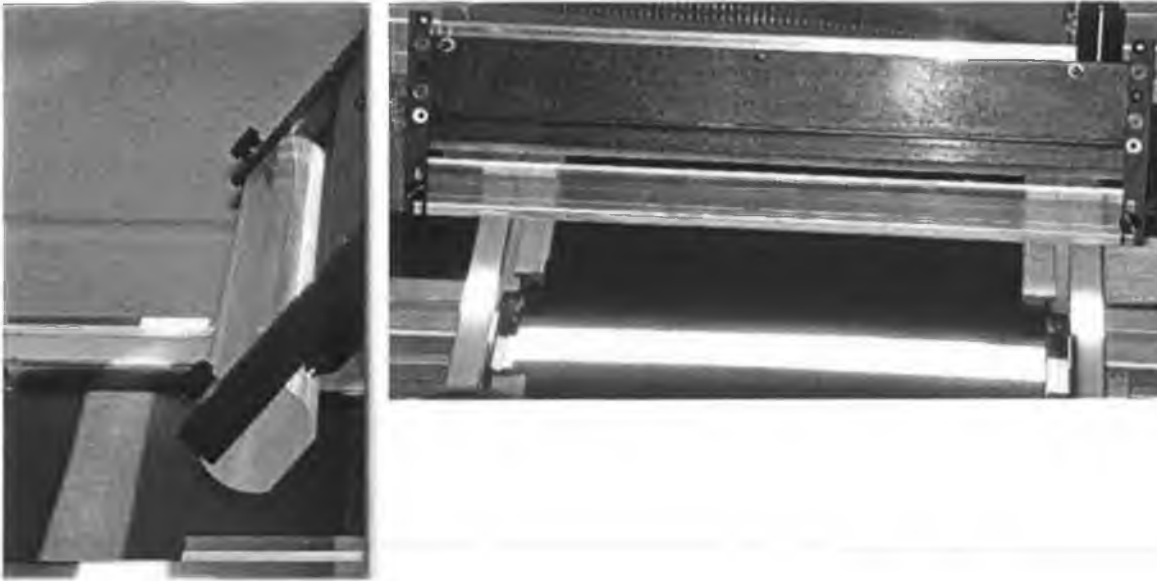


Figure 15: Modified line light and lens arrangement; side and front views.

Maximum slate depth profile variation was 5 mm translating into a 6.25 mm shift in position of the light band and of the camera view line. This means a 12.5 mm shift from the original view line. If the slate were moving on a conveyor belt, all shifts would be upwards. Concave slates would rise in the middle and convex slates would rise at the edges. The light band would be sufficiently wide to ensure the camera view line would always be illuminated for depth profile variations of 5 mm.

Standard conveyors are likely to introduce ± 3 mm of depth variation and the optical system will need to cope with this. The depth variation at any one time is likely to be ± 1 mm but will vary with usage due to dirt ingress and part aging.

The uniformity of the band of light was investigated with light incident at 45° and camera located at 0° , 20° and 46° . Graphs of intensity are shown in Figure 16. The reason for significant variation at 46° turned out to be due to miss-alignment of the fibre exit profile and the cylindrical lens. This figure was retained in the report to emphasize the importance of accurate mechanical alignment to the success of this approach. Left side of each graph in Figure 16 is closest to the lens.

Tests were repeated following alignment adjustment and the profile is shown in Figure 16.d. The profile was checked at both left and right sides. Local non-

uniformity was most likely due to variations in reflections from the slate surface. The sharp rise in intensity on the right side profile was due to local miss-alignment.

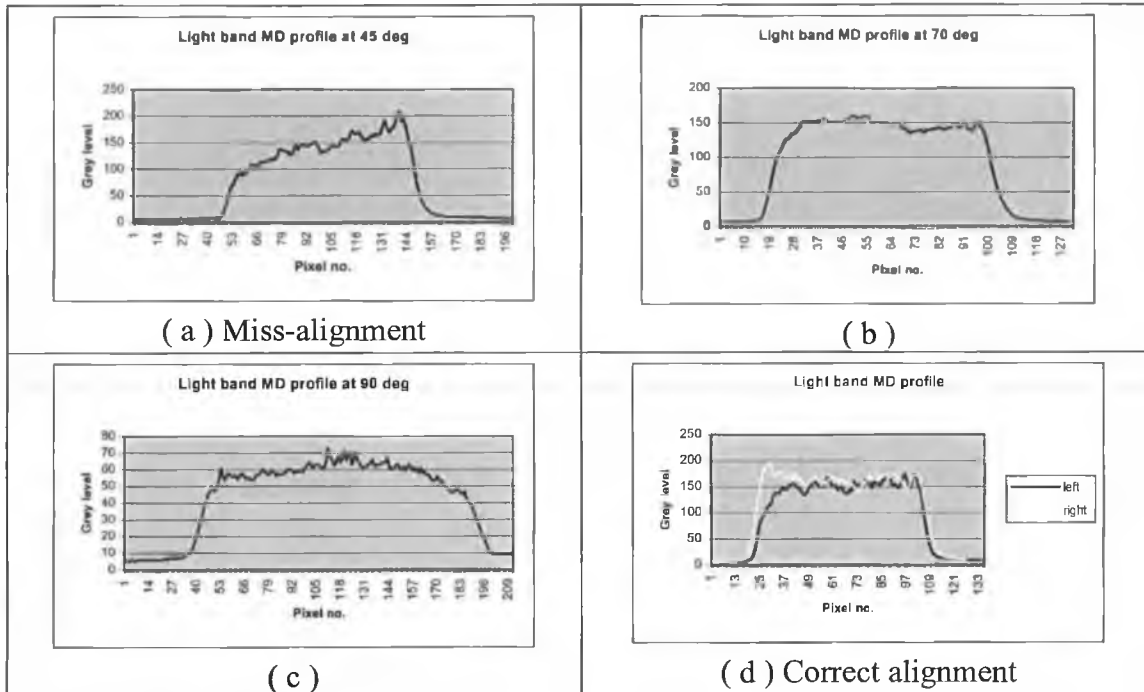


Figure 16: Light band MD profile according to camera view angle.

Tests were repeated at 20° and 0° with grey level being as low as 33 pixels for the 0° camera position. Given that background grey level was 9 pixels, this indicates there is a six-fold difference in light intensity reflected specularly and diffusely. This agrees with tests conducted on copy and glossy papers in 1998 by the Dublin Institute of Technology (DIT) physics department.

3.7.1 Test results using defocused light line

Signal amplitudes for paint and substrate faults are shown in Figure 18. All defect types were imaged. Signal strength for defects was lower by up to 100% compared to signal strength obtained using collimated light but was sufficient for detection of most defect types. Repeatability of image capture was excellent. Signal amplitude for defect types *barring* and shallow *template marks* is poor and defect detection will be difficult. No signal is generated for shallow *template marks* orthogonal to the line of sight of the camera and these will not be detected.

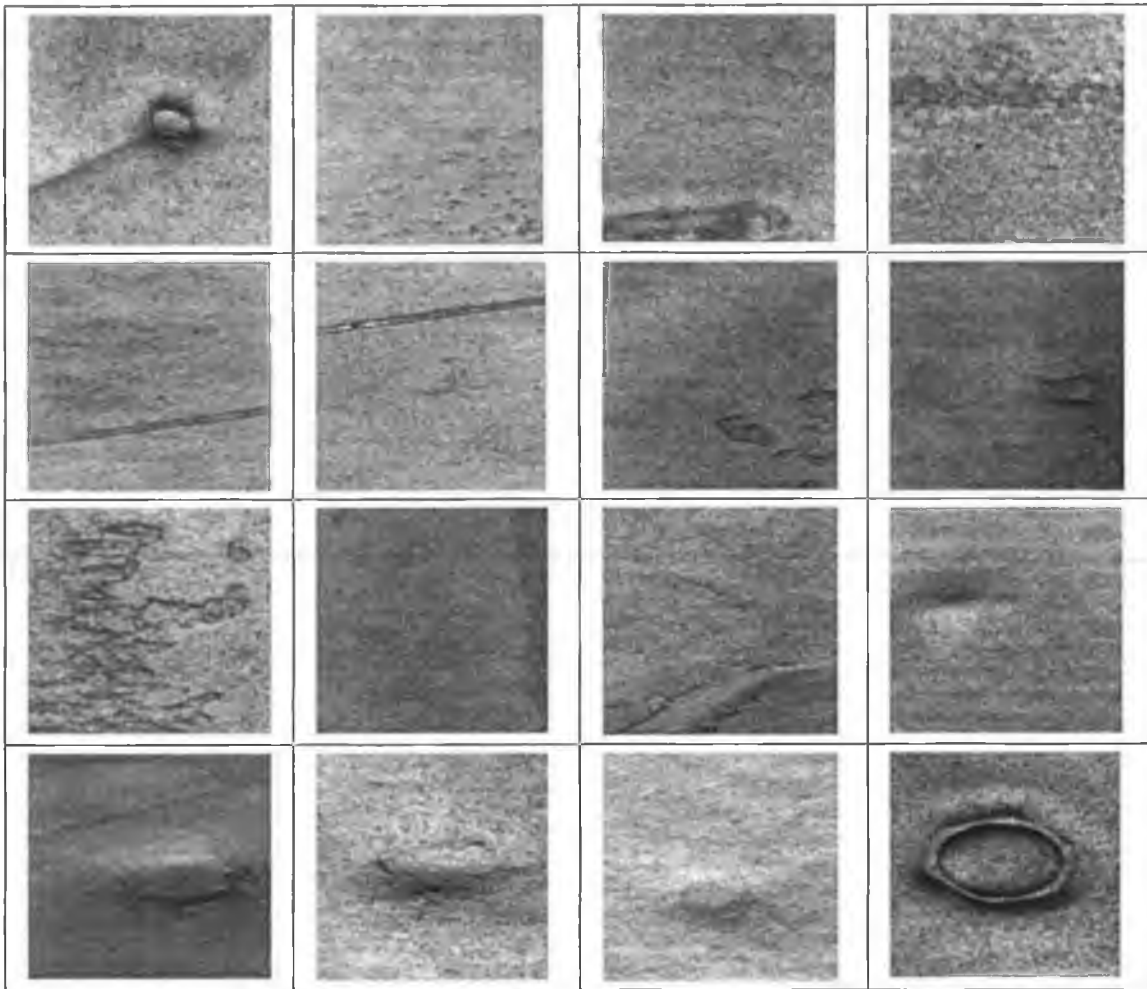


Figure 17: A selection of substrate defects of type template mark and lump.

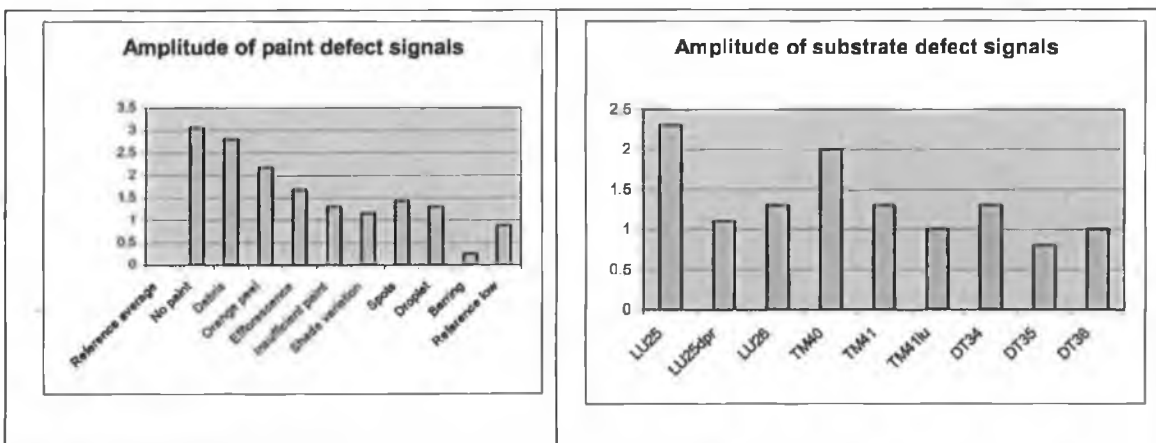


Figure 18: Amplitude of defect signals imaged with defocused light line.

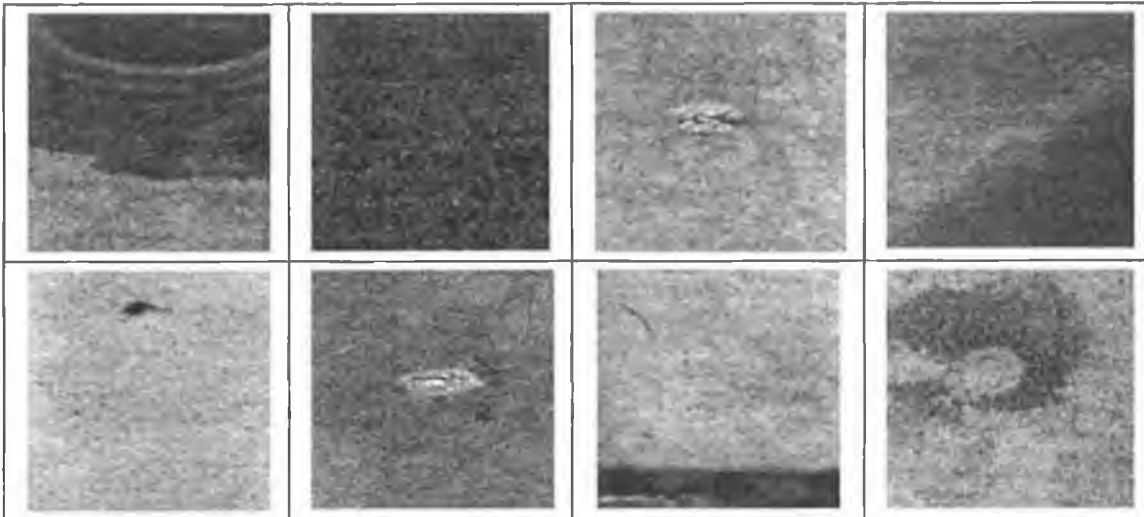


Figure 19: A selection of paint defects of type efflorescence, insufficient paint, paint droplet, shade variation, paint debris and missing paint.

3.8 Discussion

The collimated lighting method is preferred because luminance levels are sufficient and almost all defect categories can be detected. It suffers a major disadvantage in that signal level can be affected sufficiently by concavity and convexity to render defect detection impossible. A method to flatten the slate during inspection can be considered because the slate is flexible. The upper surface of the slate scratches easily and the industrial partner said any mechanical manipulation of the slate was most unlikely to be implemented on the production line.

The diffuse lighting method worked very well for detection of gross faults. Defect detection was not affected by slate profile non-uniformities of up to 5mm. The low pass filtering effect of the slow scan speed averaged much of the slate texture out. This has the advantage of lowering noise levels and the disadvantage of removing useful information about tiny defects and the amount of texture being introduced as the template condition deteriorates with use. Substrate faults can be detected using this diffuse lighting method but they are not well characterised. The fault rising edge was not detected whereas the shadow created by the falling edge was detected. This image capture method was useful for detecting large area paint faults.

The defocused fibre optic light line gives the best compromise solution for image capture. The light intensity is acceptable, the light band is sufficiently wide and

sufficiently uniform that depth profile non-uniformities do not impact negatively on signal levels and the majority of defect types have a sufficiently strong signal level.

Shallow template marks, whose direction is the same as that of the moving direction of the slate, are not detected by either collimated or diffuse lighting methods. A cross direction collimated source will enable detection of this fault type. An alternative approach is to rotate the slate and pass the slate through a second inspection station.

Tests were carried out with other camera and lighting topologies. Specular reflection dark field detection method was tested because it was felt substrate faults would be better characterised. A substrate defect will reflect light at a different angle to that of the incident light and can be detected by placing a camera where the light is reflected. Several angles were investigated but the results were poor. This was thought to be due to the large range of defect shapes causing a large variation in reflection characteristics. Locating a camera perpendicular to the slate using the collimated light source does facilitate detection of bright faults such as edge defects and wax marks but does not have particular merit for highlighting other faults.

3.9 Prototype inspection system description

The prototype inspection system was built to replicate factory conditions as closely as possible in the laboratory. The two meter long, belt-driven conveyor transports the slates past the inspection line at factory line speeds. The 762 mm wide fibre optic line light illuminates the slate and the camera captures a digital image of the slate and transfers this image to a PC located beneath the conveyor. The camera used was a Basler 2K-pixel line-scan operating at a scan frequency of 2.5 KHz.

A Euresys frame grabber was used to interface the camera to the PC. A 762 mm wide light-line illuminated with two 150W halogen lamps allows us to image the slate with either the 300 mm or the 600 mm edge facing forward. Software development was carried out on a 600 MHz Pentium II processor having 128 MB RAM. The effects of vibration are minimized by using a belt-driven conveyor and by careful selection of the belt material. A guide was placed on one side of the conveyor to minimize lateral drift and rotation of the slate.

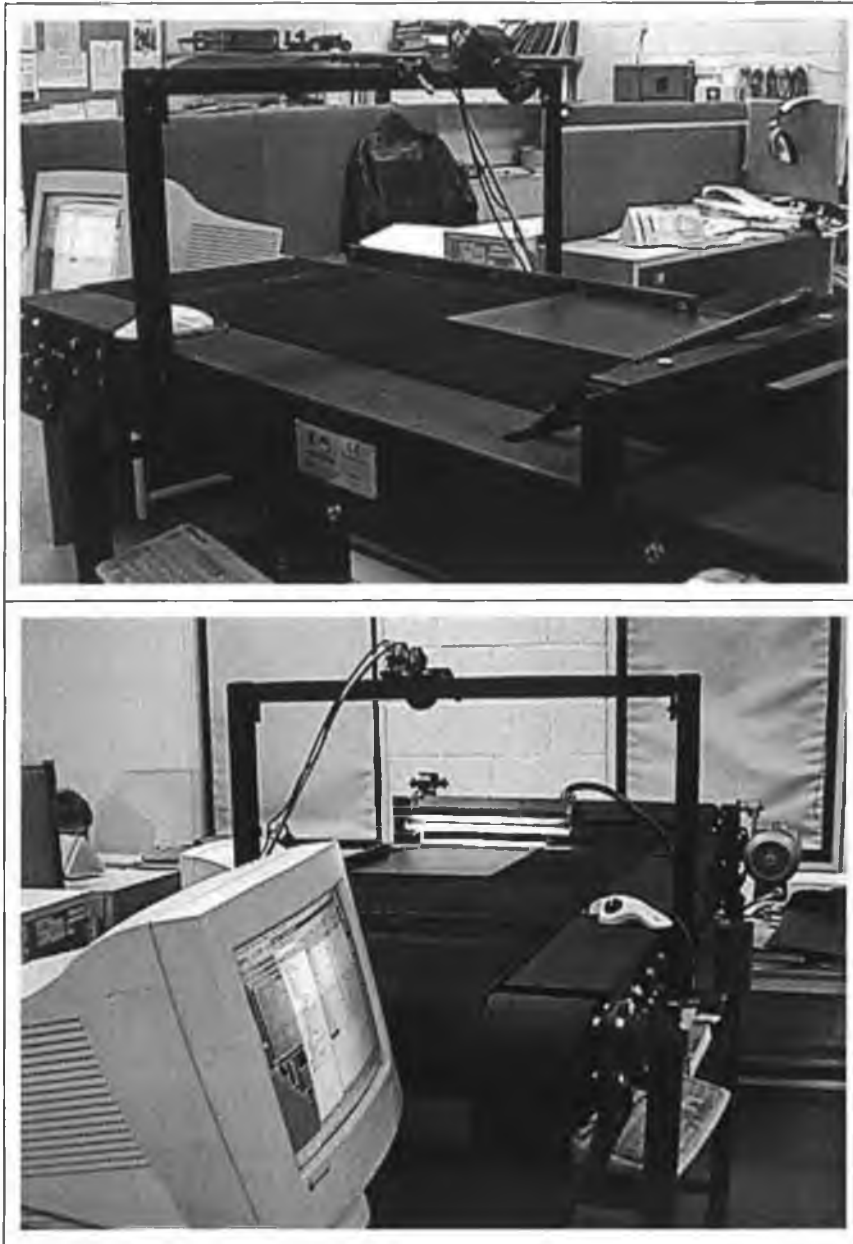


Figure 20: Conveyor and slate inspection system.

The slate under inspection is aligned against the guide towards the front of the conveyor. When aligned, the slate is released onto the conveyor belt and transported past the inspection line before dropping onto the collection tray. The inspection system is triggered to begin image capture immediately prior to the arrival of the slate at the inspection line. Image capture continues for sufficiently long to image the full slate. The frame grabber has only 8 KB frame store and the slate image is transferred dynamically to PC memory while image capture is in progress. Once the image transfer is complete, the slate image is processed using the developed slate inspection software described in Section 4.7.

4. Image Processing Algorithm Design

This section of the report describes the image-processing algorithm developed for the automatic identification of paint and substrate faults on painted slates. I begin by characterising the signals from reference and defective slates. The applicability of the candidate image processing methods to slate inspection is explored before progressing to a detailed description of the devised algorithm. There are four main components to the image-processing algorithm; global mean threshold, adaptive signal threshold, connected component labeling and edge detection. Rigorous testing was carried out on slate images captured with the laboratory test bed. Detailed results are presented, including images of all defect types and the output from the image processing algorithm. Successful defect detection was greater than 95%. All acceptable quality slates were correctly detected.

4.1 Introduction

The primary objective is to find an image processing solution that will correctly detect all defects and not reject acceptable quality slates. Correct classification by type is not a requirement. A single solution is not necessary; different image processing solutions may be appropriate depending on defect type.

A secondary objective is to find computationally efficient image processing solutions with a view to potential real-time implementation. Candidate methods that may satisfy this objective are grey level statistical methods, morphological methods, grey level difference methods, local binary patterns and edge detection methods.

4.2 Reference slate characterisation

Some information concerning the profile of reference slates has already been presented in Section 3.5.1. In summary, shading compensation is necessary to remove cross directional non-uniformities introduced by the lighting and imaging system and slate texture noise is ± 15 grey levels with outliers of up to ± 40 grey levels.

An investigation of the mean grey level of successive slates revealed significant variation. Measured mean grey level variations between successive samples are shown in Figure 21. Measurements were repeated several times on the same slates over a time frame of four weeks. The results confirmed that the variations are from the slate and not due to the imaging system. The effect of mean shifts is further illustrated on a single column of data in the right side of Figure 21. It can be seen that a threshold suitable for first third would result in many false triggers if applied to middle third and that most defects would not be detected if applied to the final third.

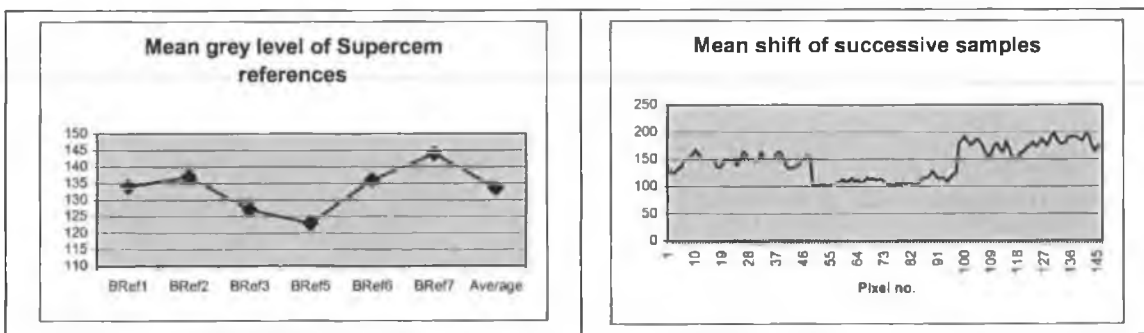


Figure 21: Mean grey level variation for successive samples.

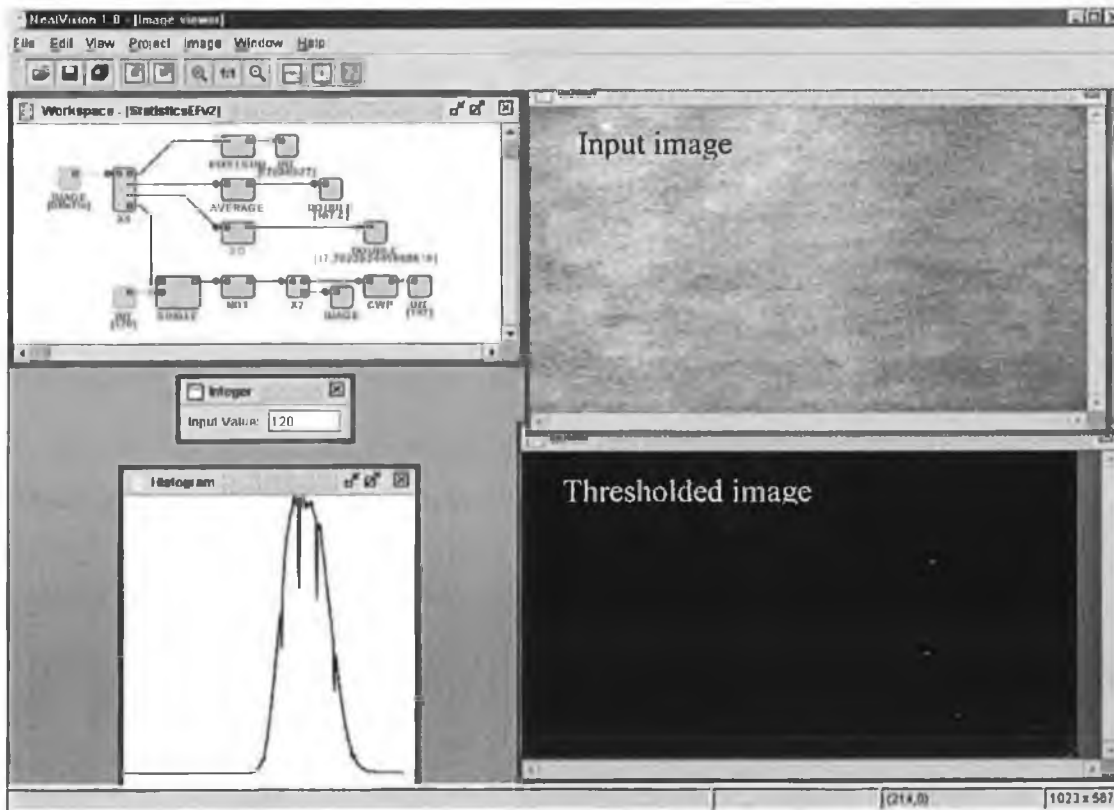


Figure 22: Reference sample under test in the Neatvision environment.

The reference image shown in Figure 22 is almost full slate width and no compensation has been applied for lighting and imaging system non-uniformities. The Neatvision program, (statisticsEFv2), used for feature extraction is on top left and grey level histogram of input image is on bottom left. The drop in light levels is evident on the right hand side of the input image and causes the relatively large spread in histogram values. The mean grey level was 167. A threshold setting of 120 causes some false triggers in the darker right hand side of the image and these can be seen as white pixels in the binary image. The application of shading compensation prior to the threshold operation is necessary to reduce the impact of cross-direction lighting non-uniformities. There appears to exist (to the human eye) non-uniformities unrelated to cross-direction lighting and these were investigated by extracting 150 x 150 pixel image sub-sections from the full slate image. The method of cell extraction is illustrated in Figure 23.

Table 6: Measurements on 150 x 150 pixel sub-sections of reference brefl.

Sample	PixelSum	Mean	SD	Threshold pixels
a1	3019	179	15.9	0
a2	3177	189	12.4	0
a3	3060	182	10.9	0
a4	3146	191	10.6	0
a5	2884	173	13.1	0
b1	3040	180	12.1	0
b2	3165	187	12.3	0
b3	3111	184	11.6	0
b4	3080	182	11	0
b5	2944	174	10.6	0
c1	2952	176	13.9	0
c2	3138	186	13.7	0
c3	2935	174	11.2	0
c4	2944	174	9.8	0
c5	2795	165	10.4	0
d1	2860	169	12.2	0
d2	2995	177	12.9	0
d3	2895	171	9.8	0
d4	2865	169	9.7	0
d5	2743	162	11.8	0
20	2987	177	11.8	0
low	2743	162	9.70	0
high	3177	191	15.9	0
mean-low	244	15	2.1	0
high-mean	190	14	4.1	0

The data shown in Table 6 is for 20 cells of sample Brefl when the full slate image grey level mean was established at 167 grey levels. The statistical features of mean, standard deviation (SD), total grey level value of all pixels (PixelSum) and number of defect pixels using threshold setting of (mean-40) were examined. Variations of $\pm 10\%$ were measured on this small sample set for each feature. There are no false triggers for the threshold test indicating the effectiveness of working with small sub-sections of the full slate image. The histogram shape is more consistent when working with smaller image sections and leads to more consistent results. Shown in Figure 24 are the mean grey levels for 150 x 150 pixel sub-sections of reference sample bref5.

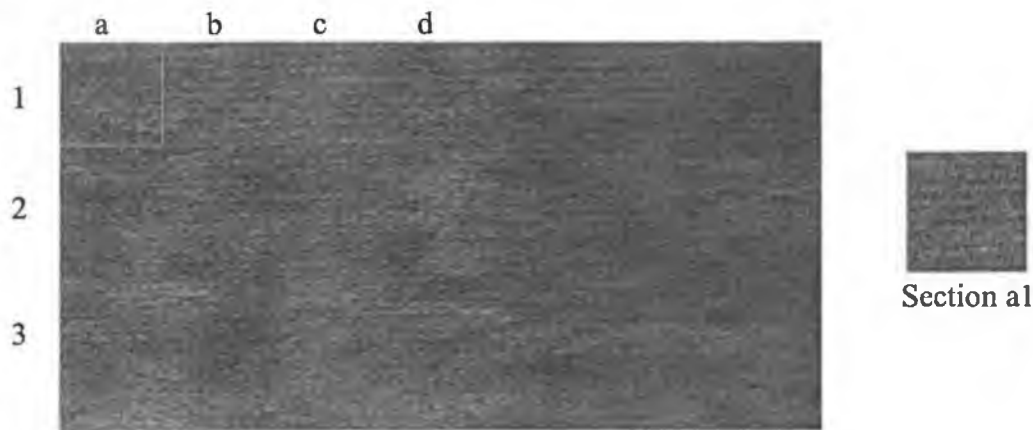


Figure 23: Slate image bref5 and section a1 shown on right.

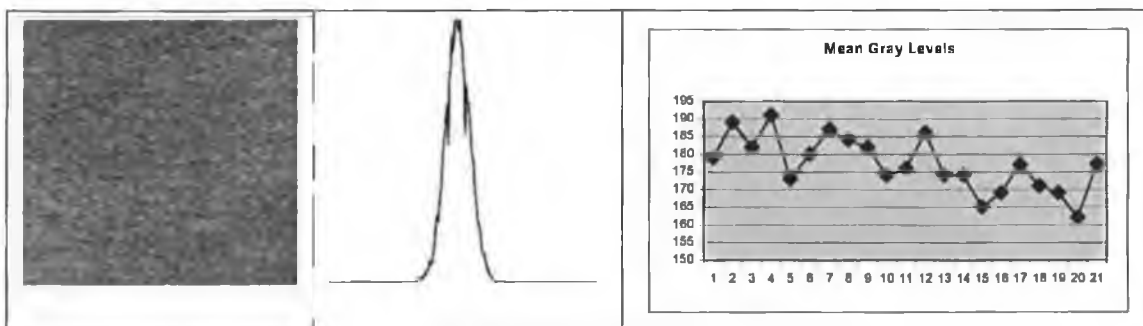


Figure 24: A 150 x 150 pixel sub-section from bref5 and its grey level histogram.

Reference image mean grey level value can vary by:

- 20 grey levels between successive samples,
- 17% within a single sample due to depth profile variations,
- ± 15 grey levels for small sub-sections within the same sample.

The image-processing algorithm must accommodate the variations in mean grey levels. For example, the full slate mean of a production batch might be set at 150 grey levels. A darker sample could have a global mean of 130 grey levels and the mean of a sub-section of a dark sample could be as low as 115 grey levels. The texture noise margin would be at mean minus forty pixels or 75 grey levels. An image section²⁰ from a bright sample could have a mean value of 185 grey levels and the upper texture noise margin would be 225 grey levels. In summary:

- The grey level mean is different for each reference type. It will be assumed the mean value for each slate type will be known from a training phase.
- The grey level mean varies from slate to slate of the same type and the limits of this variation will be known from a training phase.
- The grey level mean varies within a single slate and the limits of this variation will be known from a training phase.
- Noise (including variation due to slate texture) has a Gaussian distribution.

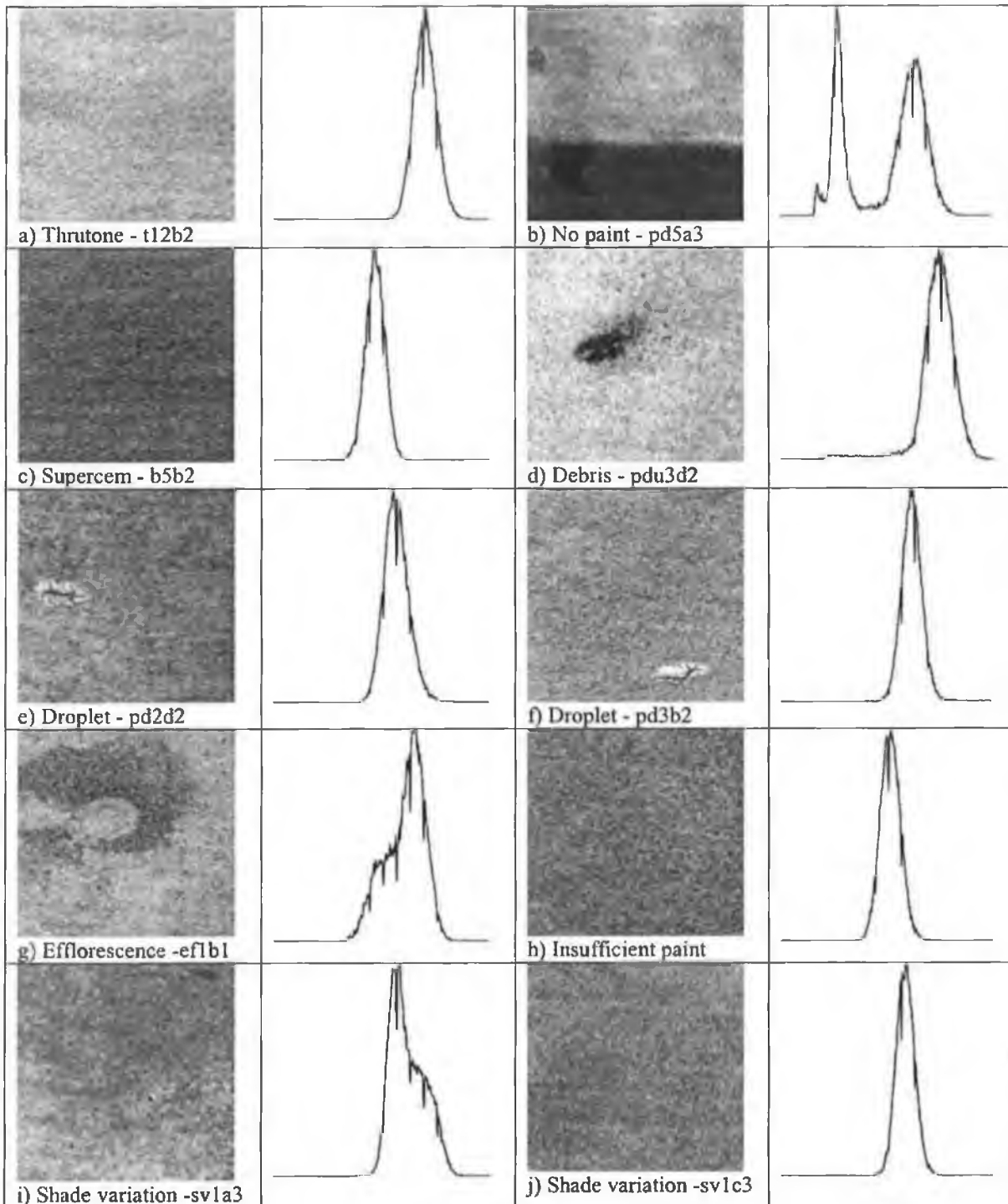
4.3 Defect slate characterisation

The grey level histograms for paint and substrate faults are shown in Figures 25 and 26 respectively. Analysis of these histograms is one of the most important steps in finding features that will enable us to distinguish defective slates from acceptable quality slates. The majority of the defects are negligibly small relative to the whole slate image. One advantage of working with smaller image sizes is the fact that the relative impact of a defect on the grey level statistics of the image is increased. The size of the image section is selected to be sufficiently large so that the statistical data satisfies the central limit theorem for normality (Hayslett, 1993) and so that the medium size defects occupy about 10% of the area of the image section. The selected image section size is 128 x 128 pixels. In summary:

- The average value of the defect pixels is generally less than the average of the background pixels. Droplets are the exception, where sections of some droplets having average values greater than the background.
- The number of pixels belonging to the defect ranges from negligibly small to the total number of pixels in the image.

²⁰ The term 'image section' and 'image sub-section' are inter-changeable.

- The number of pixels belonging to a defect relative to the total number of pixels in the image does alter the characteristics of the histogram. Note the effect on the histogram for shade variation defect type when the whole image is defective (Figure 25.j) compared to a sub-section of the image (Figure 25.i).



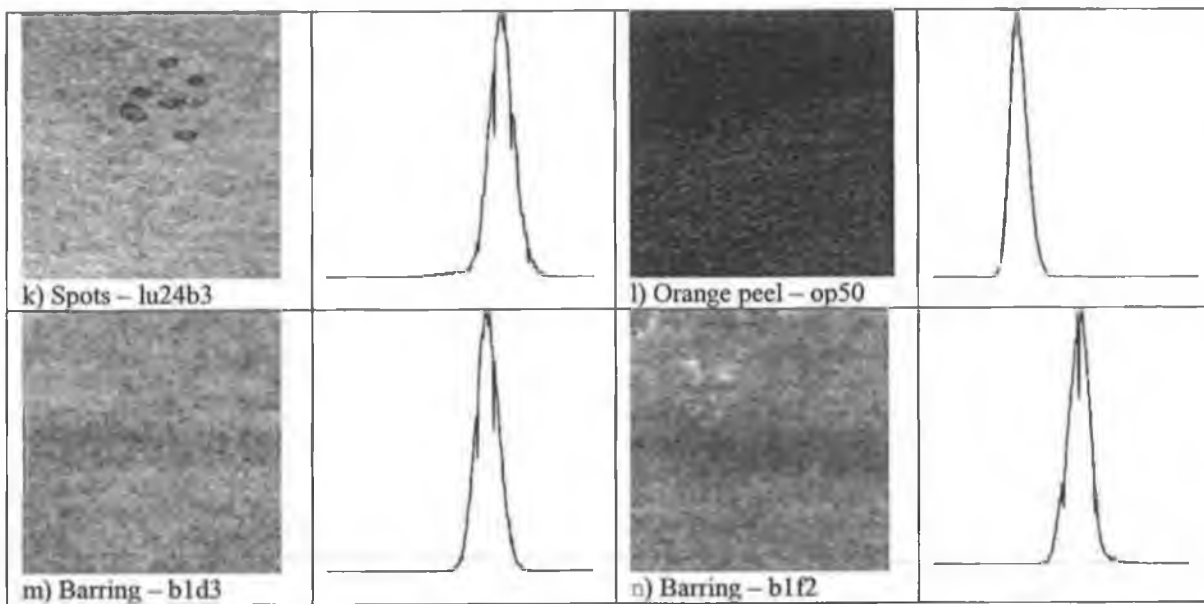
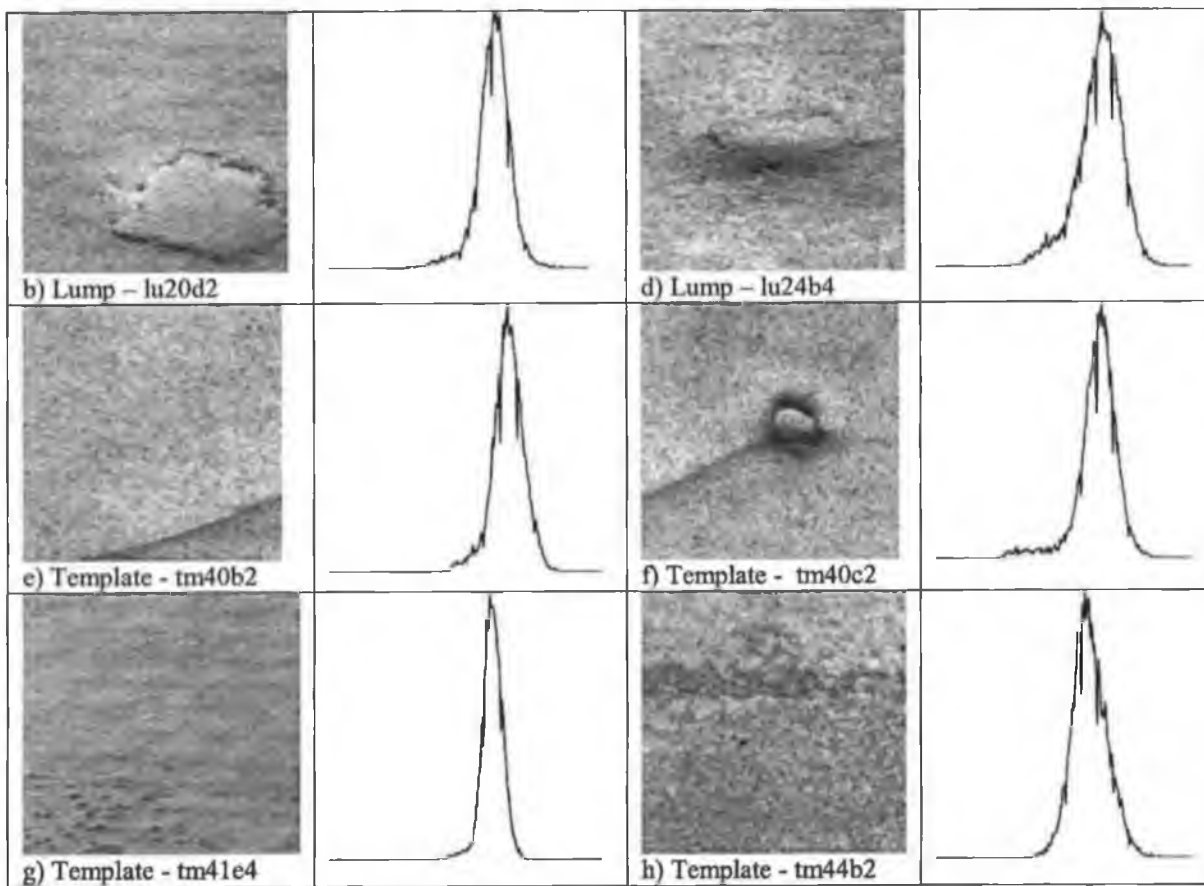


Figure 25: A selection of paint defects and their grey level histograms.



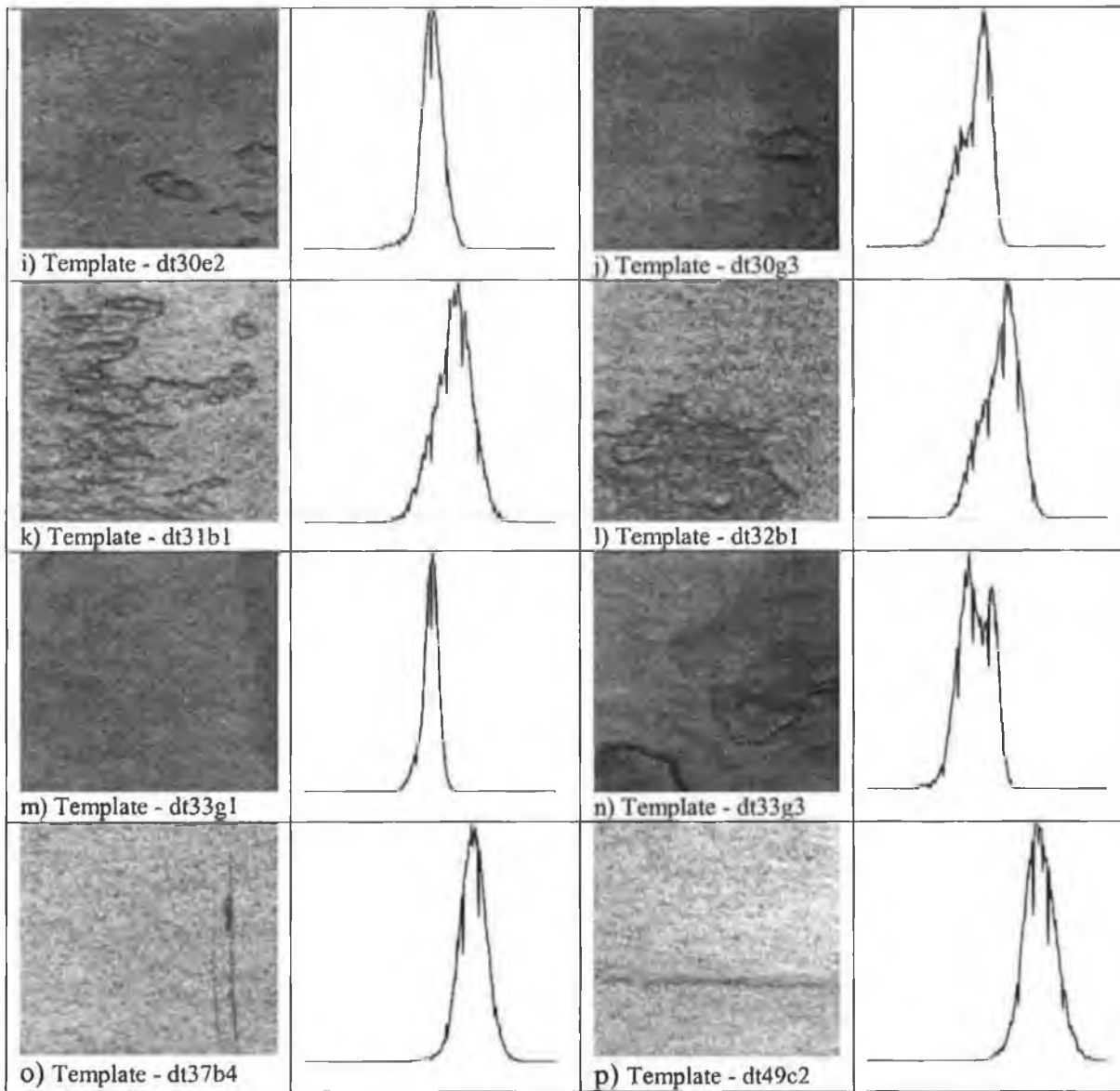


Figure 26: A selection of substrate defects and their grey level histograms.

4.4 Image processing methods investigated

4.4.1 Grey level statistical methods

One of the prior work findings was that grey level statistics might offer discriminating characteristics for detecting defective slates. Such features include grey level mean, standard deviation, skewness, kurtosis, entropy and range²¹. Some of the results obtained during experimentation are given in Section 3.6.2 and in Section 4.2. The

²¹ Range is defined as the maximum grey level minus the minimum grey level in an image. The range for images where fifty lowest value pixels and fifty highest value pixels were removed from the image histogram was also tested.

grey level mean was the only useful feature for distinguishing between acceptable and defective slates.

4.4.2 Grey level difference methods

The first order statistics of the absolute difference between pairs of grey levels is one method used for discrimination of textures. Reports of successful application in ceramics and computational efficiency encouraged its investigation on slate defect detection. The grey level difference method examines local properties, usually of one or two pixel separation. The directions 0° and 90° are usually investigated and the directions 45° and 135° are sometimes investigated.

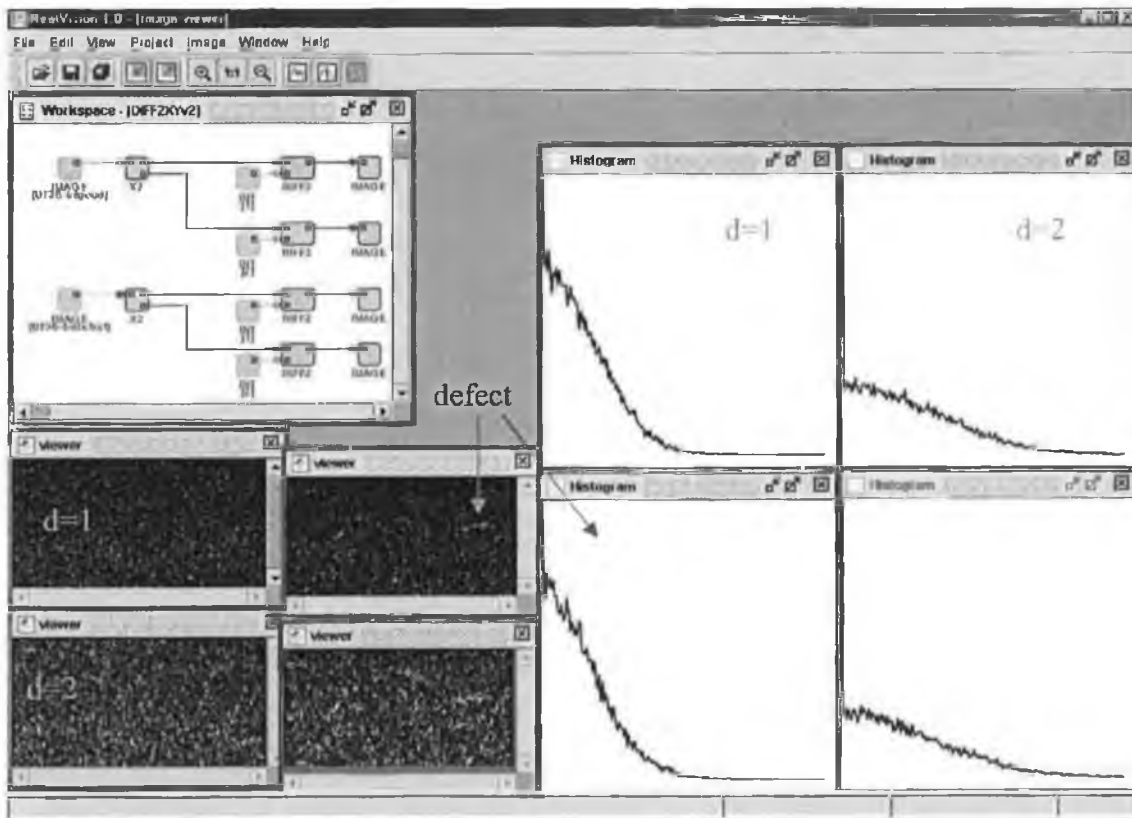


Figure 27: Difference statistic ($0^\circ + 90^\circ$) applied to reference and defect image.

Tests conducted in the Neatvision environment using images captured with the test bed produced inconclusive results. Tests were carried out in directions 0° , 90° , $0^\circ + 90^\circ$ and $|0^\circ| + |90^\circ|$ for separations of 1, 2, 3 and 4 pixels. The method was sensitive

to intensity variations within images and between successive images²². A decision on GLDM merit for slate inspection was postponed in expectation that better quality images would become available using the system prototype.

The difference formula used by Tobias et al (1995) was applied to images captured using the production prototype. The probability density function of the difference image was calculated and two sets of measurements were applied. The first was the calculation of *mean*, *standard deviation*, *largest grey level value*, *pixelsum*, *skewness* and *entropy*. Typical mean values were in the range 4 to 7 grey levels, standard deviations were in the range 0.024 to 0.046 and largest grey level values of 60 were noted. However, these statistics were influenced more by the mean grey level of the original image than the defect features. The grey level difference method outlined by Tobias et al (1995), using a classifier based on the mean and the variance of the difference histogram, is not applicable for detection of defects in slate images.

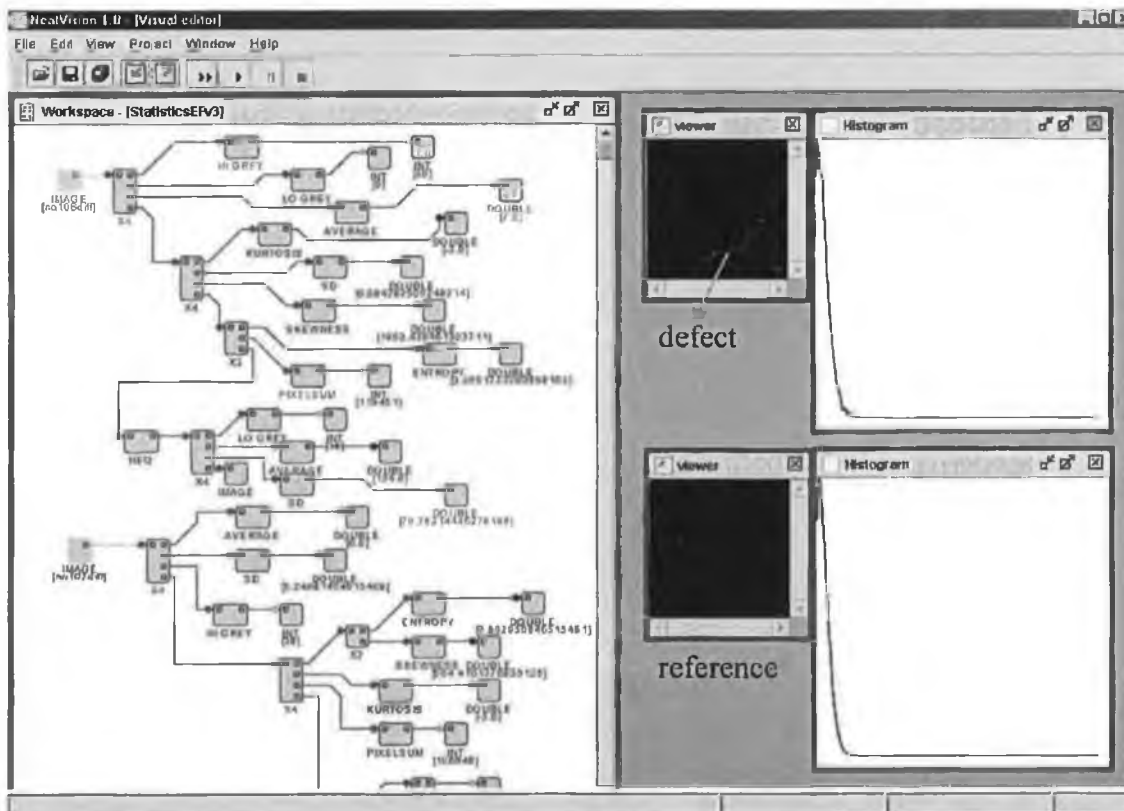


Figure 28: Comparison of DiffXY histograms for reference and defect images.

²² Histogram equalisation is usually performed on the test image prior to application of GLDM and is not done here because it would be impractical for a real-time implementation.

The second measurement set was the classical statistical features of mean, angular second moment, contrast and inverse different moment. Slate no. 128²³ was used as a training image and the threshold settings were selected based on data from the 140 image sub-sections. The threshold settings were set 30% larger than the maximum values observed for any image sub-section in order to minimise false positives. The 8 acceptable quality slates, no. 134 ~ 141, were all correctly accepted according to these inspection criteria.

Paint faults of type *no paint* and *paint debris* are detected using the grey level difference method and usually with the contrast measurement. Defect types such as *shade variation*, *insufficient paint*, *nozzle drip* and most *efflorescence faults* are not detected. Some *template marks* and *lumps* are found. In general, the detected defects present sharp edges. Substrate defects having gradual edge changes are not detected. Averaging was applied to substrate defects having gradual edge changes and most of these defects were detected at the resolution that created a sufficiently sharp edge. The block sizes used for averaging were 2 x 2, 4 x 4, 8 x 8 and 16 x 16.

Some false positives occurred using the grey level difference method on acceptable sections of slates. These false detections always occur in the brightest centre section of the image. Given that further improvements in image quality are unlikely, this method is unlikely to be robust enough to detect the full range of defects.

4.4.3 Local binary pattern methods

The local binary pattern method is reported by Pietikäinen et al (1999) as giving good results for the detection of faults in industrial problems. The method is invariant to grey scale intensity variations and is computationally efficient, thereby making it potentially attractive for this application. Tests were carried out in the Neatvision environment. The anticipated discriminatory features did not materialise. A comparison of binned histograms for LBP and contrast LBP (LBP/C) are shown for reference and defect images. The histograms are almost identical and offer no scope for reliable discrimination.

²³ All slates used in these experiments are numbered so that reviewers of this report can refer back to the original data source.

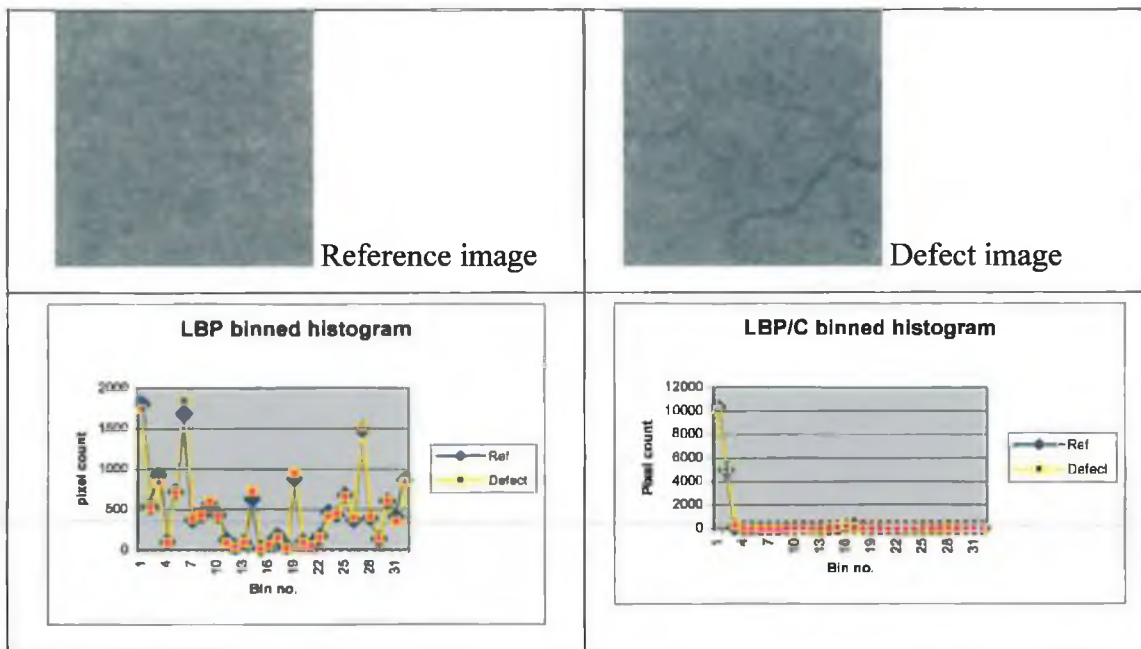


Figure 29: Comparison of LBP and LBP/C binned histograms.

4.4.4 Morphological methods

Müller and Nicholay (1994) demonstrated how to apply morphological methods to detect surface defects in ceramics and textiles. Morphology is the study of structure and shape, and morphological transformations are based on the comparison of objects in an image with objects (termed structuring elements) of known size and shape. A key to successful application of morphological methods is the selection of structuring elements matched to the size and shape of the features of interest in the image under analysis. The difficulty with slate defects is that they exist in a vast range of sizes and shapes. The list of structuring element sizes needed is large²⁴ and would mitigate against these methods being used, given our real-time implementation targets.

Morphological methods were used, in conjunction with other image-processing techniques, to detect specific defect types. In particular, morphological filters were used to remove small structures from images where these structures could be attributed to texture noise.

²⁴ The number of structuring element sizes may be reduced by adopting a multi-scale approach.

4.4.5 Convolution methods

Edge detection operators are neighbourhood operators whereby a mask of size 3 x 3, 5 x 5 or larger is moved across the image. Of the standard edge detectors, the Sobel operator produced the best results. The Sobel operator detected substrate defects having sharp edges but failed to detect gross defects when the defect edge was gradual. The edge detectors also detected a lot of the texture noise and are sensitive to grey level intensity variations within the image. The method was applied, in combination with other image processing techniques, to the detection of thin structures in images. For further details, refer to Section 4.5.4.

4.5 Algorithm design

Extensive testing was carried out to determine features of the defect images that will give an indication of the presence of defective slates. Considerable effort was expended in testing the candidate image processing methods with a view to applying an existing and proven solution. However, a reliable solution that could detect the range of defects was not found. It became necessary to devise a solution tailored to the inspection task at hand. The devised algorithm, which incorporates some aspects of the candidate techniques, is explained here.

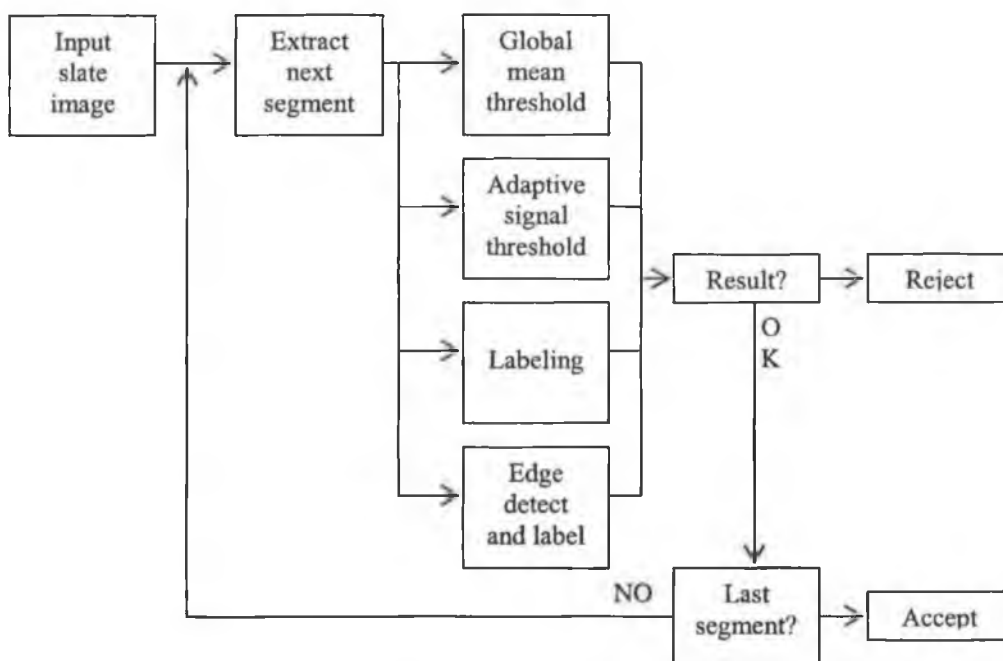


Figure 30: Slate defect detection block diagram.

There are four main components to the algorithm with each component tailored to detect specific features of fault. The components are:

1. Global mean threshold method
2. Adaptive signal threshold method
3. Labeling method
4. Edge detection method

4.5.1 Global mean threshold method

When the grey level mean of an image section is lower than the expected mean the image is considered to be defective. A global mean threshold can be established to detect gross faults such as missing paint and orange peel. A grade-specific threshold is required for low contrast faults such as efflorescence, insufficient paint and shade variation. This method is the only way found to date to reliably identify these types of defects. Monitoring of absolute values of light intensity will be necessary when using grade-specific threshold settings.

4.5.2 Adaptive signal threshold method

The adaptive signal threshold is selected by observing that slate texture noise is found in the band $(\text{mean} - 20) < x < (\text{mean} + 30)$ grey levels. Some outliers are observed in the band $(\text{mean} - 40) < x < (\text{mean} - 20)$ and in the band $(\text{mean} + 30) < x < (\text{mean} + 65)$ of reference slates. The signal thresholds were selected as $(\text{mean} - 40)$ and $(\text{mean} + 60)$ following extensive testing. Defects of type *missing paint* (when less than 50% of image is defective), *paint debris*, *droplet* and *spots* are always detected using the adaptive signal threshold. Most substrate defects can be found using this method. Exceptions are shallow and thin marks and some template mark II samples.

Defects of type *efflorescence*, *shade variation*, *insufficient paint*, whereby a section of the image is defective, are sometimes detected using the adaptive signal threshold. Detection depends on the severity of the defect. Many of these types of low contrast defect do not generate a sufficiently strong signal to make detection possible using adaptive signal threshold settings.

This method adapts to changes in light intensity. The same threshold settings are effective for both Thrutone and Supercem slates.

4.5.3 Labelling method

Connected component labeling is a method applicable to detection of low contrast defects immersed in noise. The algorithm used here is shown in Figure 31. The image is converted to binary using a threshold setting of $(\text{mean} - n)$ where n is an integer in the range $5 < n < 60$. It was found experimentally that threshold settings in the range $(\text{mean} - 20) < \text{threshold} < (\text{mean} - 10)$ were most effective for low contrast defect detection.

The binary image was filtered to reduce noise and outliers due to slate texture. An erosion is followed by a dilation, otherwise known as a morphological opening. The design requirement for this filter is to retain as much as possible of the original image while suppressing small size features.



Figure 31: Label algorithm.

The filtered image is labeled (see Haralick and Shapiro 1992) whereby the pixels associated with each image feature are grouped together and given a unique label. The labels are ordered in accordance with the size of the features. Small size features are generally (though not always) associated with slate texture and larger size features are associated with defects. This leads us to examine the larger size features for characteristics that might enable us to classify them as defective. One such characteristic is the size (or number of pixels) of the largest feature.

The size of the ten largest blobs is used as the discriminating feature between acceptable and defective images. The number of blobs and the blob size threshold setting were determined experimentally. The labeling algorithm works well for detection of samples shown in Figure 25.g and 25.i. Labelling is also effective for detecting high contrast defects such as *paint debris*, *droplets*, *spots* and *no paint* defects.

The algorithm cannot cope with intensity variations within the image under test (as it is designed to locate them) and care must be taken to ensure uniformity of light intensity on the inspection line.

4.5.4 Edge detection method

The majority of defect types and sizes are detected using either mean threshold, adaptive signal threshold or labelling. It was noted that small size and thin, narrow defects are either not well detected or are not detected using these techniques. A new processing loop was added to the algorithm to detect these defect types. As the noise model is of impulse type²⁵, the level of noise in the image is reduced by applying a 3 x 3 median filter. To highlight the defect features, the image section is subjected to a Sobel edge detector.

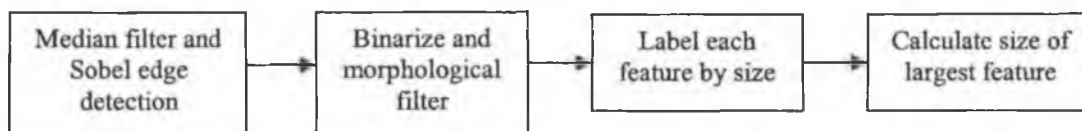


Figure 32: Edge detection algorithm.

The edge detector result is converted to a binary image using an experimentally determined threshold setting of 28. The binary image is noisy and the noise level is dependant on a number of factors including absolute grey level and grey level variations within the image. A morphological filter was selected with the objective of linking defect structures within the image. The image was dilated using a 3 x 3 square structuring element followed by an erosion using the same structuring element. The filtered image was labelled by size of blob and the size of the 10 largest blobs was used as the distinguishing feature between defects and accepts.

4.5.5 Detection of shallow template mark by vertical projection.

We will demonstrate in Section 5.4.1 that shallow and narrow template marks aligned perpendicularly to direction of travel of the conveyor are imaged with relatively poor signal amplitude. The image processing algorithm cannot reliably detect this defect.

²⁵ The Gaussian noise is usually attenuated by applying a low-pass filter.

One option considered to improve detection reliability was to alter the threshold settings to ensure detection. This approach increases detection reliability but at the expense of generating false triggers. The threshold settings have to be left sufficiently relaxed to avoid generating false triggers on acceptable quality slate images.

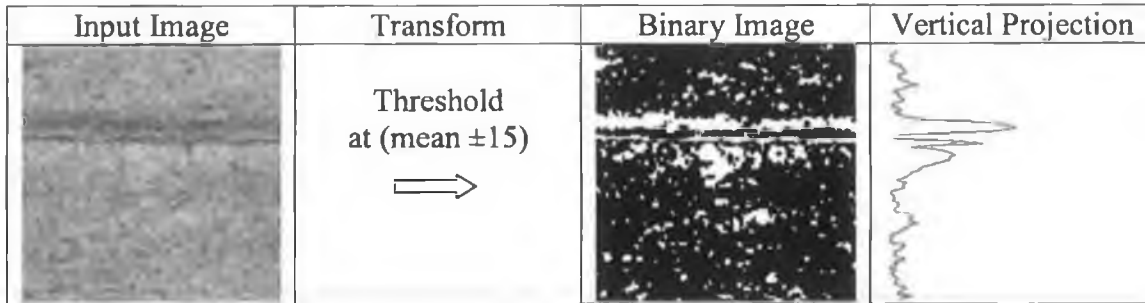


Figure 33: Vertical projection algorithm explanation.

Alternative image processing algorithms were considered. Options included: (i) the design of a morphological filter using a structuring element chosen for this specific fault type, (ii) projections, (iii) application of the Hough transform. A vertical projection was chosen for its simplicity, effectiveness and computational efficiency. The processing steps are explained graphically in Figure 33. The grey scale image is transformed to binary and projected onto the vertical axis. The defect is clearly identifiable as a peak and can be identified using a threshold, shown as a dashed line.

The projections for the images in Figure 33 are illustrated in Figure 34. The horizontal and vertical projections of the grey scale image shown in row 1 are not especially useful. A differential function ($Y = P[n] - P[n-1]$) was applied to the grey scale projections and the mark is identifiable in the graphs shown in row 2. Close examination shows that the thicker portion of the mark is not clearly identified and it is the narrow lower mark that is detected. The binary image was projected and the template mark is clearly identified on the vertical projection shown in row 3.

The algorithm was tested on sample no. 21 (shallow template mark) and on no. 57 (large depression) with good results. The shallow template mark image of sample no. 21 was not detected using the four component algorithm and was detected using the projection algorithm. Acceptable quality portions of the slate were not falsely detected. The vertical projection algorithm worked well. Robustness testing on a large sample set is needed.

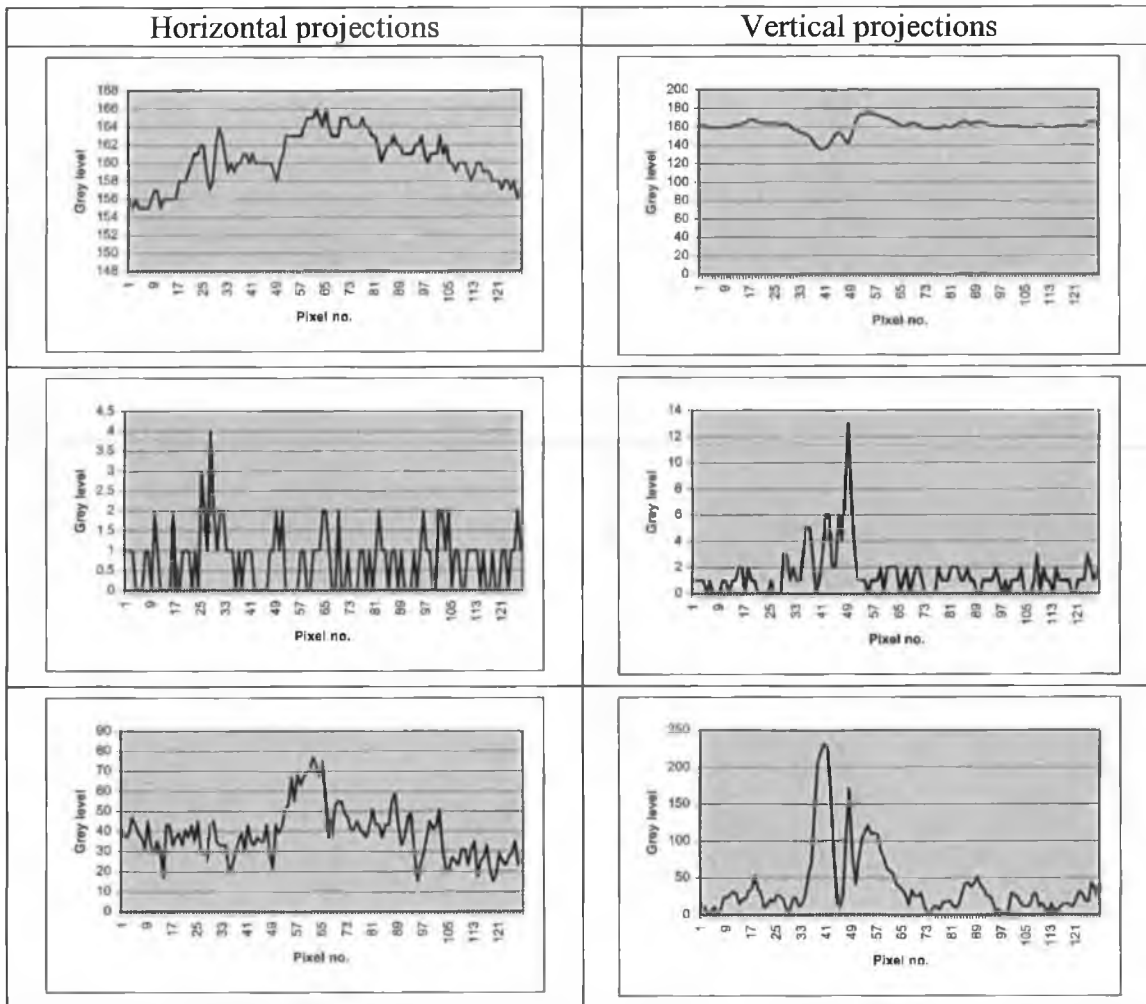


Figure 34: Projection method traces for grey and binary images.

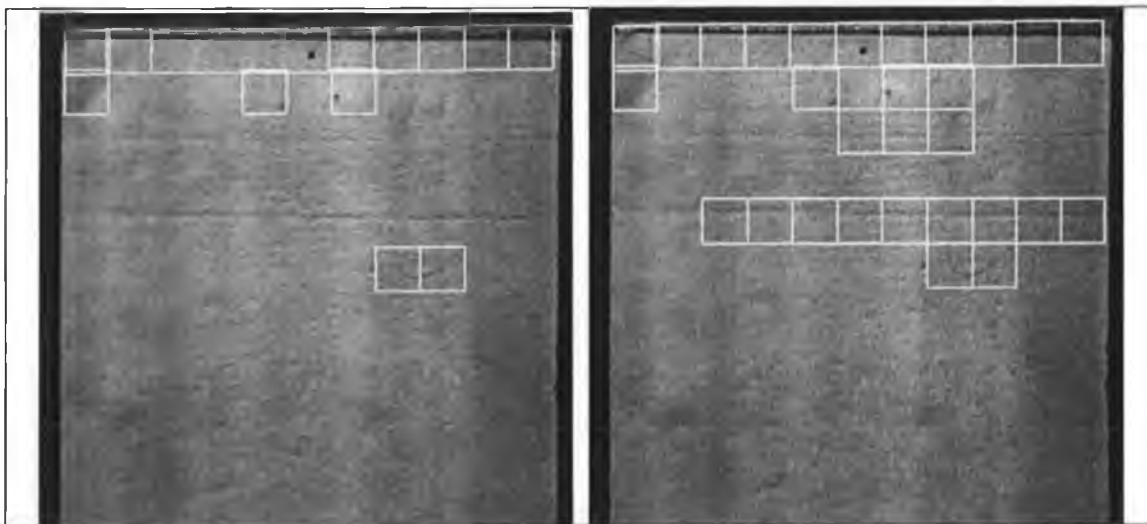


Figure 35: Comparison between the four component algorithm and the projection algorithm for detecting a shallow template mark.

4.6 Algorithm testing

Approximately one hundred samples were received from the industrial partner for analysis. These samples are representative of the defects found on Thrutone and Supercem slates. Decision threshold settings are set at 20% higher than largest observed values for reference slates. A mean threshold of 100 grey levels was used for Supercem samples. The algorithm was implemented in the Neatvision graphical image-processing environment.

4.6.1 Paint faults










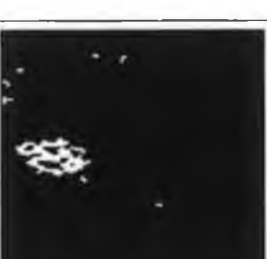


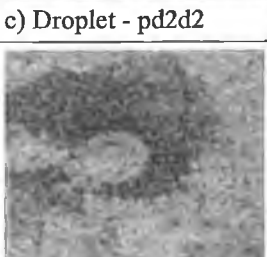


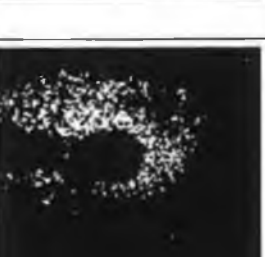
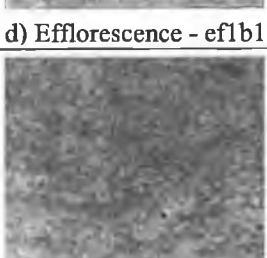



All paint defects can be found using a combination of adaptive mean threshold, adaptive signal threshold and labelling. This algorithm is close to 100% effective for the range of paint defects examined to date.

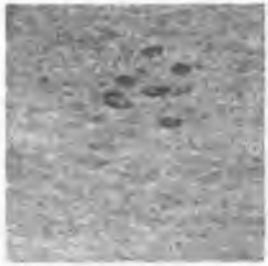















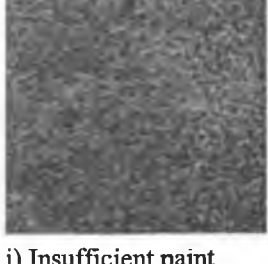



Table 7: Processing loop results for selected paint defects.

Sample	Mean threshold		Threshold (mean- 40)		Threshold (mean- 20)		Threshold and label		Correct result
	Data	Result	Data	Result	Data	Result	Data	Result	Result
Tref12b2	179	No	31	No	2059	No	102	No	Yes
Bref5b2	119	No	5	No	611	No	13	No	Yes
Pd2d2	144	No	86	Yes	2473	No	275	No	Yes
Ef1b1	154	No	1877	Yes	744	Yes	3649	Yes	Yes
Sv1a3	158	No	171	Yes	6015	Yes	1174	Yes	Yes
Lu24b3	167	No	288	Yes	1191	No	300	No	Yes
Pd5a3	128	Yes	13446	Yes	20933	Yes	16404	Yes	Yes
Pdu3d1	187	No	1527	Yes	354	Yes	1773	Yes	Yes
Pd3b2	157	No	204	Yes	1730	No	140	No	Yes
Ip77b2	128	Yes	10	No	1922	No	30	No	Yes
Sv1c3	149	Yes	5	No	781	No	33	No	Yes
Op50	79	Yes	0	No	6	No	0	No	Yes
Barrd3	154	No	0	No	838	No	114	No	No
Barrf2	145	No	41	No	1580	No	444	No	No
Thresh	150		76		2500		510		

The algorithm has potential weak points for very small droplets, barring and for very mildly insufficient paint defects. Very small droplets generate a small number of defective pixels and may be difficult to distinguish from slate texture noise. Insufficient paint defects covering the whole image were detected using the global

mean threshold and marginal samples may be difficult to distinguish from acceptable quality slates.

Input Image	Edge Detection	Threshold at (mean-10) and label	Threshold at (mean-40)
 <p>a) Thrutone - t12b2</p>			
 <p>b) Supercem - b5b2</p>			
 <p>c) Droplet - pd2d2</p>			
 <p>d) Efflorescence - ef1b1</p>			
 <p>e) Shade - sv1a3</p>			

 <p>f) Spots - lu24b3</p>		 <p>not detected</p>	
 <p>g) No Paint - pd5a3</p>			
 <p>h) Debris - pdu3d2</p>			
<p>Input Image</p>	<p>Edge Detection</p>	<p>Threshold at (mean-10) and label</p>	<p>Threshold at (mean-40)</p>
 <p>i) Droplet - pd3b2</p>			
 <p>j) Insufficient paint</p>			

















			
k) Shade - sv1c3			
			
l) Orange Peel - op50			
			
m) Barring - b1d3			
			
n) Barring - b1f2			
Input Image	Edge Detection	Threshold at (mean-10) and label	Threshold at (mean-40)

Figure 36: Image processing image output for selected paint faults.

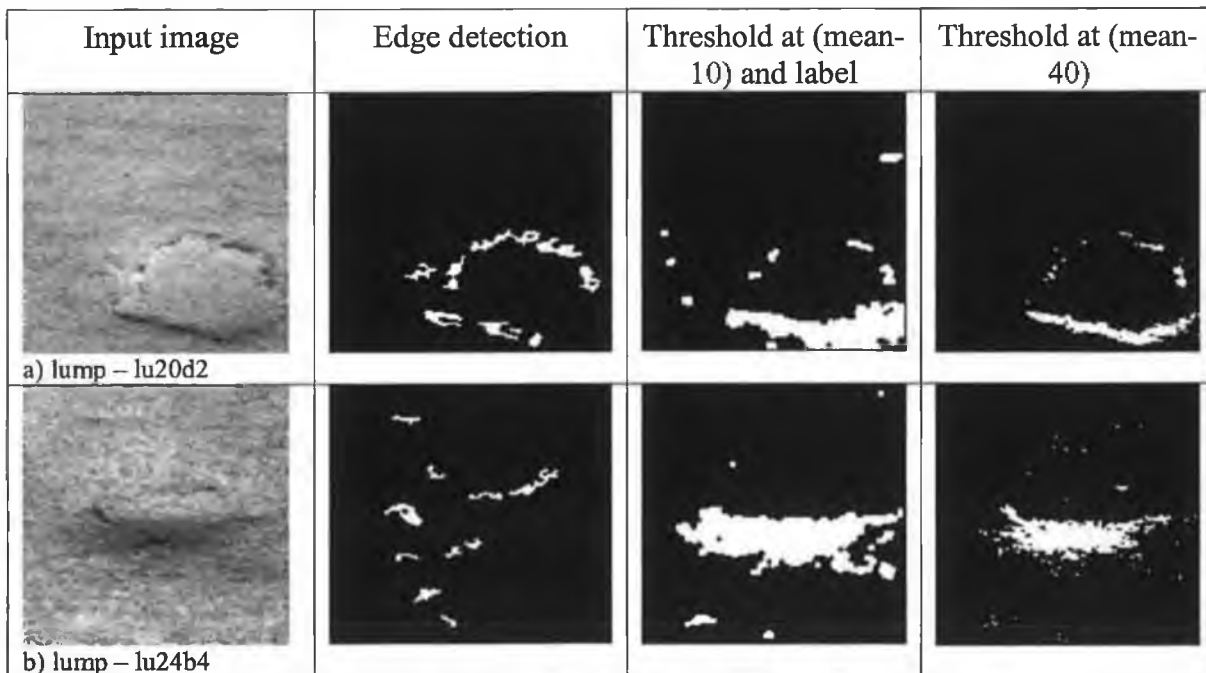
4.6.2 Substrate faults



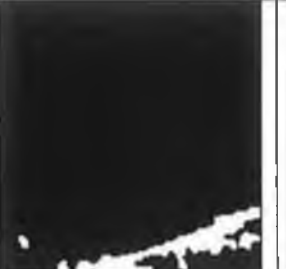
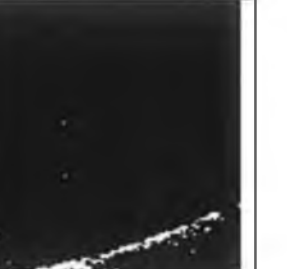







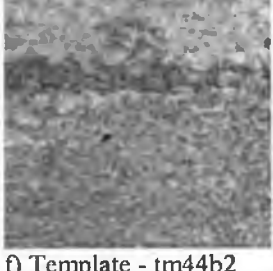

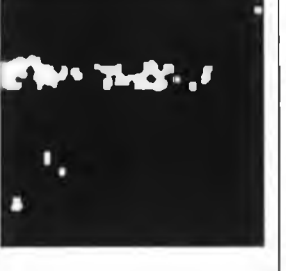

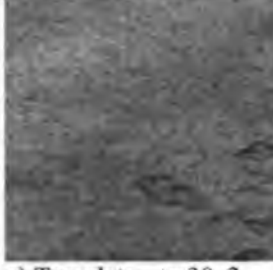







All lumps and larger depressions were found with the adaptive signal threshold. Shallow depressions are detected using the labeling algorithm. Most template marks were successively detected. Template marks proving difficult to detect are shallow or thin marks and most samples at hand were detected by either the edge detection or

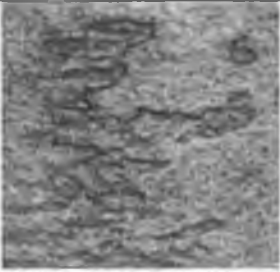























labeling components of the algorithm. All type II template mark samples (60 image sub-sections) were correctly detected.

Table 8: Processing loop results for selected substrate defects.

Sample	Mean threshold		Threshold (mean- 40)		Threshold (mean- 20)		Threshold (mean - 20) and label		Correct result
	Data	Result	Data	Result	Data	Result	Data	Result	
Lu20d2	162	No	634	Yes	2192	No	1073	Yes	Yes
Lu24b4	163	No	1306	Yes	3990	Yes	1992	Yes	Yes
Tm40b2	167	No	485	Yes	3597	Yes	902	Yes	Yes
Tm40c2	163	No	865	Yes	2311	No	1190	Yes	Yes
Tm41e3	159	No	137	Yes	1183	No	118	No	Yes
Tm44b2	153	No	193	Yes	2406	No	497	No	Yes
Dt30e2	130	No	176	Yes	947	No	255	No	Yes
Dt30g3	113	No	304	Yes	2857	Yes	1564	Yes	Yes
Dt31b1	151	No	538	Yes	3485	Yes	364	No	Yes
Dt32b1	145	No	296	Yes	1568	No	637	Yes	Yes
Dt33g1	127	No	0	No	419	No	90	No	No
Dt33g3	115	No	218	Yes	2532	Yes	1089	Yes	Yes
Dt37b4	170	No	238	Yes	2105	No	235	No	Yes
Tm49c2	184	No	364	Yes	3750	Yes	696	Yes	Yes
Thresh	150		76		2500		510		



 c) Template - tm40b2			
 d) Template - tm40c2			
 e) Template - tm41e3		not detected	
 f) Template - tm44b2			
Input image	Edge detection	Threshold at (mean-10) and label	Threshold at (mean-40)
 g) Template - tm30e2			
 h) Template - tm30g3			

			
l) Template - tm31b1			
			
j) Template - tm32b1			
			
k) Template - tm33g1			
			
l) Template - tm33g3			
Input image	Edge detection	Threshold at (mean-10) and label	Threshold at (mean-40)
			
m) Template - tm37b4			
			
n) Template - tm49c2			

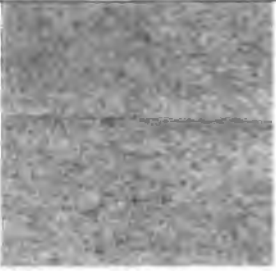




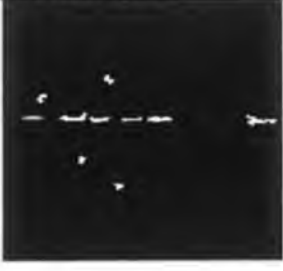


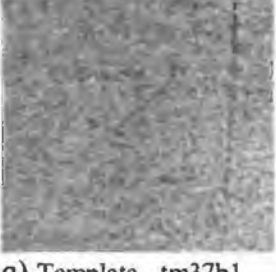











			
o) Lump - lu5a3	not detected		
			
p) Lump - lu5b3			
			
q) Template - tm37b1			
			
r) Lump - ef27e3			
			
s) Depression - ef13da1			
Input image	Edge detection	Threshold at (mean-10) and label	Threshold at (mean-40)

Figure 37: Image processing image output for selected substrate faults.

Processing time varies with sample content from 530 msec to 3000 msec for a 150 x 150 pixel image. A full slate image will be ~3.4MB and processing in Neatvision

could take 8 ~ 10 minutes. Processing speed depends on the number of blobs in an image. Substantial speed improvements will be realized when the algorithm is coded in C and using code segments optimised for speed of execution (refer to Section 4.7.3).

4.6.3 Preliminary robustness testing

Twenty two consecutive reference samples were obtained from the industrial partner. Mean values vary from 159 to 190 with an average mean value of 177 grey levels. Range of means between samples is ± 18 grey levels. The range of mean values of sub-sections of reference images Tref10, Tref11 and Tref27 is from 168 to 194 with average means of 180, 181 and 188 respectively. Range of means within a single slate image is ± 12 grey levels.

The summary of label data taken from several Thrutone reference samples is shown in Table 9. Binarisation thresholds (mean - 10), (mean - 20), (mean - 30) and (mean - 40) were tested. The average data is shown on the left of the table with lowest acceptable values shown in middle of table and highest acceptable values shown on right side of table. Threshold settings were set at 20% higher than the highest values.

Table 9: Summary data for Thrutone reference slates.

Th	Average data			Minimum data			Maximum data		
	CWP	#Blobs	CWP10	CWP	#Blobs	CWP10	CWP	#Blobs	CWP10
10	6234	152	1190	4803	113	744	7717	193	2248
20	1476	32	247	665	12	60	2064	66	425
30	192	3	30	30	0	0	401	11	163
40	21	0	6	0	0	0	63	4	44

Defective slates from the same batch as the 22 references were collected on the same day. Some variations in the shapes of template marks, lumps and droplets were observed. Some of the results are presented in Table 10. The results were very good with all slates being correctly classified.

Table 10: Processing loop results for various substrate defects.

Sample	Threshold (mean- 40)		Threshold (mean- 10)		Edge detection		Threshold (mean – 10) and label		Correct result
	Data	Result	Data	Result	Data	Result	Data	Result	
Tm47b2	207	Yes	8068	No	419	Yes	596	No	Yes
Tm44b2	193	Yes	6612	No	997	Yes	674	Yes	Yes
Tm40b3	314	Yes	3975	No	89	No	1266	Yes	Yes
Tm40c2	865	Yes	5021	No	609	Yes	1650	Yes	Yes
Tm41e3	137	Yes	5423	No	257	Yes	322	No	Yes
Dt30e2	176	Yes	3502	No	568	No	267	Yes	Yes
Dt30g3	304	Yes	5724	No	98	No	3710	Yes	Yes
Dt31b1	538	Yes	7147	No	1218	Yes	603	No	Yes
Dt33g1	0	No	2142	No	2	No	815	Yes	Yes
Dt32b1	485	Yes	6838	No	211	Yes	1819	Yes	Yes
Dt33g3	218	Yes	6459	No	143	No	3236	Yes	Yes
Dt37a1	41	No	6542	No	212	Yes	288	No	Yes
Dt37b3	204	Yes	6894	No	320	Yes	283	No	Yes
Dt37b4	238	Yes	7197	No	363	Yes	331	No	Yes
Tm49b2	192	Yes	7938	No	195	No	804	Yes	Yes
Tm49c2	364	Yes	10377	Yes	271	Yes	1370	Yes	Yes
Lu2c2	402	Yes	10904	Yes	619	Yes	908	Yes	Yes
Lu5a3	3	No	5530	No	161	No	140	No	No
Lu5b3	33	No	8396	No	236	Yes	374	No	Yes
Lu5c3	6	No	7645	No	88	No	499	No	No
Thresh ²⁶	76		9260		202		510		

4.6.4 Discussion

Successful classification of slates as acceptable or defective is greater than 95%. A number of defect images were not detected but the slate was still correctly identified as defective based on other image sections from the same slate. All acceptable quality slates in this study were correctly classified.

Each new set of samples introduces further challenges, some of which may require algorithm modification. It is worth noting that this is a normal part of the robustness testing of any new algorithm.

Processing the slate as a matrix of smaller images has a number of advantages in terms of overcoming the worst effects of mean grey level variations within the slate

and increasing processing speed of the labeling algorithm. One potential shortcoming of this approach is when a small defect that would merit rejection of the slate is divided in two by image subdivision and where the halved reject is too small to be considered as a defect. This problem will occur in a small number of cases and a solution can be devised. Potential solutions include processing of overlapping image sections and comparing results of neighbour image sections.

Grading of a slate as accept or reject is based on an area count of either the area of the largest blobs in the image or all the defective pixels in an image. More sophisticated techniques can be considered. These include measuring the length, width and fractal perimeter of each blob. A vertical or horizontal projection of defect pixels onto the end line may also produce useful distinguishing features. The relative position of each blob within the image can also produce distinguishing features. These techniques have not been explored in depth as the defect pixel count is producing good results. It is useful to be aware that alternative grading possibilities are available should improvements to the current technique become necessary.

Tests using grey level difference methods and local binary patterns did not produce useful results. The reason is thought to be due in part to the variation in slate texture introduced by uneven transport of the slate. The efficacy of the grey level difference method was adversely affected by grey level variation between samples and within samples.

4.7 Transfer to the production prototype

The image-processing algorithm was ported from the Neatvision environment to the MS Visual C++ 6.0 environment and expanded to automatically cater for slate edges, nail holes and to process a full slate width image. The slate is segmented from the background belt conveyor using a simple threshold. The belt material and color were carefully chosen so as not to reflect light into the camera. The slate is processed in small sub-images of size 128 x 128 pixels. Each sub-image is checked for *global mean threshold*, *adaptive signal threshold*, *labeling* and *edge detection and labeling*. A result is produced for each processing component and these results are compared to

²⁶ Thresh = Threshold setting. A data figure exceeding the threshold indicates a defect.

experimentally determined thresholds. If any result exceeds the threshold settings then the sub-image is considered defective. Test result output is in the form of a text file and an image of the slate with white boxes drawn around the defect sections.

4.7.1 Slate edge detection and region to inspect selection

The developed algorithm was modified to automatically detect slate edges and to set the inspection region. An optical proximity sensor was used to indicate the slate is close and to initiate a frame capture sequence. Cutting slots in the conveyor base facilitated slate edge detection. The belt width is narrower than the slate width so that these slots are in the image area of the camera when no slate is present. This facilitates fast segmentation of the slate from the background. The camera signal from these slots is close to the camera black level when no slate is present and there is a very sharp signal transition when a slate arrives in the field of view. A threshold operation is sufficient for edge detection. The front and side edge lines are tracked until edge end positions are found. These edge end positions will be in the same location when the corners are correctly formed. When the edge end positions are significantly different, it indicates the corner is damaged. A similar process is implemented for the end edge corners.

The first approach used to verify that the slate edge is defect free is explained here. A straight line was drawn between the detected corner positions and the inspection start locations were set relative to this line. Rotation was accounted for using the equation for a straight line. The evenness of the edge was checked using a distribution check of the edge locations. A well-formed edge has a narrow distribution with a high peak and an uneven edge has a wide distribution. The four component algorithm is then applied and an edge fault such as a bit of missing material will be detected using the adaptive signal method.

This edge checking method worked well for perfectly flat slates but resulted in false triggers for slates having the 5 mm depth profile variation. The image follows the curve of the slate and false triggers occur when there is too much error between the assumed straight edge and the imaged curved edge. The devised solution was to divide the edge into short line lengths of 30 mm length and to verify the exact edge

location for these short segments. This necessitates segmentation of the slate image from conveyor belt material and a simple threshold is effective for most slates. However, the threshold method is unreliable for unpainted slates as the signal response of unpainted slates is not significantly different to that of the conveyor.

4.7.2 Nail hole inspection

Nail holes are detected by a threshold operation in the image section where the holes are expected. The algorithm finds the front left corner position and begins searching for the nail hole at a fixed offset from the detected corner location. There is some variation in the exact location of the holes in the image due to rotation and the variable forward motion of the conveyor. This is especially obvious for the hole located close to the end edge and the search area is increased to ensure the hole can be found. The threshold method of hole detection works reliably because the signal generated by nail holes is greater than that generated by any defect type.

When a nail hole is found, a simple area count check is made to ensure a minimum size for the hole. Neighbouring image data is then transferred to cover and completely eliminate the hole from the image. The defect detection algorithm can therefore be applied to these sections of the image without fear of false trigger generation.











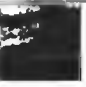


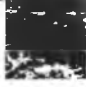
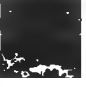



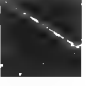

4.7.3 Tests using prototype inspection system

Images of slates were captured at factory production line speeds on the production prototype described in Section 3.9. The original samples were retested using the production prototype and it was found that the threshold settings had to be increased by 30% so as to ensure reference slates were not miss-classified as defects.

Enlargement of sections of slate images showing input image, result image and data for each processing section are shown in Table 11. The numbers to the right of the images are the processing result which is compared to the threshold shown on row 1. The result column has a coded result. A code of 8, as shown in Table 11, indicates

the label test failed and a code of 18 indicates that both the (mean - 40) threshold test and the edge test failed.

Table 11: Image and data output for selected defect types.

Sample	Input	(Mean-13)	Label	Edge	Result
Thresholds		3500	800	60	
No 18-14 Reference		 444	 42	 0	OK
No 15-14 Efflorescence		 2560	 1109	 26	Fail 8
No 15-34 Efflorescence		 3713	 2242	 91	Fail 28
No 16-13 Template mark		 2560	 1109	 26	Fail 8
No 16-30 Template mark		 1502	 447	 975	Fail 18

The detection results using the production prototype were generally in agreement with those found during the experimental phase of the project. Major variations were that the barring defect is now undetectable because the threshold settings are further removed from the mean grey level of a sub-section and shade variation defects are no longer picked out clearly using the adaptive signal threshold, but are always detected using the labeling test. All other defect types are detected and reference slates accepted. Processing time for reference slates is now 12 seconds. The processing time required for all of a defective slate is up to 30% longer than for a reference slate and the time increase is in proportion to the type and severity of the defects. However, processing can be terminated when a defect is found and the time required to process a defective slate will usually be less than that required for reference slates.

The image processing algorithm was optimised for speed using a combination of fast algorithm implementations available in the VSL and the Intel image processing library (IPL) routines. The results obtained using the IPL routines differ marginally from those obtained using standard C language routines and some modifications to threshold settings were required. The morphological filter applied after the IPL Sobel edge detector was also modified to ensure satisfactory results. The average

processing speed was reduced to 3 seconds per slate. The target speed will be met when suitable processing power is available. The project was progressed with robustness testing on more than 300 slates collected from the production line. This work is described in detail in Chapter 5.

5. Robustness Tests

5.1 Introduction

This section of the report details robustness tests on reference and defect slates. Colour slates were also tested. The reference slates had already passed inspection at the factory and were packed in bundles. The defective slates had been rejected by the factory inspection procedures.

5.2 Experimental details

The conveyor speed was set at 38 m/min and camera exposure was set to 400 μ sec giving a scan frequency of 2,500 Hz. The cross direction resolution was 0.221mm and the moving direction resolution was 0.244 mm. The shorter exposure time requires an increase in illumination intensity. Both lamp controllers were tuned to 100% output for most of the tests. Bulbs were changed on the final week of tests and an intensity setting of 90% was sufficient when using new bulbs.

Full length, slate images were captured to buffer memory and inspected using the development program "inspectorv2". The reference slate TR14 (imaged in February) was used as a training image. The shading compensation curve was generated from this Thrutone reference sample and applied to all the test images.

All slates were tested several times. Many variations on defect types and sizes were presented and four new defect types were discovered. The new defect types are wax marks, nozzle drip (like barring in appearance), surface cracks and cracks in slate. Several small modifications were made to the algorithm and there was a significant level of experimentation with the various threshold settings. The optimum settings were selected with a view to minimizing rejection levels of acceptable quality slates while detecting defective slates. The majority of slates were tested again using the final threshold settings.

The threshold settings for converting the slate image from grey scale to binary data are as follows.

- Adaptive signal threshold setting (mean – 45) and (mean + 60)
- Adaptive signal threshold setting for labeling (mean – 15) and (mean + 15)
- Edge detector output threshold setting 100

The threshold settings for deciding if an image sub-section is defective are as follows.

- Global mean threshold test (Thrutone) 107
- Global mean threshold test (Supercem) 97
- Adaptive signal threshold test 38
- Adaptive signal threshold pre-label test 3500
- Adaptive signal threshold & labeling test 900 (1350 for edge sections)
- Edge detector and labeling test 80

The threshold setting for Supercem slate grey level mean test was 120.

5.3 Experimental results

Table 12: Summary of inspectorv2 inspection results.

Type	Correct	Incorrect	Correct result
Reference excl. wax	147	1	99%
Reference incl. wax	134	14	91%
Defective	155	4	97%

5.3.1 Reference slates

Reference slates were collected in packed bales from the industrial partner on three occasions in March and April, 2002. 15 Thrutone samples were collected for the first test. 20 Thrutone and 2 Supercem samples were collected for the second test. 30 Thrutone, 40 Supercem and 38 assorted colour samples were collected for the third test.

The mean grey level data is shown in Figure 38 for the first sixteen references. The global mean threshold settings were selected based on this data. The grey level mean value of the two reference Supercem samples no. 152 and no. 153 was 138 and the image sub-section variations were similar to that of Thrutone samples. The global mean threshold settings for Supercem samples were set 10 grey levels lower than

those set for Thrutone. Also shown in Figure 38 are the maximum and minimum grey levels measured for any image sub-section. The mean grey level is 148 ± 10 grey levels and the range for image sub-sections is 148 ± 31 grey levels. There are 140 image sub-sections per slate.

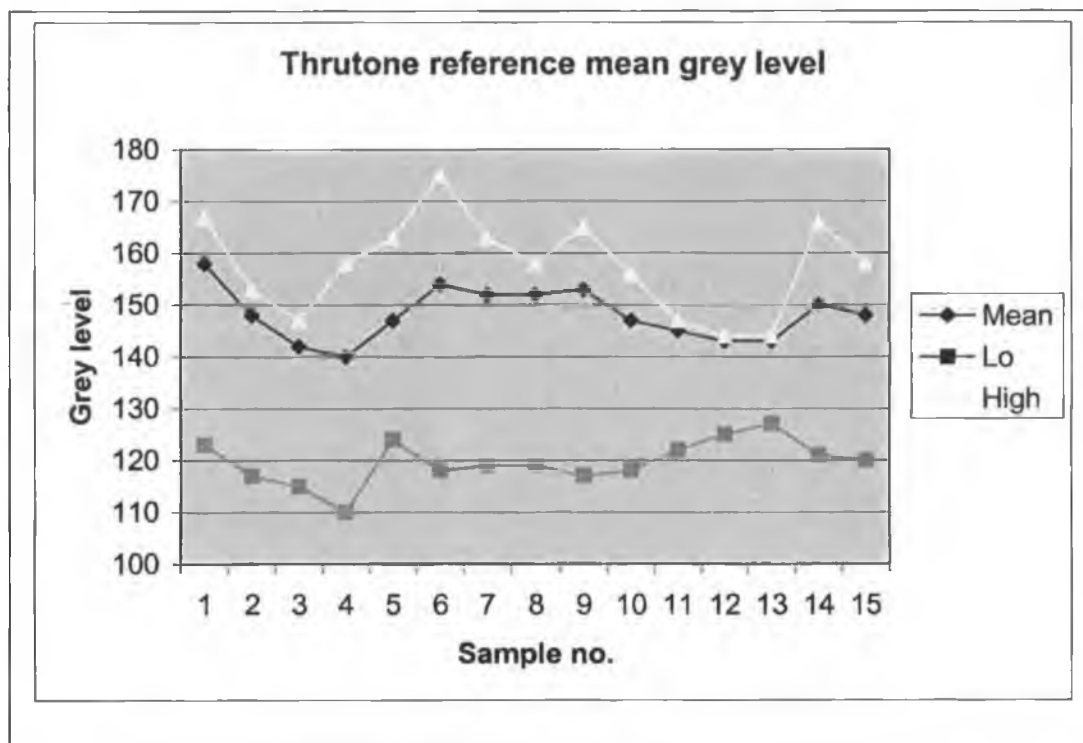


Figure 38: Mean grey levels for reference images.

Many of the reference slates contained handling marks introduced during transportation and handling despite being packaged for transportation. The slate inspection program did detect the larger and more obvious scratches and scuff marks. These marks would not have been present on the production line and these samples were considered as having been accepted. A small number of these reference slates had defects and with one exception, these defective reference slates were correctly detected by the developed slate inspection system. The one falsely accepted defective sample was accepted because the droplet was divided in half between two image sub-sections and the halved defect size was not sufficiently large to trigger a defect.

Nine per cent of the reference slates were rejected and the reason for failure was due to the detection of wax²⁷ marks. It has not yet been clarified whether these²⁸ wax

²⁷ A new type of wax was introduced on the paint line process in January, 2002. A large splash of wax on the surface is a cause for rejection.

marks are introduced during handling and transportation or whether they are present on the production line. This glossy wax mark has a spectral profile similar to that of droplets and the inspector cannot distinguish them at this time.

The efficiency of the inspector with respect to accepting good quality slates is either 91% or close to 100%, depending on how one chooses to interpret the wax mark detection.

Table 13: Summary of inspection of reference slates.

Type	Qty	Correct result	Fail reason	Defect qty	Defect type
Thrutone	38	35	Wax marks	1	Lump
Supercem	2	2		0	
Thrutone	30	28	Wax mark & droplet	2	Droplets
Supercem	40	32	Wax marks	3	Efflorescence
Colour	38	36	Wax marks	6	Droplet, debris, depression, edge mark
TOTAL	148	134 (91%)		12 (8%)	

Three out of 38 reference samples were classified as defective giving a 92% correct classification rate. The three fails were for wax marks. A further two samples failed due to detection of scuff marks introduced by handling. These samples were considered as having been accepted by the inspector as scuff marks would not be present on the production line.

Thrutone references are no. 128 through to no. 142 and no. 78. No. 130 was considered defective because of a wax mark on its left edge. No. 78 was considered defective because of a wax mark and a thumb-print close to the left edge

Thirty Thrutone reference samples were collected on April 19. Two pieces had small droplet defects of which one was detected by the inspector. The second droplet was not detected because it was divided in half between two image sub-sections and the halved defect size was not sufficiently large to trigger a defect. One good quality

²⁸ This wax mark appears as a glossy spot on the slate surface and is not a reason to reject the slate. There is a suggestion that this wax mark is caused by friction between slates in a bundle and that it is not present on the production line. This theory is subject to verification.

slate was incorrectly classified. 28 of the 30 samples were correctly marked as acceptable or defective giving a 93% success rate.

Forty Supercem reference samples were collected on April 19. Three pieces had efflorescence type defects and were identified as being defective. Eight slates were classed as defective because wax marks were detected. 32 of the 40 samples were correctly marked as acceptable or defective giving an 80% success rate. The wax mark defects caused as many as 7 image sub-sections on a single slate to be marked as defective. It is possible these marks were introduced during transport.

Thirty-eight coloured reference slates were collected on April 19. The colour range was grey, light grey, red, orange, brown, chocolate brown and light green. The reflected light intensity varied with slate colour and the lamp controller intensity setting was varied to facilitate image capture at similar intensity settings for all colour samples. Six of the 38 samples had defects including droplet, paint debris, depression and edge damage. 36 of the 38 samples were correctly marked as acceptable or defective giving a 95% success rate. The incorrectly classified samples were due to detection of wax marks.

Eleven of the 108 samples collected on April 19 had defects even though the human inspectors had passed them as being of acceptable quality. The inspector detected ten of these 11 defects. Wax marks generate false triggers and the inspector classified 11 of the 108 samples as being defective for having wax marks.

5.3.2 Defective slates

159 new defective slates were inspected during the robustness tests. The slates were collected from different batches of production spanning a three month time frame. Several size variations were discovered in defect shapes. Most of these size variations were correctly identified as being defects.

Large and shallow depressions presented difficulties. Some samples were not detected because the signal from the image capture system had poor signal amplitude. However, they were detected when imaged with the 300 mm edge facing forward.

The previously unseen nozzle drip defect was very difficult to detect, as were many of the shade variation samples. In many cases, large area defects spanning 20 or more image sub-sections might be detected on only 2 or 3 sub-sections. Detection results by defect type are presented in Table 14 and details of the robustness tests on defective slates are given in Appendix A.

Table 14: Summary of defect detection rates.

Type	Fail qty	Pass qty	Correct result
Missing paint	0	4	100%
Insufficient paint	0	9	100%
Efflorescence	0	15	100%
Shade variation	0	12	100%
Nozzle drip	0	14	100%
Droplets	0	8	100%
Dust	0	4	100%
Wax	1	7	87%
Template marks	2	33	94%
Template marks II	0	5	100%
Lumps	0	13	100%
Depressions	1	3	75%
Bad edge	0	18	100%
Misc. types	1	12	92%
TOTAL	5	157	97%

5.4 Additional experiments and results

5.4.1 Testing with slate rotated 90°

Two defect types were not well detected when imaged with the 600 mm edge facing forward. These defects are shallow template marks aligned with direction of movement of the conveyor and large area, shallow depressions where the grey scale distribution varies slowly. It was thought detection could be improved if the slate was imaged with the 300 mm edge facing forward.

These samples were tested with the slate rotated 90° to see whether detection is improved. The detection of large depressions is improved considerably. The image capture of shallow template marks is also improved and the defect is now clearly visible in the image. The detection capability has improved but detection is not

assured in all cases. The inspection output for sample no. 21 (shallow template marks) and no. 57 (large depression) is shown in Figure 39.

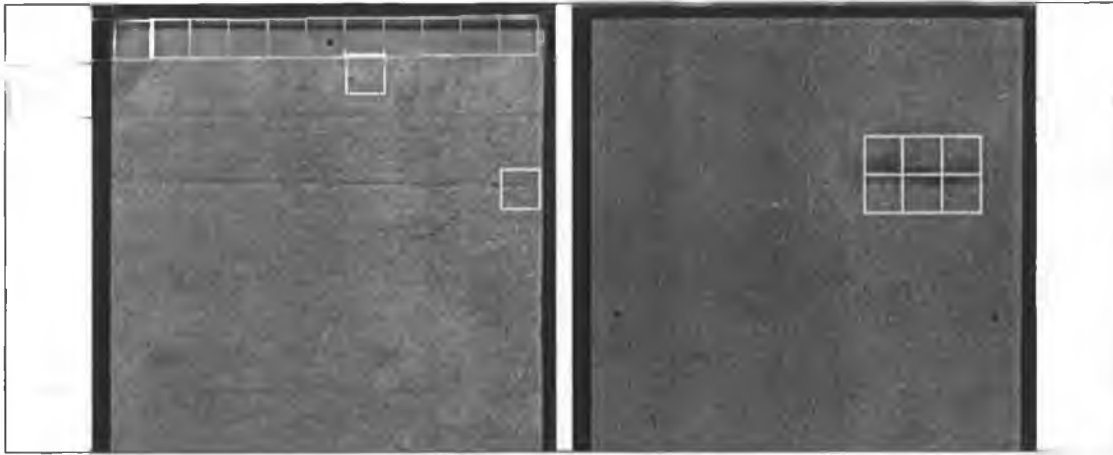


Figure 39: Inspection output for samples with 300 mm edge facing forward.

5.4.2 Full slate imaging

The full slate was imaged at lower resolution using the same equipment to investigate the impact on detection capability. The camera to slate separation was increased by ~300 mm to enable the full slate image to be captured. The cross-direction resolution is now 0.303 mm. Thrutone reference sample no. 251 was used as a training image from which the shading compensation curve was calculated.

Table 15: Inspection results for samples tested when full size slate was imaged.

No.	Type	Result	Comment
249	Reference	OK	
250	Reference	OK	
33	Large depression	Defect	
57	Large depression	Defect	
150	Small lump	Defect	
164	Efflorescence	Defect	
173	Nozzle drip	Defect	
188	Debris and nozzle drip	Defect	
194	Lump	Defect	
207	Efflorescence	Defect	Also depression
TM41	Template mark	Defect	Tiny lumps not detected

Eleven samples were tested and all were correctly classified as acceptable or defective. The cluster of tiny lumps on sample TM41 was not detected because the resolution setting of the imaging system is now too low.

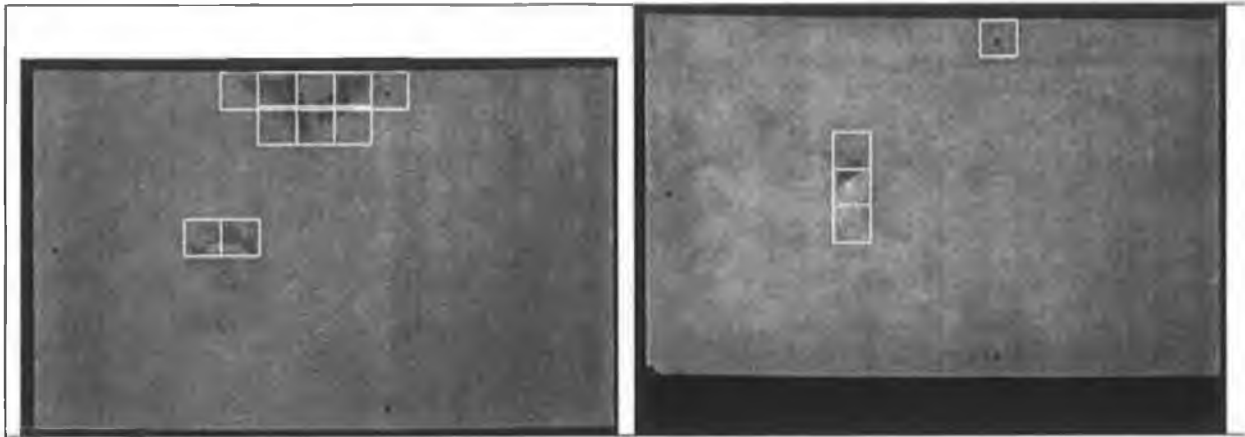


Figure 40: Inspection output of full slate for sample no. 164 and no. 194.

5.4.3 Conveyor speed characterization

The constancy of conveyor speed was measured by repeatedly imaging the same slate. The timing of image capture is measured by a digital controller and is considered to be repeatable.

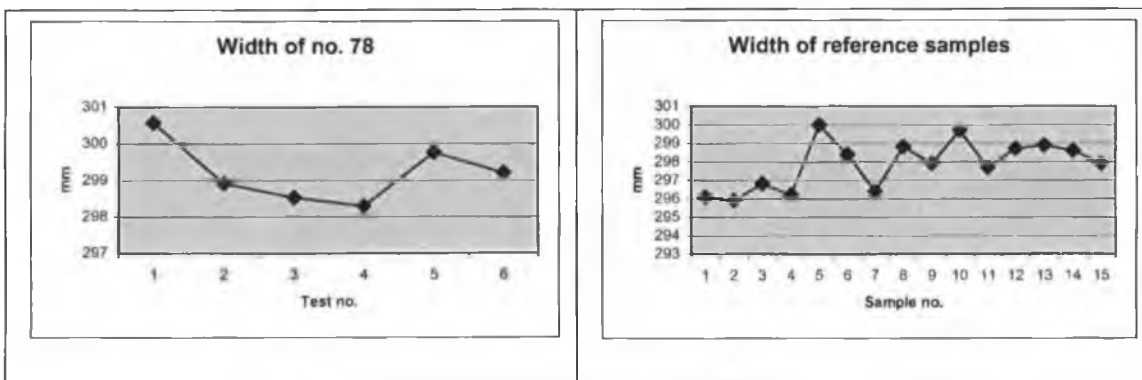


Figure 41: Graphs of variation in slate width measurements.

Sample no. 78 is 300.7 mm wide. Five of the measurements on sample no. 78 (taken over a two hour time frame) are shown in Figure 38.a. The variation is within 1% of expected value. The non-repeatability of width measurements is assumed to be due to conveyor speed variations. The measurement of 16 samples is shown in Figure 41.b where a measurement variation of 1.3% was observed.

This open-loop approach to slate width measurement is not sufficiently accurate or repeatable. If a slate of width 298.0 mm was measured with a 1% negative error, the

inspector would produce a width result of 295.02 and incorrectly classify the slate as being too narrow. A more accurate approach involves attaching a speed encoder to the conveyor and measuring the distance travelled (with respect to time) from slate front edge to slate end edge. An alternative approach, made possible on the latest frame grabbers, is to feedback the speed encoder signal to the digital camera exposure control. The exposure time of the camera is varied in response to conveyor speed variations, thereby ensuring constant pixel moving direction dimension. With constant pixel size assured, slate width can be measured accurately.

5.5.4 Effect of slate colour on inspection capability

There are eight different coloured slates manufactured at this site. These are black, grey, light grey, green, red, orange, brown and dark brown. Six samples of each colour were collected and tested on the inspector. The mean grey level varies with colour and brighter colours such as light grey produce a more intense response than darker colours such as dark brown. The mean grey levels are shown in Figure 42 and are repeatable for each colour.

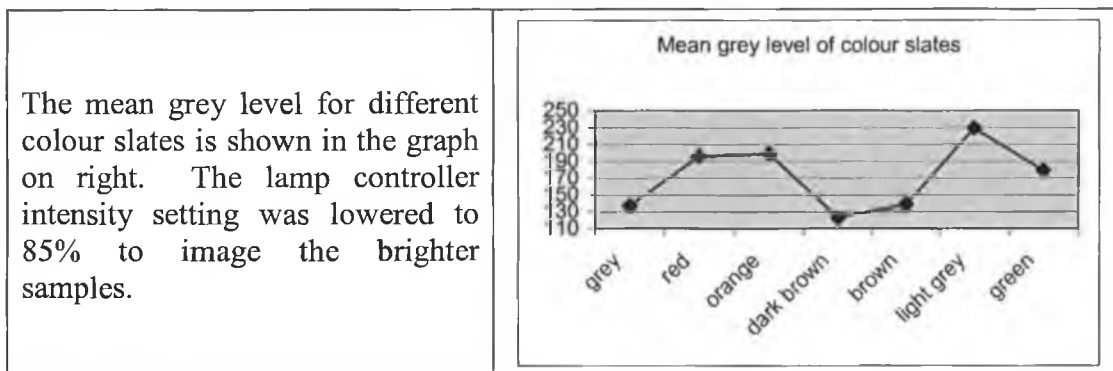


Figure 42: Mean grey levels of colour slates.

The lamp controller has an intensity control function and this was used to normalise the mean grey level at 140 grey levels for all samples to test the inspection algorithm. Most of the slates were references and these were correctly accepted as being of good quality. A small number had defects and these defects were correctly identified. The conclusion of this test is that the inspection algorithm can be applied to inspect the colour range.

5.6 Discussion

The robustness of the inspector image capture, opto-mechanical arrangement and the image processing algorithms has been verified.

The devised system can inspect Thrutone, Supercem and coloured slates equally well.

Wax mark detection as a defect type is the principal source of erroneous classification of good quality slates as defective. The wax mark appears brighter than the background and has a signal profile similar to that of paint droplets. There exists the possibility that the wax mark is introduced by handling and transportation and will not be present at the inspection station.

All defect categories can be detected. Gross defects are always detected. Smaller size defects such as shallow template marks and tiny lumps are at the margin of detection capability of the inspector. Very low contrast defects such as nozzle drip and some shade variation defects are also at the margin of detection capability of the inspector.

Changing the resolution of the image capture arrangement does not affect the detection of gross defects and the acceptance of good quality slates. The minimum defect size detectable is reduced in proportion to the drop in image capture resolution.

6. Conclusions

Test results demonstrate that automating the visual inspection of painted slates can be achieved and installation in a factory is a realistic target. Greater than 95% of slates are correctly identified as being acceptable or as being defective.

Robustness testing of the algorithm in factory-style conditions was an important part of the development process. It made it possible to verify that the devised opto-mechanical system and the image-processing algorithm is feasible to be implemented in an industrial environment.

A small number of the less obvious defect types will not be detected with this implementation. The addition of further image capture arrangements would enable some of these un-imaged defects to be detected. The industrial partner has indicated that these defects make up a very small percentage of the total number of rejects.

The industrial partner now has the technical information on which to base a decision on whether to proceed with the next steps towards procurement of an automated inspection system for the painted slate product.

6.1 Proposed next steps to commercialisation

The devised automated inspection solution can be given serious consideration as a replacement for the existing manual inspection system. Challenges to be overcome to achieve commercialization of this research include some research and a lot of development work.

An extensive robustness test involving several thousand slates is recommended. Some surprises were found during tests on 300 slates, including the discovery of previously unseen defect types. Testing on a very large sample set is recommended to ensure the full range of defect types and sizes is known and can be detected. It is further recommended that testing be carried out beside the production line so that surface damage introduced by handling and transportation is not a factor in the tests. Variations in slate color and gloss levels will have an effect on inspection and are

worthy of investigation by testing samples over several months. It is likely that algorithm modifications will be needed to facilitate the detection of previously unseen defect types and defect sizes.

A small number of defect types are not detectable unless the slate is rotated 90°. It would be useful to determine an accurate percentage of slates that can only be detected in this way.

The prototype inspector will need to be tested in line and be programmed to cope with a continuous line of slates and a variable inter-slate separation. A smoother transport mechanism is recommended to achieve further reductions in vibration and slate rotation. In-line testing is also recommended, as part of the development work. An automated inspection system will have to be programmed to deal with mechanical issues on the production line such as slates on top of each other and slates arriving side by side. A mechanical system for rejection of defective slates will be required. An interface between the inspection system and the reject mechanism will be needed so that the inspection system can control the timing of the reject mechanism.

A five-fold increase in processing power is needed to ensure processing of a slate image is completed at production line speeds. This speed increase should be achievable using a combination of a fast PC, a fast frame grabber card having on-board frame store and fast DMA transfer capability and further optimization of the software.

6.2 Equipment recommendations for industrial version of inspector

The prototype inspection system was built using standard system components that are readily available from industry suppliers. An industrial version can also be built from standard components. These components will need appropriate external enclosures to protect them in the factory environment.

While it is difficult to specify the equipment prior to conducting a rigorous system engineering analysis, the principal selections will relate to image resolution and

processing power. Either a 2K pixel or a 4K pixel camera will be used depending on minimum defect size to be detected. There are several possible design options available for processing the slate image. I recommend one of the following two approaches as industry standard components can be used. The first is to add significant on-board processing power to the frame grabber and the second is to select a frame grabber having 16 MB frame store memory and fast DMA transfer capability. In the latter case, all processing is carried out using the PC resources and a powerful PC is recommended.

Table 16: Equipment recommendations for factory inspector.

No.	Item	Model
1	Conveyor	Smoother type than currently in use and with centralizing guides on both sides of the slate.
2	Camera	Either a single 4K pixel line-scan or two pieces 2K pixel line-scan to achieve desired resolution.
3	Lens	Use a machine vision model.
4	Frame grabber	Either a Euresys Multi Plus which has on-board processing or a frame grabber having a 16MB frame-store and fast DMA transfer function such as a Coreco CamLink.
5	Fiber-optic light line	Fostec 30" triple entry with focusing lens.
6	Lamp controllers	Three units of Fostec DCRIII.
7	PC	Use a fast PC (e.g., Dell P4, 2GHz) with 128MB or 256MB fast RAM and running Windows NT.

6.3 Further applications of an automated inspection system

The algorithm structure gives some possibility to identify many of the defects by type. Defect type classification introduces the possibility to use the inspection system not only as a quality control tool but also as an early warning tool for process problems. In particular, large area paint faults such as insufficient paint, shade variation, orange peel and efflorescence have the possibility to be distinguished by type.

Substrate faults are introduced during the forming process. No action is possible on the paint process line as the slates are formed several days prior to painting. Inspection of slates during the forming process would be useful for detection of repetitive faults. Typical faults worthy of inspection are the absence of nail holes,

narrow slates and repetitive template marks introduced when the mould becomes contaminated.

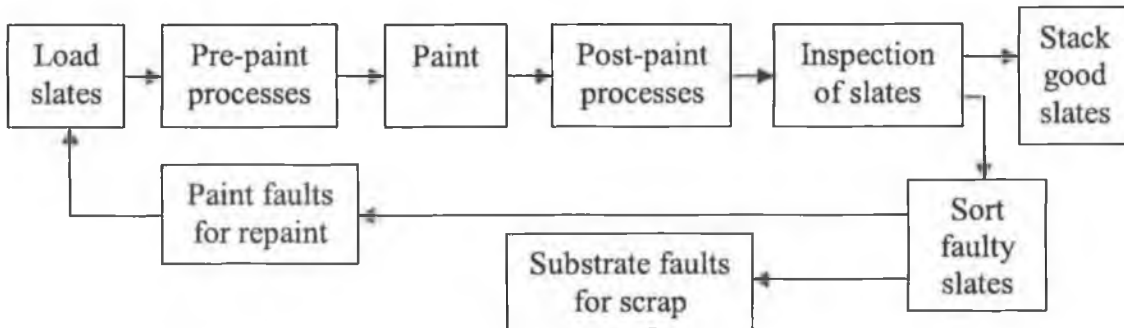


Figure 43: Paint process line with automated sorting of defective slates.

Paint faults can be categorised as random and repetitive. Random fault types include debris, droplets, spots, missing paint and wax splashes. Repetitive paint fault types include insufficient paint, shade variation, nozzle drip and efflorescence. An early warning of the presence of these fault types can be used to minimise the production of defective slates.

The repetitive paint faults are large area and therefore detectable using diffuse lighting techniques and low resolution camera systems. This method of image capture is not particularly sensitive to angle of inspection. An inspector could be placed immediately after the paint booth and act as an early warning system for paint defects.

References

Boukouvalas C., De Natale F., De Toni G., Kittler J., Marik R., Mirmehdi M., Petrou M., Le Roy P., Salgari R., Vernazza G. (1997), - "An integrated system for quality inspection of tiles", Proc. International Conference on Quality Control by Artificial Vision OCAV'97, pp 49-54, (Toulouse, France).

Boukouvalas C., Kittler J., Marik R., Petrou M. (1994), "Automatic grading of ceramic tiles using machine vision", Proc. of IEEE Intl. Symposium on Industrial Electronics, pp 13-18.

Boukouvalas C., Kittler J., Marik R., Mirmehdi M., Petrou M. (1995), - "Ceramic tile inspection for colour and structural defects", Proc. AMPT '95, pp 390-399.

Boukouvalas C., Kittler J., Marik R., Petrou M. (1997), "Automatic colour grading of ceramic tiles using machine vision", IEEE Transactions on Industrial Electronics, vol. 44, no. 1, pp 132-135.

Boukouvalas C., Kittler J., Marik R., Petrou M. (1999), - "Colour grading of randomly textured ceramic tiles using colour histograms", IEEE Transactions on Industrial Electronics, vol. 46, no. 1, pp 219-226.

Davies E.R. (1997), - "Principles and design graphs for obtaining uniform illumination in automated visual inspection", Proc. 6th IEE Intl. Conf. on *Image Processing and its Applications*, Dublin (14-17 July), IEE Conf. Publication no. 443, pp. 161-165.

Davis L., Rosenfield A., Weszka J. (1997) "Region extraction by averaging and thresholding", IEEE Transactions on SMC-5, pp. 383-388.

Finney G., Gomm B., Williams D., Atkinson J. (1994), - "Inspection of ceramic tableware for quality control using a neural network vision system", Proc. of SPIE 2193, pp 145-154.

Fioravanti S., Fioravanti R., De Natale F., Marik R., Mirmehdi M., Kittler J., Petrou M. (1995), - "Spectral and rank order approaches to texture analysis", European Transactions on Communications, 6(3), pp 287-300.

Haralick R. (1979), - "Statistical and structural approaches to texture", Proc. of the IEEE, vol. 67, no. 5.

Haralick R., Shanmugam K., Dinstein I. (1973), - "Textural features for image classification", IEEE Transactions on Systems, Man, and Cybernetics, vol. 3, no. 6.

Harwood D., Ojala T., Pietikäinen M., Kelman S., Davis L. (1995), - "Texture classification by center-symmetric auto-correlation, using Kullback discrimination of distributions", Pattern Recognition Letters, vol. 16, pp 1-10.

Huet B. and Hancock E.R. (1996), - "Structural indexing of infra-red images using statistical histogram comparison", Proc. IWISP '96, pp 653-656.

Ghita O. (2000), - "A real-time low-cost vision sensor for robotic bin picking", PhD Thesis, DCU.

Julesz B. (1965), - "Texture and visual perception", Scientific American.

Kälviäinen H., Kukkonen S., Hyvärinen T., Parkkinen J. (1998), - "Quality control in tile production", Proc. of SPIE 3522, pp 355-365.

Kauppinen H. (2000), - "A two stage defect recognition method for parquet slab grading", IAPR Barcelona, Spain.

Kittler J., Marik R., Mirmehdi M., Petrou M., Song J. (1994), - "Detection of defects in colour texture surfaces", IAPR Proc. Of Machine Vision Applications 94, pp 558-567.

Laitinen T., Silven O., Pietikäinen M. (1990), - "Morphological image processing for automated metal strip inspection", SPIE 1350, pp 241-250.

Marik R., Petrou M., Kittler J. (1997), - "Bump and depression detection on ceramic tiles", IEEE Colloquium (Digest) no.41, pp 5/1-5/3.

Müller S. and Nickolay B. (1994), - "Morphological image processing for the recognition of surface defects", Proc. of SPIE 2249, no. 58, pp 298-307.

Ojala T., Pietikäinen M., Harwood D. (1996), - "A comparative study of texture measures with classification based on feature distributions", Pattern Recognition vol. 29, no.1, pp 51-59.

Ojala T., Pietikäinen M., Nisula J. (1996), - "Determining composition of grain mixtures by texture classification based on feature distributions", Intl. Journal of Pattern Recognition and Artificial Intelligence vol. 10, no.1, pp 73-82.

Ojala T., Pietikäinen M., (1999) - "Unsupervised texture segmentation using feature distributions", Pattern Recognition vol. 32, no.1, pp 477-486.

Peñaranda J., Briones L., Florez J. (1997), - "Colour machine vision system for process control in ceramics industry", Proc. of SPIE 3101, pp 182-192.

Petrou M. (1993), - "Optimal convolution filters and an algorithm for the detection of wide linear features", Proc. of IEE, vol. 140, no. 5, pp 331-339.

Porter A.L., Rossini F.A., Eshelman J., Jenkins D.D., Cancelleri D.J. (1985), - "Industrial Robots – A strategic forecast using the technological delivery system approach", IEEE Transactions on Systems, Man, and Cybernetics, vol.15, no. 4, pp 521-527.

Pietikäinen M., Ojala T., Nisula J., Heikkinen J. (1994), - "Experiments with two industrial problems using texture classification based on feature distributions", SPIE 2354, pp 197-204.

Pietikäinen M. and Kauppinen H. (1999), - "Texture '99, Workshop on Texture Analysis in Machine Vision", Oulu, Finland.

Tamura H., Mori S., Tamawaki T. (1987), - "Textural features corresponding to visual perception", IEEE Trans. on Systems, Man and Cybernetics, vol. 8, no. 6.

Tobias O., Seara R., Soares F., Bermudez J. (1995), - "Automated visual inspection using the co-occurrence approach", IEEE Midwest Symposium on Circuits and Systems, pp 154-157.

TSI Ltd (1997), - Eagle Eye 4000 web inspector operation manual, Ireland.

TSI Ltd (1998), - Eagle Eye 2000 web inspector product brochure, Ireland.

Unser M. (1986), - "Sum and difference histograms for texture classification", IEEE Transactions on Pattern Analysis and Machine Vision, vol. 8, no. 1.

Wang L and He D. (1990), - "A new statistical approach for texture analysis", Photogrammetric Engineering and Remote Sensing, vol. 56, no. 1, pp. 61-66.

Weszka J., Dyer C., Rosenfield A. (1976), - "A comparative study of texture measures for terrain classification", IEEE Transactions on Systems, Man, and Cybernetics, vol. 6, no. 4.

Whelan P.F., Drimbarean A., Soille P. (1999), - "Online registration of watermarks from continuous web paper", IMVIP '99, pp 267-279.

Whelan P.F. (1997), - "System engineering issues in industrial inspection", IEE Colloquium on Industrial Inspection, (Digest) no. 41, pp. 1/1-1/5.

Bibliography

Davies E.R. (1997) *Machine Vision: Theory, Algorithms, Practicalities*, Academic Press (2nd edition)

Fanchi J.R. (2000), - Maths refresher for scientists and engineers, Wiley.

Haralick R.M. and Shapiro L.G. (1992), - Computer and Robot Vision, Addison – Wesley Publishing Company.

Hayslett H.T. (1993), - “Statistics”, Reed Elsevier.

Hubel D. (1988), - “Eye, Brain and Vision”, Scientific American.

Levine M. (1985), - “Vision in Man and Machine”, McGraw-Hill.

Neatvision, - An image analysis and software development environment, www.neatvision.com.

Pinson L. J. (1985), – Electro-optics, Wiley.

Soille P. (1999), - “Morphological Image Analysis: Principles and Applications”, Springer-Verlag, Berlin.

Sonka M., Hlavac V., Boyle R. (1998), - Image Processing, Analysis, and Machine Vision”, Brooks/Cole, USA.

Whelan P. and Molloy D. (2000), - “Machine Vision Algorithms in Java: Techniques and Implementation”, Springer-Verlag, London.

Publications arising from this research

Carew T., Ghita O. and Whelan P.F. (2001), - “Detecting visual faults on painted slates”, Proc. IMVIP2001, September 5-7, Maynooth, Ireland.

Carew T., Ghita O. and Whelan P.F. (2001), - “A vision system for detecting paint faults on painted slates”, Proc. ICCAS2001, ICASE International Conference on Control, Automation and Systems, October 17-21, Korea.

~~**Carew T., Ghita O. and Whelan P.F. (2002)**~~, - “A vision system for detecting surface faults on painted slates”, The 8th Mechatronics Forum International Conference (*Mechatronics 2002*), University of Twente, Enschede, Netherlands.

Appendix A - Detailed Robustness Tests Results

A.1 No paint and insufficient paint

Two unpainted samples were imaged (no. 142 and no. 149) and these were found to have mean grey levels of 53. Six insufficient paint samples were imaged (no. 154 ~ no. 160) and these were found to have an average grey level of 105.

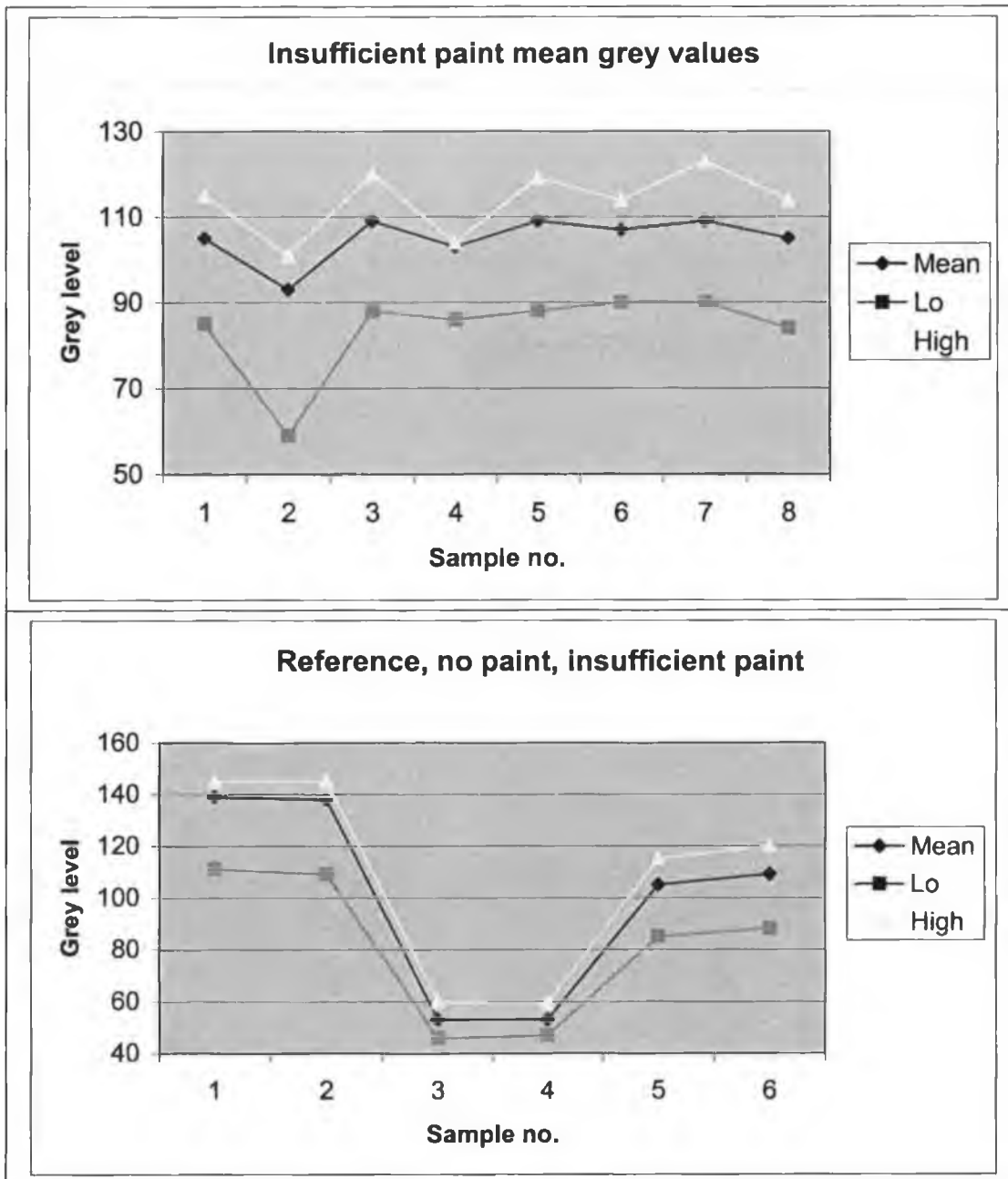


Figure A.1: Insufficient paint and no paint sample mean grey levels.

All samples are correctly identified as defects. There is potential to use the grey level mean to identify the samples by defect type. There is overlap between the lower limits of acceptable mean values for an image sub-section and the upper limits of mean values observed on insufficient paint image sub-sections. However, a sufficient number of image sub-sections have mean values below the threshold for the mean test to be successful.

Table A.1: Paint fault detection results.

No.	InspectorV2 result	Comment
26, 42	Defect	Missing paint at edge
142, 149	Defect	Unpainted slate
49, 51, 154 ~ 160	Defect	Insufficient paint

A.2 Efflorescence

All samples were successfully detected. These are no. 15, 60, 64, 68, 76, 102, 108, 109, 110, 111, 148, 161, 164, 165 and no. 207. The sample range had a variety of sizes of defect and located at various positions on the slate, including the edges.

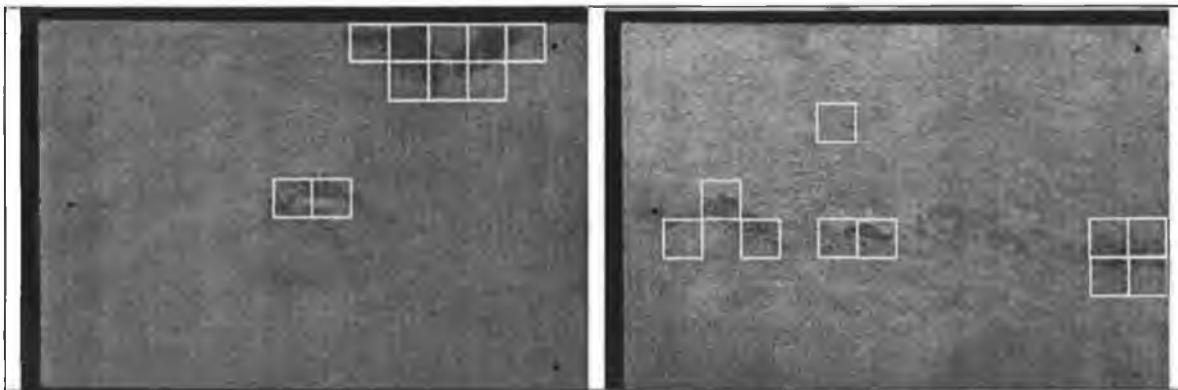


Figure A.2: Efflorescence samples no. 164 and no. 165 detection results.

A.3 Shade variation

The shade variation samples tested are successfully detected as defects at the interface between acceptable quality and defective quality slate. All samples were detected and are no. 29, 95 ~ 98, 119, 183 ~ 186, 190 and no. 201.

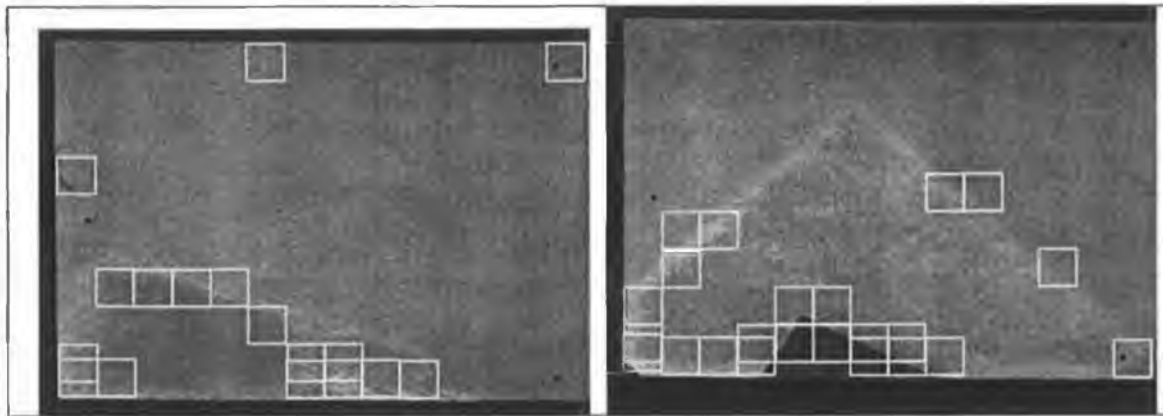


Figure A.3: Shade variation samples no. 183 and no. 185 detection results.

A.4 Nozzle drip

12 of the 13 samples were successfully detected using the image processing algorithm. Most samples are detected with the label algorithm. Some samples were also detected with the global mean threshold and a small number are also detected with adaptive mean threshold set to (mean-15).

Table A.2: Nozzle drip sample inspection results.

No.	Th=(mean-13)	Th=(mean-15)	Mean	Slate mean test
50	Defect	Defect	120	Pass
173	OK→Defect	OK→Defect	110	Fail
174	Defect	Defect	114	Fail
175	Defect	Defect	126	Pass
176	Defect	Defect	110	Fail
177	Defect	Defect	117	Fail
178	Defect	Defect	120	Pass
179	Defect	Defect	124	Pass
180	Defect	Defect	125	Pass
181	Defect	Defect	113	Fail
182	Defect	Defect	119	Fail
187	Defect	Defect	126	Pass
188	Defect	Defect	113	Fail
191	Defect	Defect	117	Fail

One sample, no. 173, was not detected using any of the image processing components and a new test was devised to categorize this sample as defective. The slate global mean test was introduced based on the full slate image grey level mean. Sample no. 173 failed this test and was classed as defective.

Mean of nozzle drip samples is shown on right. No. 1 and no. 15 are Supercem reference samples having slate mean grey level of 139. A slate mean threshold can be set at 120 grey levels. Eight of thirteen samples will fail this test.

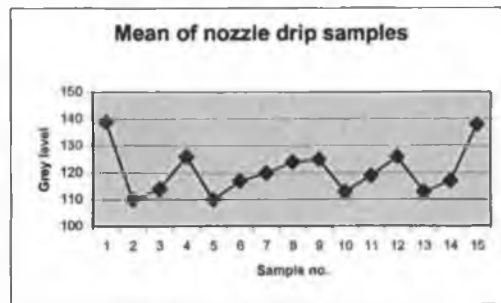


Figure A.4: Mean grey levels of nozzle drip samples.

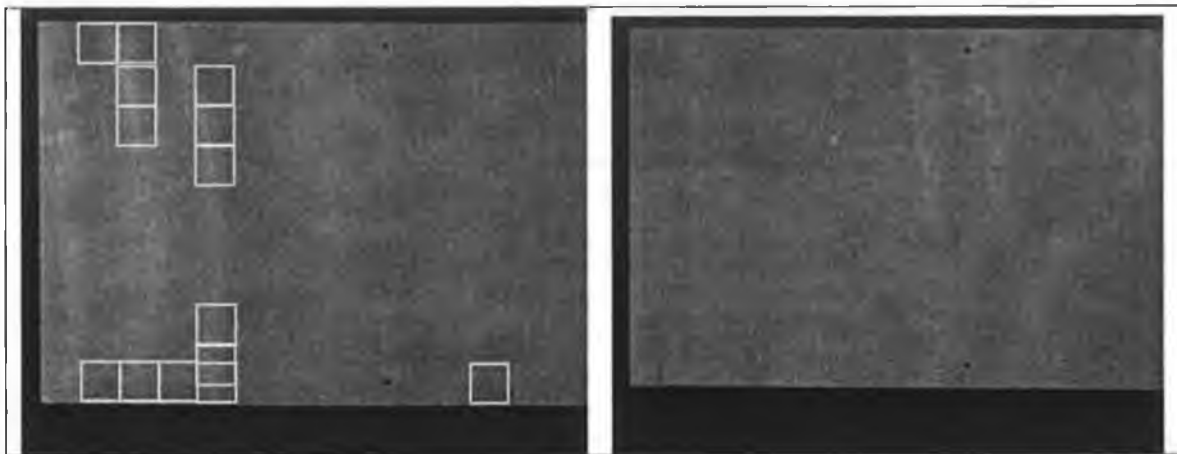
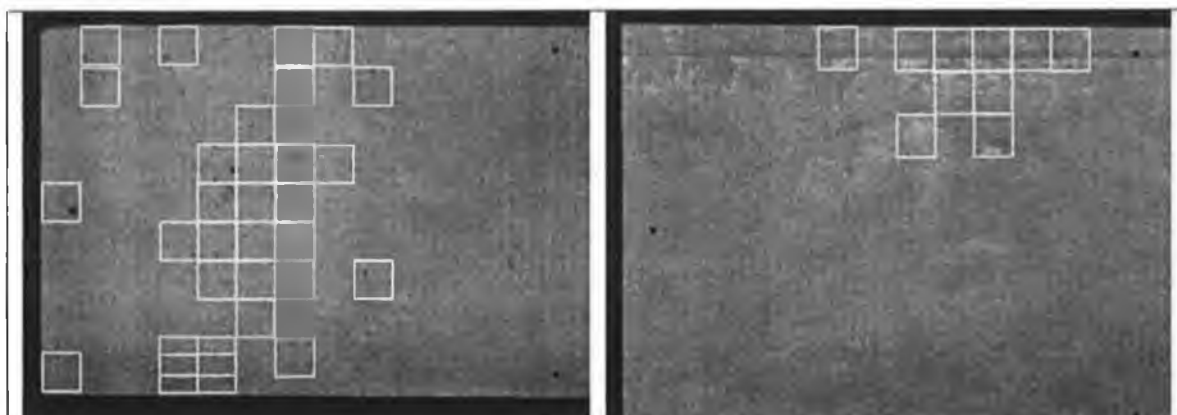


Figure A.5: Nozzle Drip samples no 181. and no. 173 detection output.

A.5 Paint droplets, wax marks and paint debris

These are small size defects and are generally well detected. Paint debris samples are no. 124, 145, 195 and 200. Paint droplet samples are no. 11, 41, 52, 59, 70, 99, 120 and 122. Wax marks are no. 1, 40, 59, 76, 119, 121, 143 and no. 202. Wax mark sample no. 1 was not detected because no signal was generated from the image capture system. This wax mark is of lighter colour than the slate and diffuse with the result that it is not distinguishable from the darker but glossy slate surface.



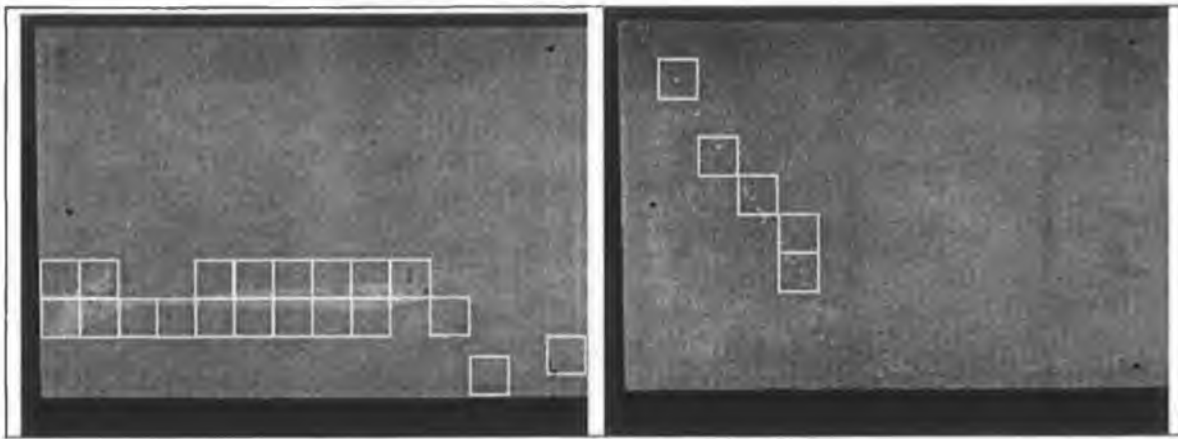


Figure A.6: Small paint fault detection result output.

A.6 Template marks

Template marks include sample no. 12, 13, 15, 17, 19, 37, 44 ~ 47, 58, 64, 65, 68, 72 ~ 74, 113, 116, 117 and 198. More samples are listed in Table 6. A large range of template mark shapes and sizes were investigated and most are well detected.

Table A.3: Template mark defect detection results.

No.	Type	Result	Comment
22	Line, narrow at angle	Defect	
23	Blob	Defect	
27	Large area, varied	Defect	
28	Blob	Defect	
30	Shallow, large area	Defect	
34	Thin line in direction of travel of conveyor	OK	
67	Small protrusion	Defect	
69	Faint lines in CD	OK	Also wax detected
75	Edge mark	Defect	
115	Protrusion	Defect	
203	Nut impression	Defect	Also wax

A.7 Template marks II

This class of template marks are well detected and are no. 32, 39, 71, 112 and 195.

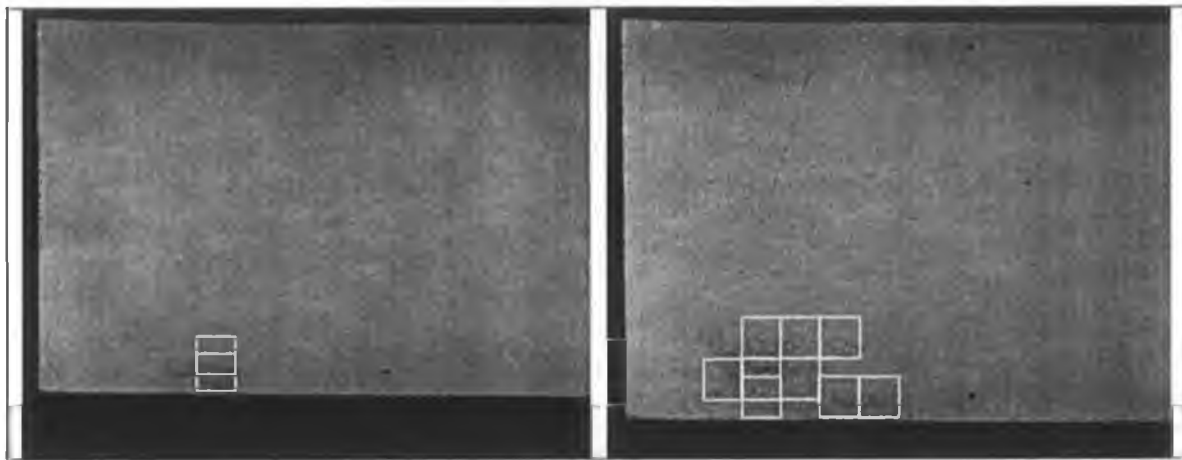


Figure A.7: Template marks no. 39 and no. 195 detection output.

A.8 Lumps

Lumps are well detected and include samples no. 8, 9, 31, 54, 56, 62, 66, 111, 114, 193, 194, 196, 213 and TM41. The sample range includes shallow and high types, small and medium sizes and a cluster of tiny lumps (TM41).

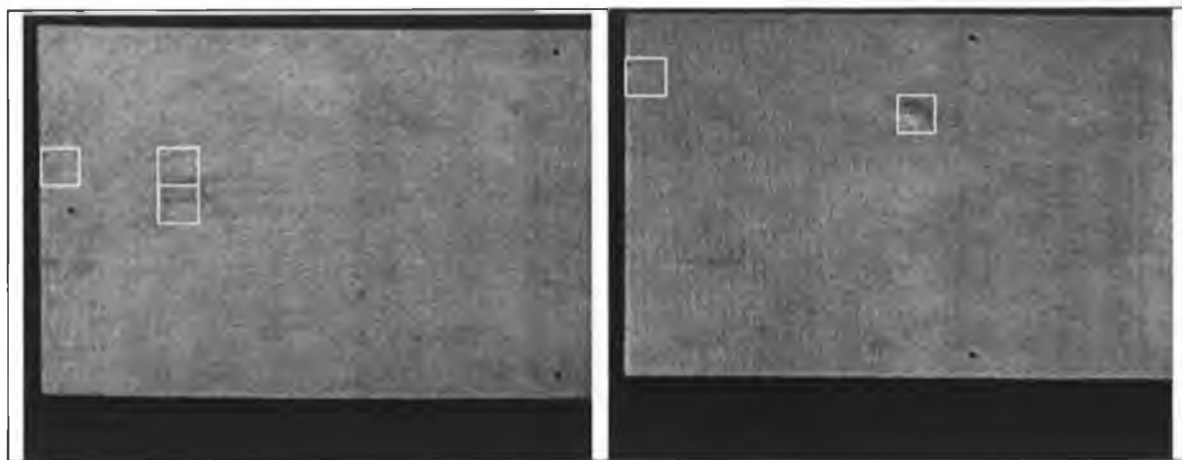


Figure A.8: Detection output for no. 56 and no. 66 lump defects.

A.9 Depressions

Table A.4: Depression inspection results.

No.	Type	Result	Comment
3	Tiny depressions	OK	Too small and shallow
33	Large shallow	Defect	
38	Large shallow	OK	Detected when 300mm edge facing forward.
70	Medium size	Defect	
205	Large shallow	Defect	
207	Large shallow	Defect	

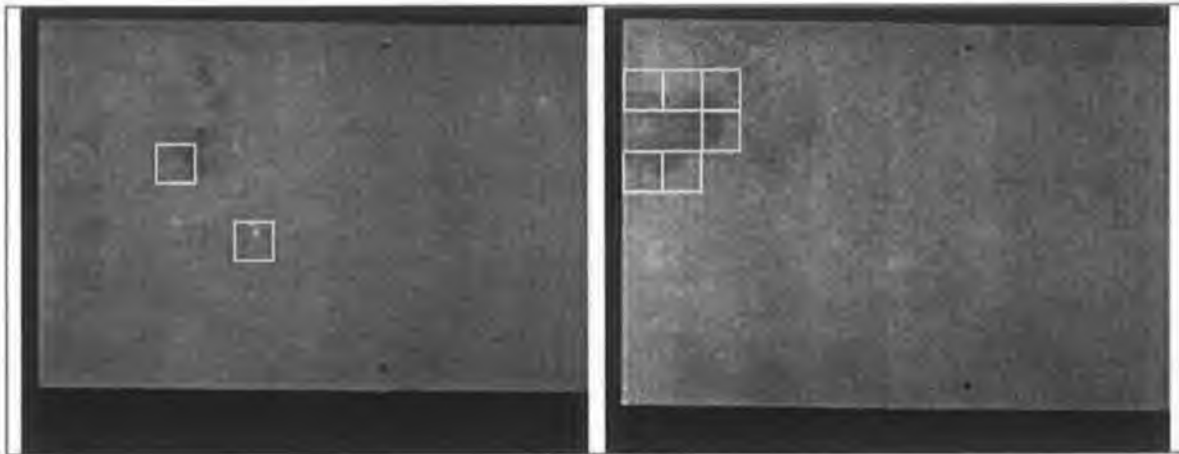


Figure A.9: Depression no. 205 and no. 38 detection output.

A.10 Bad edge

Table A.5: Bad edge defect detection details.

No.	Type	Result	Comment
10		Defect	
20	Horizontal edge	Defect	
21	Vertical edge	Defect	
25	Horizontal edge	Defect	
56	Notch on left edge	Defect	
79	Corner missing	Defect	
80	Section of edge narrower	Defect	
81	Poor lower edge	Defect	
82	Poor lower edge	Defect	
83	Thicker top edge	Defect	
84	Uneven edge	Defect	
85	Notch on top left	Defect	
86		Defect	
87		Defect	
88	Notch on left edge	Defect	Also tiny marks
89	Poor top edge	Defect	
199	Lower edge	Defect	
206	Large corner missing	Defect	

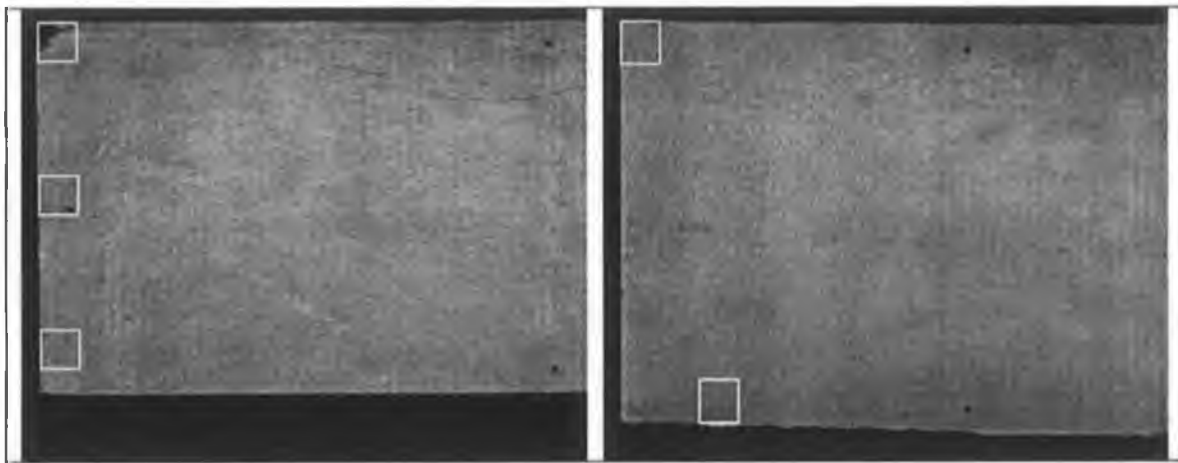


Figure A.10: Bad edge no. 79 and no. 82 detection output.

A.11 Miscellaneous defect types

Table A.6: Miscellaneous defect type detection results.

No.	Defect type	Result	Comment
4	Orange peel	Defect	
105	Orange peel	Defect	
35		Defect	
36		Defect	
7	Cracks in paint	Defect	
63	Crack in slate	Defect	
14	Spots	Defect	
100	Surface cracks	Defect	Barely detected
101	Surface cracks	Defect	
106	Surface cracks	Defect	
107	Surface cracks	Defect	
S61	Crack and debris	OK	Debris detected

Appendix B - Prototype Inspector Equipment List

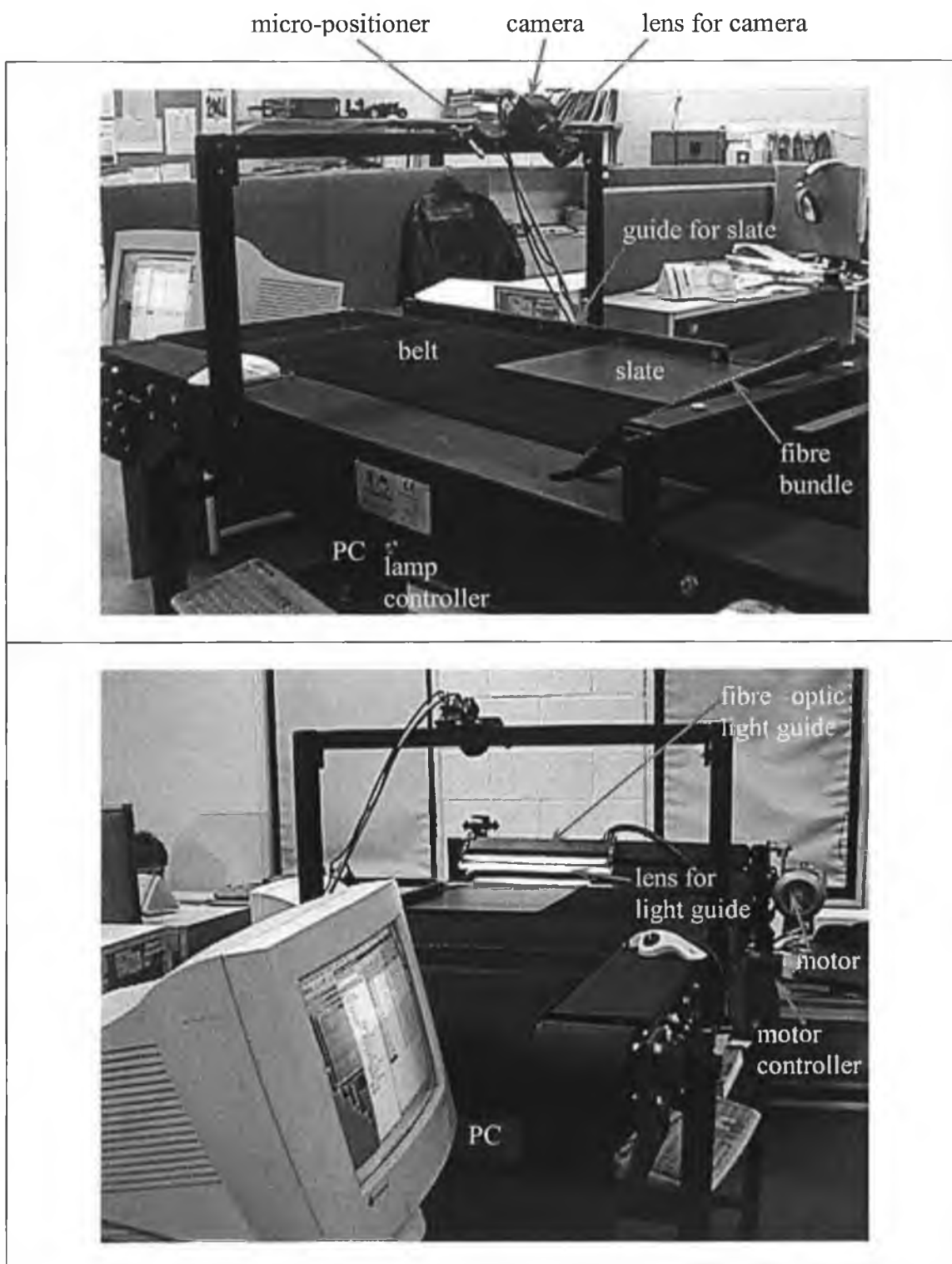


Figure B.1: Conveyor and slate inspection system.

Table B.1: Equipment list.

No.	Item	Model	Supplier	Cost (euro)
1	Conveyor	2-meter long, belt-driven	Noreside Conveyors	6,500
2	Camera	Basler L102	Kane Computing	3,700
3	Lens		Firstsight Vision	600
4	Frame grabber	Euresys Multi	Kane Computing	1,900
5	Fiber-optic light line	Fostec 30" dual entry with lens	Caulfield Industrial	4,000
6	Lamp controllers	Fostec DCRIII	Caulfield Industrial	1,700
7	PC	Gateway 2000 PII	Gateway 2000	1,500

Appendix C - Popular Image Processing Techniques

C.1 - Difference statistics

The first order statistics of the absolute difference between pairs of grey levels is one method used for discrimination of textures. The grey level difference method examines local properties, usually of one or two pixel separation. The directions 0° and 90° are usually investigated and the directions 45° and 135° are sometimes investigated. The method is sensitive to intensity variations within an image and it is usual to perform a histogram equalisation prior to calculation of the differences.

The difference statistic is computed in the following way. Select a suitable pixel separation. Select a difference formula for the principal directions of interest. Compute the probability density for the difference formula. Compute statistics of the probability density function. Compare the statistical results to those of references and decide whether the image contains a defect.

The difference formula favoured by Tobias et al (1995) is

$$D_d(x,y) = I(x+1,y) + I(x,y+1) - I(x-1,y) - I(x,y-1) \quad (C1-1)$$

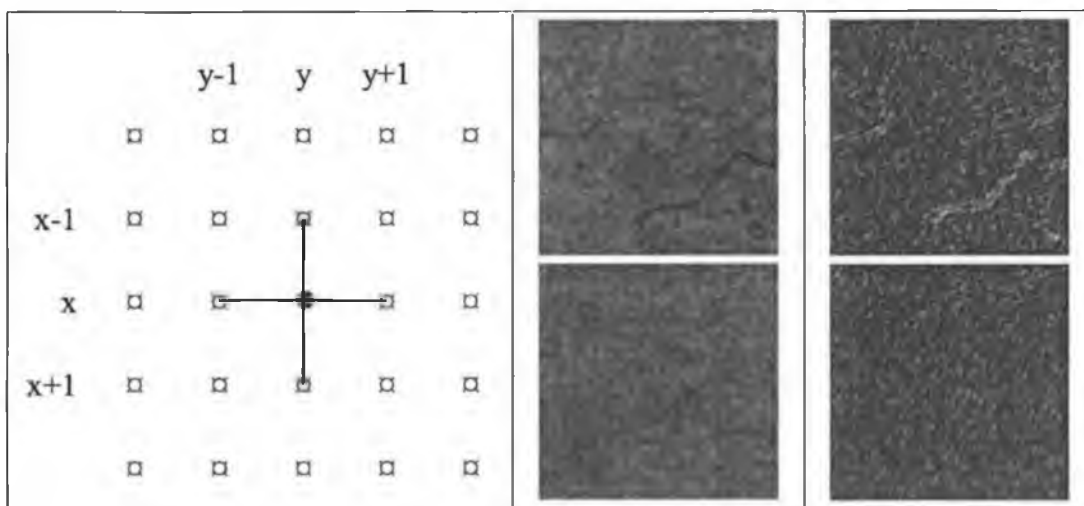


Figure C.1: Difference statistic calculation, source and difference images.

In general, difference histograms will peak near zero for a small d while they are more spread out for larger values of d . Weszka et al (1976) noted that if a texture is coarse, and d is small compared to the texture element size, the pairs of points at separation d

should usually have similar grey levels, so that values are concentrated near the origin. Conversely, for a fine texture with d comparable to the element size the grey levels of points d should often be quite different and histogram values should be more spread out. One observation from the above is that choosing appropriate imaging resolution for the features to be distinguished is an important consideration. Ojala et al (1996) define several difference measures and these are listed here.

g_4	g_2	g_3	$p_2(g_1-g_0, g_2-g_0)$	(C1-2)
g_5	g_0	g_1	$p_4(g_1-g_0, g_2-g_0, g_3-g_0, g_4-g_0)$	(C1-3)
g_6	g_7	g_8	$p_8(g_1-g_0, g_2-g_0, \dots, g_8-g_0)$	(C1-4)

$$\text{DIFFX} = |I(x,y)-I(x+1,y)| \quad (\text{C1-5})$$

$$\text{DIFFY} = |I(x,y)-I(x,y+1)| \quad (\text{C1-6})$$

$$\text{DIFF2} = |I(x+1,y)-I(x-1,y)+I(x,y+1)-I(x,y-1)| \quad (\text{C1-7})$$

$$\text{DIFF4} = |I(x+1,y)-I(x-1,y)+I(x,y+1)-I(x,y-1)+I(x+1,y+1)-I(x-1,y-1)+I(x-1,y+1)-I(x+1,y-1)| \quad (\text{C1-8})$$

The statistical features computed from the grey level difference probability density function are:

$$\text{Contrast: } CON = \sum i^2 P_d(i) \quad (\text{C1-9})$$

$$\text{Mean: } MEAN = \frac{1}{m} \sum i P_d(i) \quad (\text{C1-10})$$

$$\text{Angular second moment: } ASM = \sum P_d(i)^2 \quad (\text{C1-11})$$

$$\text{Entropy: } ENT = -\sum P_d(i) \log P_d(i) \quad (\text{C1-12})$$

C.2 - Local Binary Patterns

Local Binary Patterns (LBP) are a two-level version of the Texture Spectrum Method proposed by Wang and He (1990) and can be useful for discriminating different types of texture. LBP is invariant against any monotonic grey scale transformation. This makes the method invariant to changes in average illuminance and potentially useful in this application involving uneven illumination. It is simple to compute and is calculated as follows:

1. The 3x3 neighbourhood is thresholded by the value of the centre pixel.
2. The values of the pixels in the thresholded neighbourhood are multiplied by the weights given to the corresponding pixels.
3. The values of the eight pixels are summed to obtain a number for this neighbourhood.

Pixels			Example	Thresholded	weights	
P_1	P_2	P_3	6 5 2	1 0 0	1 0 0	$LBP = 1+8+32+128=169$
P_4	P_5	P_6	7 6 1	1 0	8 0	$LBP/C = (6+7+9+7)/4$
P_7	P_8	P_9	9 3 7	1 0 1	32 0 128	$-(5+2+1+3)/4 = 4.5$

Figure C.2: Local binary pattern calculation.

The LBP and LBP\C histograms are computed from the LBP and LBP/C images. The histograms are binned with the number of bins usually set to 32 with 16 bins sometimes used.

The binned histograms are compared using any one of a number of non-parametric statistical tests. Ojala et al (1996) use the G test log-likelihood measure to compare a test sample S to a reference sample M

$$G = 2 \sum_{n=1}^N s_n \log \frac{s_n}{m_n} \quad (C2-1)$$

where s_n and m_n correspond to sample and model probabilities of bin n , respectively. The value of the log-likelihood measure indicates the probability that the two sample distributions come from the same population: the higher the value the lower the probability that the two samples are from the same population. A classifier such as k

nearest neighbour is usually applied to classify the sample under test. In the case of slates, an accept/reject decision is sufficient and a simple threshold can be applied.

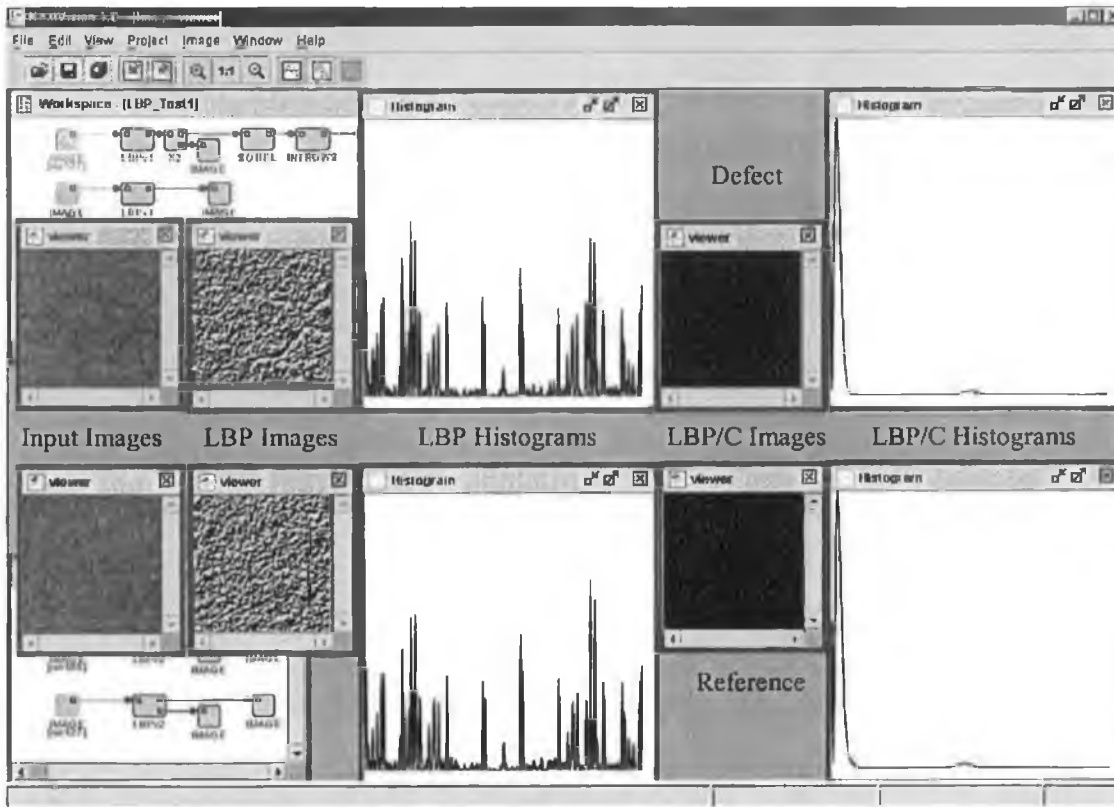


Figure C.3: Typical LBP images and histograms.

C.3 - Application of binary morphology

Morphology deals with the geometric structure within an image and is usually referred to as the science of structures and shapes. It is often called mathematical morphology because the analysis is based on set theory, integral geometry and lattice algebra (Soille, 1999).

The basic concept in morphology is to compare the objects to be analysed with an object of known shape and size. The known object is called a structuring element (SE) and usually has a simple geometric shape such as a square, circle, hexagon or line. The result of the comparison is a modified form of the input object; locations where the structuring element fits the input image are marked and reveal structural information about the image. Morphological operations can be used to fulfil most image processing and analysis requirements including filtering, image segmentation and image measurements.

Erosion and dilation are the basic operators of morphology. All other operations are built up as combinations of these two operators. Dilation refers to the filling or growing of an image and erosion refers to the shrinking of an image. A dilation expands an image set A by a SE B and an erosion reduces an image set A by a SE B (Whelan and Molloy, 2001). The image set A is reduced or expanded when the SE B fits the image set A , and remains unchanged when the SE B does not fit the image set.

To illustrate these concepts, slate images will be probed with a line structuring element of size 5 pixels. A horizontal line is used in the first instance and a vertical line is then applied to the same image. The key to the figures is as follows:

- Top left: input image of portion of slate.
- Top middle: binary version of input image using threshold of (mean-15).
- Top right: dilation of binary image to join line structures.
- Bottom right: first erosion to remove non-line structures.
- Bottom middle: second erosion to remove non-line structures.
- Bottom left: third erosion to remove non-line structures.

The images show that the image structures of interest are segmented only when the SE fits the image set. E.g., vertical lines are extracted using a vertical SE.

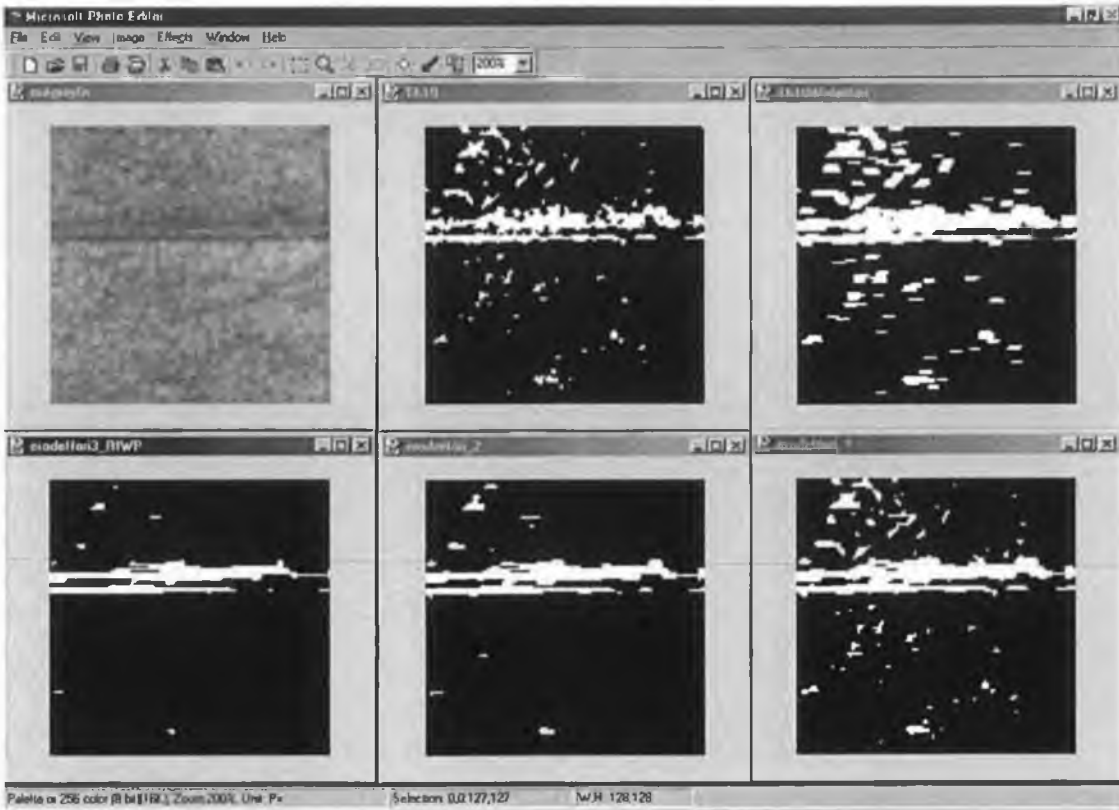


Figure C.4: Horizontal line SE applied to detection of horizontal template mark.

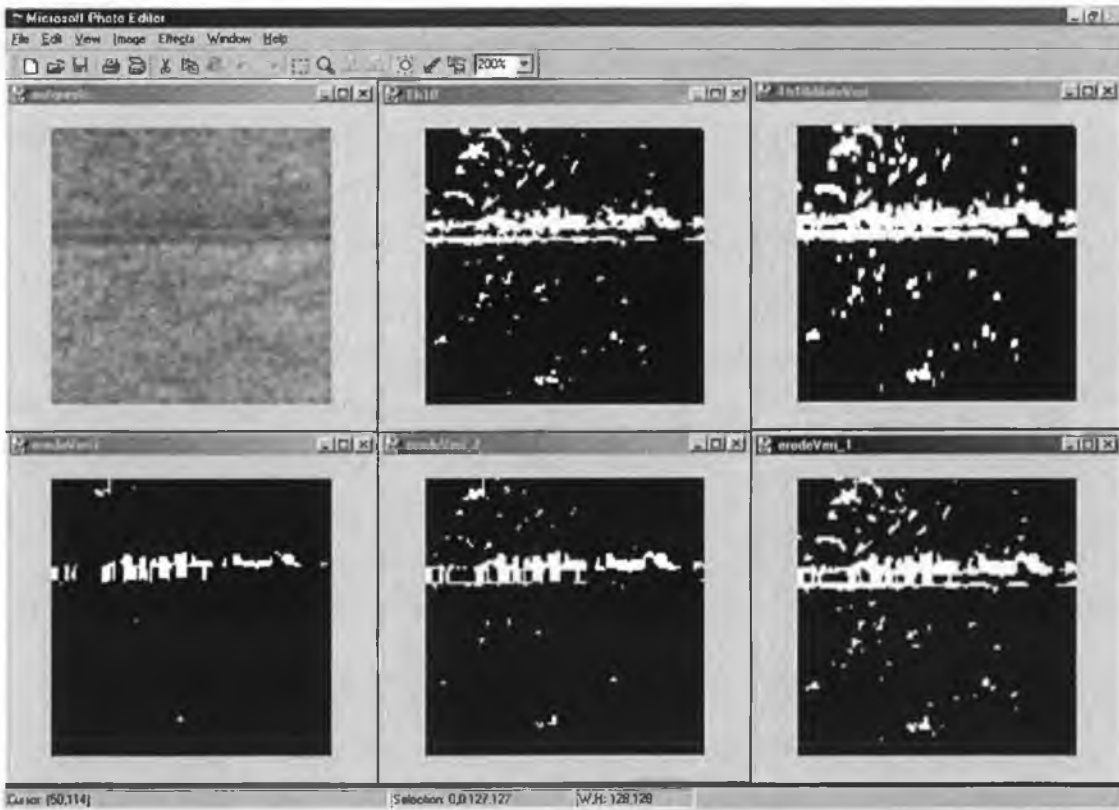


Figure C.5: Vertical line SE applied to detection of a horizontal template mark.

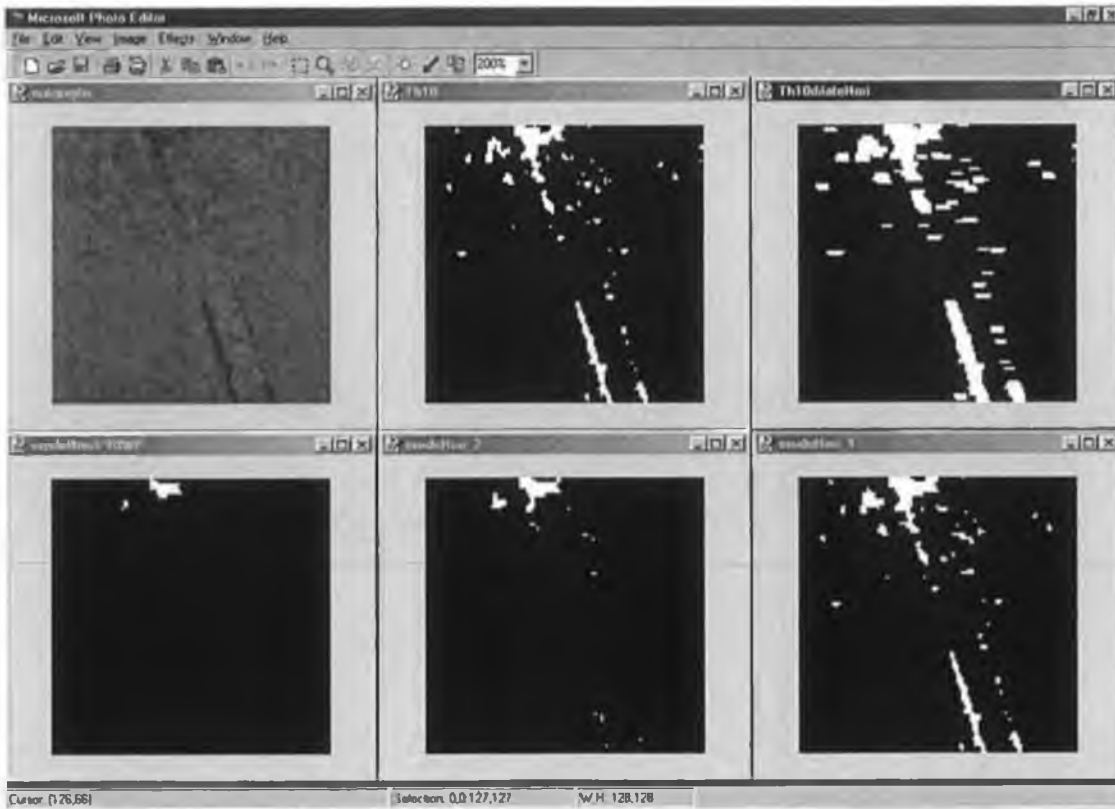


Figure C.6: Horizontal SE applied to detection of a vertical template mark

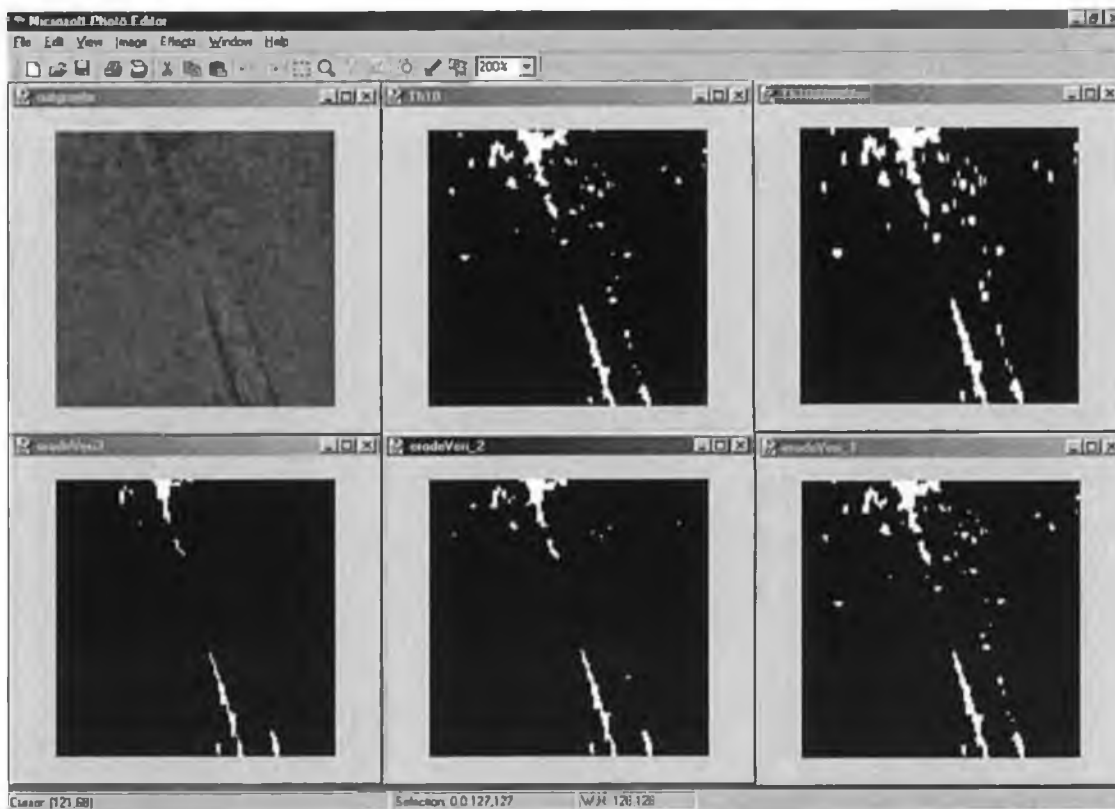


Figure C.7: Vertical SE applied to detection of a vertical template mark

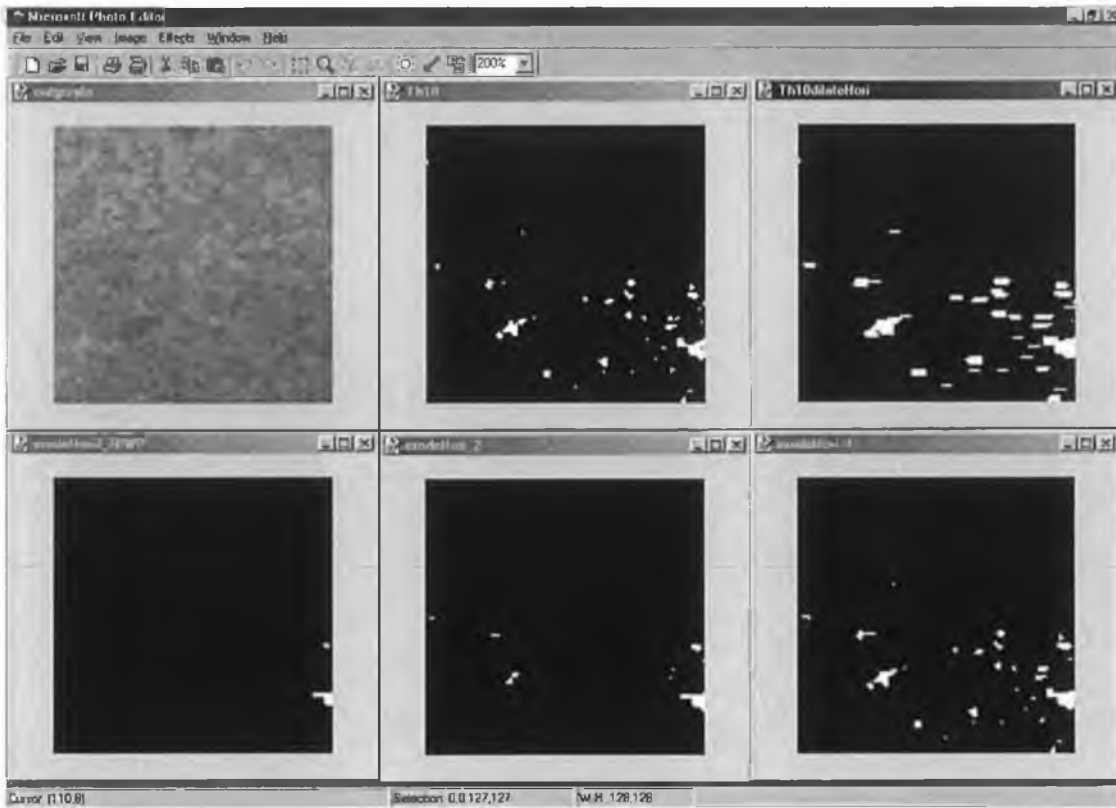


Figure C.8: Horizontal line SE applied to a reference image.

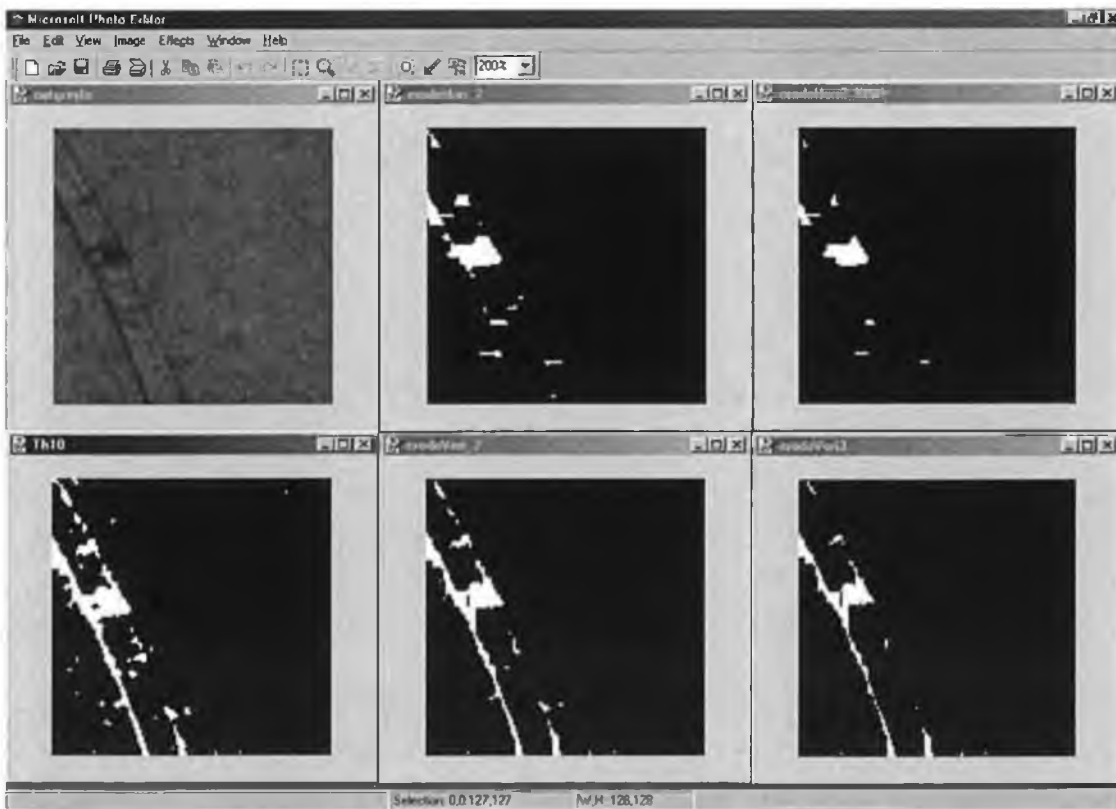


Figure C.9: Comparison of vertical and horizontal (top row) SE results when applied to a vertical template mark.

Appendix D - Classification of Defects by Type

Brief investigations were made into application of the defect detection algorithm to the task of defect classification by type. Each of the four components of the algorithm was designed to detect specific image features. These features are as follows:

Table D.1: Relation of algorithm component to defect type.

Method	Feature to detect
Global mean threshold	Reduction in overall intensity
Adaptive signal threshold	Localised and gross dark or bright regions
Labelling	Localised and low contrast dark or bright regions
Edge detection and labelling	Edges

The algorithm component triggered for several of the defects were collated into Table 24. Examination of the data shows that there is rarely a unique signature for specific types. Reliable classification of other defect types will not be possible using the algorithm in its present format. This is due to the large range of shapes and sizes of the defects, which can trigger one, two or three components of the algorithm. The size of a defect can also change the number of algorithm components triggered.

The main scope for defect classification comes from the intensity measurement. It will be possible to distinguish no paint, orange peel and insufficient paint defect types. Please refer to Figure 41 in Appendix A.

Minor modifications to the algorithm should bring about significant improvements to the classification. For example, droplets and wax marks are generally bright defects whereas other types are dark defects. The grey scale to binary transformation can be modified to check whether the defect is bright or dark, thereby facilitating their distinction from other types.

Large lumps and template marks generate more intense signals than do shade variation and nozzle drip defect types. The grey scale to binary transformation of the labeling component can be extended to check at several intensity levels rather than at a single intensity level as is the case now. The signal amplitude graphs given in Figure 14 indicate the potential for this proposed classification based on intensity of signal generated by a defect.

Table D.2: Algorithm component triggered by defect type.

Type	Mean	Global mean	Local mean	Adaptive signal	Labelling	Edge detection & labelling
No paint - all	53	yes	yes	no	no	no
No paint - small		no	no	yes	no	no
No paint - medium		no	no	yes	yes	no
No paint - large		no	yes	yes	yes	no
Orange peel	70	yes	yes	no	no	no
Insufficient paint - all	105	yes	yes	no	no	no
Insufficient paint - partial	95	no	yes	no	no	no
Efflorescence - very dark		no	maybe	maybe	yes	no
Efflorescence - dark		no	no	no	yes	no
Shade variation		maybe	maybe	no	yes	no
Nozzle drip		maybe	no	no	yes	no
Paint debris		no	maybe	yes	maybe	maybe
Droplet		no	no	maybe	no	yes
Spots		no	no	maybe	no	yes
Template mark - excess material		no	maybe	maybe	maybe	maybe
Template mark II		no	no	maybe	maybe	maybe
Lump		no	no	maybe	yes	maybe
Depressions		no	no	maybe	maybe	no
Wax mark		no	no	maybe	yes	yes
Tiny lumps - cluster		no	no	no	no	yes
Paint splash		no	no	no	yes	no
Template mark - nut impression		no	no	yes	yes	no
Template mark - distorted surface		no	no	maybe	yes	no

The current algorithm classifies labelled regions as defective based on a simple area measurement. No attempt has been made to characterise the defects according to their shape or absolute size. There are several other metrics that can be applied and it is possible one or more of these metrics will enable unique classification of certain defect types.

The current algorithm is designed with execution speed as an important criterion. Classification of defects by type is for statistical purposes and is not a time critical function. Images of defective slates can be stored for analysis using a new algorithm designed with defect type classification as the design criterion.

Substrate faults can be distinguished from paint faults if slates are imaged using triangulation and with an area camera. Illuminating the slate with a narrow band of collimated light and imaging this band of light using an area camera implements triangulation imaging. A reference slate having a flat surface profile will not deform the band of light.



Figure D.1: Reference slate and large depression imaged by triangulation.

A substrate defect is a localised depth (or height) variation and will shift the position of the band of light. An area camera can pick up this positional deviation. The deviation will be in proportion to the height variation and the severity of the defect can be measured.

Shown in Figure 61 are a portion of a reference slate (on left) and a portion of a slate having a large depression (on right). The reference slate generates a straight edge along the bright to dark transition whereas the defective slate generates a curve in the edge line where the defect is present. Metrics can be applied to the edge profile to detect the size and extent of the depth profile variation.

In summary, the possibility to classify defects by type and by size does exist. The algorithm in its current format has limited usefulness for type classification. Further work is necessary to extend the algorithm to enable type classification.

Appendix E – Defect Naming Abbreviations

Defect naming abbreviations are explained here.

Table E-1: Defect naming abbreviations used in the report.

Tref	Thrutone reference
Bref	Supercem reference
Lu	lump
Lu20	Sample number 20 and of type lump
Ip	Insufficient paint
Pd	Paint droplet
Pdu	Paint debris
Op	Orange peel
Ef	Efflorescence
Mp	Missing or no paint
Sv	Shade variation
Tm	Template mark
Dt	Template mark type II
Be	Bad edge
Lu25dpr	Depression on lump sample number 25. Lump is primary defect type
B	Barring
B1f2	Image sub-section f2 from barring sample number 1. F is the column identifier and 2 is the row identifier
Tm41c4	Image sub-section c4 from template mark sample number 41. C is the column identifier and 4 is the row identifier
Thresh	Threshold setting used for data shown in a table. Any data exceeding the threshold shown indicates a defective image sub-section
CWP	Count White Pixels. The number of pixels in an image sub-section which exceed the threshold
CWP10	The number of pixels in the ten largest blobs of an image sub-section
No 18-14	Image sub-section 14 of sample number 18